The Effect of Muscle Length on Post-Tetanic Potentiation of skMLCK $^{-/-}$ and C57BL/6 Mouse EDL Muscles

Angelos Angelidis

Submitted in partial fulfillment of the requirements for the degree of Master of Science in Applied Health Sciences (Kinesiology)

Faculty of Applied Health Sciences, Brock University

St. Catharines, Ontario

Abstract

Post-tetanic potentiation of force in fast skeletal muscle is inversely related to muscle or sarcomere length, diminishing at longer lengths. This relationship has been mainly attributed to the structural effects of the primary mechanism of potentiation, phosphorylation of the regulatory light chain (RLC) of myosin, which is catalyzed by skeletal myosin light chain kinase (skMLCK). The purpose of this thesis was to compare the relationship between isometric twitch force potentiation and muscle or sarcomere length in fast twitch extensor digitorum longus (EDL) muscles from wildtype and skMLCK$^{-/-}$ mice. It was hypothesized that in addition to reduced potentiation, skMLCK$^{-/-}$ muscles without the ability to phosphorylate the RLC would also display an altered length-dependence of potentiation compared to wildtype muscles with RLC phosphorylation. The main finding was that although twitch potentiation was greater in WT muscles at all lengths, the relationship between potentiation and muscle length was similar in both WT and skMLCK$^{-/-}$ muscles. This indicates that the length-dependence of potentiation cannot necessarily be attributed to RLC phosphorylation. Thus, additional mechanisms, possibly related to Ca^{2+} handling, thick filament mechanosensing and length-dependent activation may participate in the length-dependence of potentiation displayed by murine fast muscle models.

Key Words: Potentiation, RLC, skMLCK, Length, Myosin

Acknowledgements:

I would like to thank Rene for providing me with the guidance and necessary resources to complete this thesis. I would also like to thank the members of my advisory committee, Dr. Gabriel and Dr. Fajardo, for their advice and support, as well as Dr. Brian MacIntosh for his help as my external examiner.

A special thank you to Dr. Gittings for his technical assistance and advice. Additionally, I would like to thank Shawn Bukovac and the animal care personnel for their help throughout this project.

My family and friends have supported me throughout this process and I am grateful for their love and understanding.

Table of Contents:

List of Figures:

List of Tables:

List of Abbreviations:

$+dF/dt$	Instantaneous Rate of Force Development
$-dF/dt$	Instantaneous Rate of Force Relaxation
½ RT	Half-Relaxation Time
ADP	Adenosine Diphosphate
AMP	Adenosine Monophosphate
ANOVA	Analysis of Variance
ATP	Adenosine Triphosphate
ATPase	Adenosine Triphosphatase
Ca^{2+}	Calcium Divalent Cation
CaM	Calmodulin
CEU	Calcium Entry Units
CPA	Cooperative Phosphorylation Activation
CSQ	Calsequestrin
DHPR	Dihydropyridine Receptor
DWORF	Dwarf Open Reading Frame
ECC	Excitation-Contraction Coupling
ECCE	Excitation-Coupled Calcium Entry
EDL	Extensor Digitorum Longus
ELC	Essential Light Chain of Myosin
GTP	Guanosine Triphosphate
IHM	Interacting Heads Motif
L_0	Optimal Length
LDA	Length-Dependent Activation
M1	First Meridional Reflection of Myosin
M3	Third Meridional Reflection of Myosin
M6	Sixth Meridional Reflection of Myosin
MCU	Mitochondrial Calcium Uniporter
Mg^{2+}	Magnesium Divalent Cation

ML1	First Myosin Layer Line Reflection
MLCP	Myosin Light Chain Phosphatase
MLN	Myoregulin
MyBP-C	Myosin Binding Protein C
MYPT2	Myosin Targeting Subunit 2
n	Number of Subjects in Sample
NCX	Na^{2+}/Ca^{2+} exchanger
pCa	Negative $\log_{10}$ of Calcium Concentration
Pi	Inorganic Phosphate
PKA	Protein Kinase A (or cyclic AMP-dependent protein kinase)
PKCε	Protein Kinase Cε
PLN	Phospholamban
P_o	Peak Tetanic Force
PO_2	Partial Pressure of Oxygen
Pot	Potentiation
P_t	Peak Twitch Force
RFD	Rate of Force Development
RLC	Regulatory Light Chain of Myosin
RLC-P	Regulatory Light Chain Phosphorylation
RyR	Ryanodine Receptor
RSK2	Ribosomal S6 Kinase II
S6	Spacing of the Sixth Meridional Reflection of Myosin
sAnk1	Small Ankyrin 1
SD	Standard Deviation
SEM	Standard Error of Mean
SERCA	Sarcoplasmic-Endoplasmic Reticulum Calcium ATPase
skMLCK	Skeletal Myosin Light Chain Kinase
$skMLCK^{-/-}$	skMLCK Knockout
SLN	Sarcolipin
SOCE	Store-Operated Calcium Entry

SR	Sarcoplasmic Reticulum
SRX	Super Relaxed State of Myosin
STIM1	Stromal Interaction Molecule 1
TnC	Troponin C
TnI	Troponin I
TPT	Time to Peak Tension
T-tubule	Transverse Tubule
V_{max}	Maximal Rate of Reaction, or Maximal Velocity
WT	Wild Type

Chapter One: Introduction

Skeletal muscle contraction is a highly regulated process with various sites of modulation in place, reflecting the distinct functional needs of each species and phenotype (Gordon et al., 2000; Lehman, 2016; Irving, 2017). Each site of contraction regulation or modulation is influenced by a variety of genetic and environmental factors, leading to a wide range of phenotypes depending on the species, muscle type and function, and imposed external conditions (Schiaffino & Reggiani, 2011). Traditionally, skeletal muscle contraction in vertebrates has been thought to be thick filament based, but thin filament regulated (Gordon et al., 2000). Recent advances, however, have pointed to a more complex model of contraction regulation (Irving, 2017), involving thick filament mechanosensing mechanisms (e.g., Fusi et al., 2015; 2016). In other species, phosphorylation or calcium-based mechanisms have also been characterized (Padron et al., 2020). These mechanisms act to initiate the structural and biochemical thick filament changes necessary for the contractile process, allowing the myosin heads to bind to the actin binding sites. In addition to these basic mechanisms, the importance of two other major sarcomeric proteins in contraction, MyBP-C (Myosin-Binding Protein C) (Song et al., 2021) and titin (Linke, 2018), is becoming increasingly understood. These processes, along with other, modulatory mechanisms, facilitate contraction. Structurally, the thick filament exhibits a highly organized arrangement, termed the interacting heads motif (IHM), which has been shown to be present consistently, albeit with small differences, across species and muscle types (Alamo et al., 2018). IHM is facilitated by a set of intra- and inter-molecular interactions on the thick filament, and presents as a pseudo-helical array in small mammals (Jung et al., 2008; Zoghbi et al., 2008; Alamo et al., 2018). This arrangement likely provides thick filament-based regulation over certain important functions related

to muscle energetics and/or force. By inhibiting cycling myosin heads, the biochemical "Super-Relaxed State" (SRX) improves muscle economy at rest (McNamara et al., 2014), and may be at least partially facilitated structurally by the IHM (Nag & Trivedi, 2021). In addition, the interacting heads motif provides the structural base for activity-dependent potentiation in tarantula skeletal muscle (Alamo et al., 2018; Padron et al., 2020), and possibly in rodents (Padron et al., 2020; Hill et al., 2021), although this has not been directly demonstrated.

Activity-dependent potentiation is a well-described phenomenon, which encompasses the contractile-history dependent enhancement of contractile function (MacIntosh, 2010; Vandenboom, 2017). In rat and mouse muscle, activity-dependent potentiation has been researched extensively, and its implications on contraction have been well characterized (Vandenboom et al., 2013). The primary mechanism of activity-dependent potentiation is currently thought to be phosphorylation of the regulatory light chain (RLC) of myosin (Zhi et al., 2005). RLC phosphorylation results in structural changes of the thick filament and a change in orientation of the myosin heads (Levine et al., 1996), as well as the biochemical transition from the SRX to the "Disordered-Relaxed State" (DRX) (McNamara et al., 2014), thereby leading to increased probability of actin-myosin interaction (Sweeney et al., 1993). In permeabilized fibers, RLC phosphorylation results in enhanced Ca^{2+} sensitivity (force production at a given level of intracellular calcium) (Szczesna et al., 2002). Additional mechanisms of potentiation appear to be present, as it has been observed in the absence of RLC phosphorylation in a plethora of models (e.g., Rassier et al., 1999b; Gittings et al., 2017). Of particular interest, the mouse lumbrical muscle has been shown to exhibit both post-tetanic (Smith et al., 2013) and staircase potentiation (Smith et al., 2014), with virtually non-existent RLC phosphorylation. The mechanistic explanation for

these observations involves stimulation-induced increases in resting calcium (Smith et al. 2013; 2014). In the context of this thesis, skMLCK$^{-/-}$ EDL muscle, another model showing RLC phosphorylation-independent potentiation (Zhi et al., 2005; Gittings et al., 2017), presents an opportunity to examine the length-dependence of potentiation, a functional relationship with potentially important implications in understanding the mechanism through which RLC phosphorylation enhances contractile function. Moreover, new insights regarding the additional mechanisms of potentiation can be obtained, through examination of their interaction with muscle or sarcomere length, in the absence of RLC phosphorylation.

In rat gastrocnemius muscle in situ and mouse EDL fiber bundles in vitro, potentiation appears to be inversely related to sarcomere length (e.g., Rassier & MacIntosh, 2002). The proposed mechanistic explanation for this relationship involves the interaction between the structural changes brought on by RLC phosphorylation, and the changes in interfilament lattice spacing at different sarcomere lengths. Specifically, it has been proposed that since at longer sarcomere lengths interfilament lattice spacing is reduced, this spatial configuration may render the protruding myosin heads redundant, thus decreasing the observed effect of potentiation (MacIntosh, 2010). This hypothesis is additionally based on the phenomenon of length-dependent activation (de Tombe et al., 2010), whereby the peak of submaximal force production occurs at lengths longer than the optimal length for tetanic force production. This discrepancy is explained by the increased Ca^{2+} sensitivity observed at longer sarcomere lengths. The exact molecular underpinnings of length-dependent activation are unknown (de Tombe et al., 2010; Ait-Mou et al., 2016), but a major initial theory implicated the reduction in interfilament lattice spacing at longer lengths as the main mechanism (de Tombe et al., 2010). Thus, the dual structural (redundancy of myosin head protrusion) and functional

(already enhanced Ca^{2+} sensitivity) implications of reduced interfilament lattice spacing are thought to potentially explain the length-dependence of potentiation. However, this model cannot sufficiently explain some of the findings in the literature. For example, a disconnect has been observed between length-dependent activation and the sarcomere length-interfilament lattice spacing relationship (Konhillas et al., 2002; 2002b, de Tombe et al., 2010). As an example, while cardiac, fast and slow skeletal rat muscles display different magnitudes of length-dependent activation, the slope of the sarcomere length-interfilament lattice spacing relationship does not differ between them. In addition to these and other early experiments (see discussion in de Tombe et al., 2010), recent data from cardiac, as well as skeletal muscle, have provided more mechanistic, in-depth evidence that it is not interfilament lattice spacing per se that mediates length-dependent activation (de Tombe et al., 2010; Mateja et al., 2013; Williams et al., 2013; Ait-Mou et al., 2016; Li et al., 2016). This suggests that although such spatial changes may explain some length-dependent aspects of contraction, and by extension potentiation, they cannot be considered the sole factor responsible (Williams et al., 2013). Structural studies in intact cardiac (Caremani et al., 2019; Park-Holohan et al., 2021) and skeletal muscle (Caremani et al., 2019b; Caremani et al., 2021) have additionally demonstrated that findings from permeabilized fiber and isolated filament experiments related to thick filament structure and function may not directly correspond to the intact muscle environment (Irving & Craig, 2019), and it is still unclear how RLC phosphorylation or other potentiation mechanisms would be structurally manifested in a whole muscle model. An additional example of a finding that possibly challenges the proposed model is related to the effects of caffeine on potentiation (Rassier et al., 1998). Specifically, caffeine has been shown to abolish the length-dependence of potentiation along with length-dependent activation, with both outcomes thought to be mediated by

its positive effect on Ca^{2+} sensitivity (Rassier et al., 1998; Rassier & MacIntosh, 2000). However, potentiation was increased with concomitant increase of basal twitch force at a long muscle length, indicating that a ceiling effect on Ca^{2+} sensitivity cannot, in isolation, explain the findings (Rassier et al., 1998). Thus, it becomes apparent that more information is necessary in order to understand why potentiation is dependent on sarcomere or muscle length. The existence of additional potentiation mechanisms (e.g., Smith et al., 2013), as well as the more nuanced contemporary view of length-dependent activation (e.g., Mateja et al., 2013; Ait-Mou et al., 2016), indicate that probably a more complex set of interactions explain this relationship. Additionally, while previously thought to be unchanged (Balnave & Allen, 1996), it has recently been shown that in intact mouse fast skeletal muscle fibers, calcium release during activation may be inhibited at short sarcomere lengths (at least for higher stimulation frequencies) an effect reversed by caffeine (Rassier & Minozzo, 2016), thus further complicating the picture.

The purpose of this thesis was to investigate the length-dependence of potentiation utilizing skMLCK$^{-/-}$ and wildtype mouse EDL muscles. The rationale for using skMLCK$^{-/-}$ EDL muscles was that they are a unique murine fast twitch muscle, in that they do not contain the enzymatic machinery for RLC phosphorylation, but still display a smaller magnitude of potentiation (e.g., Gittings et al., 2017). This allowed for exploring to what extent the length-dependence of potentiation can be attributed to the structural and functional changes brought on by RLC phosphorylation, and to what to other mechanisms. Moreover, additional insights into the alternative mechanism(s) of potentiation were obtained, by examining its relationship with length in the absence of RLC phosphorylation. On the other hand, wildtype muscles allowed for comparison

of past findings with the experimental model and conditions used here, while also enabling direct comparisons with the skMLCK$^{-/-}$ model.

Chapter Two: Literature Review

The following review will discuss general aspects of muscle function, focusing on contraction regulation and activity-dependent potentiation. In the first section, relevant aspects of skeletal and where necessary, cardiac muscle physiology will be discussed. An overview of all the relevant components of the contractile apparatus and the sarcomere will be given. In the second section, activity-dependent potentiation will be addressed, focusing both on its mechanisms and its effects on muscle function. Finally, the third section will focus on the length-dependence of potentiation, while also providing the necessary background on the length-dependence of force.

2.1 Structural and Functional Aspects of Skeletal Muscle

I. Structure of Muscle and Microanatomy of the Muscle Fiber

Skeletal muscle is composed of myofibers, which represent the individual muscle cell (Mukund & Subramaniam, 2020). Bundles of fibers are further organized into fascicles and finally a whole muscle, with intermediate extracellular matrix in each level of organization (Mukund & Subramaniam, 2020). Each individual muscle fiber comprises numerous myofibrils as well as other functional systems, namely the t-tubular system and the sarcoplasmic reticulum, which surround the myofibrils and are essential for contraction (Mukund & Sabramaniam, 2020). In turn, each myofibril is composed of sarcomeres, which are the functional units of muscle, containing the

molecular machinery necessary for contraction (Gordon et al., 2000; Irving, 2017). Remarkably, even though the aforementioned description of skeletal muscle structure has been accepted for years, recent findings suggest that instead of individual myofibrils, sarcomeres within a fiber instead form a "unified matrix" characterized by sarcomere branching (Willingham et al., 2020). The implications of this finding are not yet clear. In addition to this basic structure, skeletal muscle contains other organelles (e.g., mitochondria) with various functions, and a vast number of cytoskeletal proteins and structures with scaffolding, signaling and regulatory roles (Henderson et al., 2017).

II. The Sarcomere

Sarcomeres are the basic contractile units of striated muscle. Each sarcomere comprises three main filament structures: thick myosin filaments; thin actin filaments, with the associated regulatory proteins troponin C, I and T and tropomyosin; and titin (Henderson et al., 2017). In addition to these major components, the sarcomere includes various proteins on many sites, which act to ensure its structural integrity, as well as modulate and regulate the totality of its functions, from contraction to the numerous processes related to adaptation to imposed conditions (Henderson et al., 2017). Schematically, the sarcomere presents two Z-discs (one on each side), which define its borders with adjacent sarcomeres and bind the actin-containing thin filaments. Next to the Z-disc is the I-band, the area with no overlap between thin and thick filaments, which is shared between serial sarcomeres. The A-band represents the area where the thick filaments extent (regardless of whether they overlap with the thin filaments or not). In the middle of the sarcomere is the M-band, where the thick filaments are attached, while the thick filament area adjacent to the M-band with no thin filament overlap is called H-zone. During sarcomere shortening, the Z-disc is translocated closer to the M-band through the action of myosin on actin.

In addition to the well-characterized role of actin and myosin in the contractile process, recent progress has elucidated the role of other components of the sarcomere in contraction regulation and modulation. Proteins that may be of importance to this thesis will be mentioned later in this review where necessary. Briefly, titin is a giant sarcomeric protein, extending from the Z-disc all the way to the M-line, with different isoforms expressed in skeletal (N2A) and cardiac (N2BA and N2B) muscle (Linke, 2018). Titin interacts both with the thin and thick filaments, as well as Myosin-Binding Protein C (MyBP-C), and alternative splicing of its I-band region results in isoforms of different stiffness (Linke, 2018). Titin appears to have a central role in mechanosensing processes and length-dependent activation (LDA) (Linke, 2018). MyBP-C is a protein expressed in all striated muscle types, with minor structural differences between cardiac and skeletal paralogs (additional N-terminal immunoglobulin domain, different phosphorylatable residues, and an additional 28 amino acid loop in the C5 domain) (Heling et al., 2020), which appears to modulate contraction through its interaction with thin and thick filaments, as well as titin (Moss et al., 2015; Heling et al., 2020). This process is regulated by its phosphorylation at different residues (Ponnam et al., 2019), as well as by Ca^{2+} (Previs et al., 2016), and a number of additional post-translational modifications (e.g., Patel, Wilder & Solaro, 2013). MyBP-C is localized at the C-zone of the A-band (middle part of the half thick filament) (Heling et al., 2020). As will be discussed later, the post-translational modifications and exact function of the skeletal fast and slow MyBP-C paralogs are largely unknown (Robinett et al., 2019; Li et al., 2019), but they appear to be essential for normal sarcomere structure and contractile function, as revealed by knockout models (Geist et al., 2018; Song et al., 2021). Collectively, these proteins and potentially others, act as sites of contraction modulation

which may interact with RLC phosphorylation, although their function in skeletal muscle is not as well-understood as in cardiac muscle.

III. Myosin and the Crossbridge Cycle

Myosin is a superfamily of molecular motor proteins with a plethora of functions (Sweeney & Houdusse, 2010). In striated muscle, myosin class II molecules form thick filaments, which power contraction (Sweeney and Houdusse, 2010). Structurally, myosin II molecules consist of six polypeptide chains: two heavy chains, two essential light chains (ELC) and two regulatory light chains (RLC). The two heavy chains form a head and neck region on their N-termini, while their C-termini coil around each other to form a helical backbone region (Craig & Woodhead, 2006). The head region comprises a pair of globular heads, with each head presenting with two subdomains interspersed by an outer and an inner cleft which appear to close upon actin binding, creating the actin-binding interface (Houdusse & Sweeney, 2016). Additionally, each head contains a nucleotide-binding domain. The converter domain connects the myosin head and the neck region. The neck region acts as a lever arm, transducing the forces produced by the structural changes of the motor domain to the rest of the thick filament, and binds the essential and regulatory light chains, which have important functions in the contractile process (e.g., Vandenboom, 2017). During contraction, numerous structural and kinetic changes in the myosin motor domain drive the interaction of myosin with actin and result in the powerstroke, the movement of the lever arm which facilitates the translocation of actin filaments (Geeves & Holmes, 2005; Sweeney & Houdusse, 2010; Houdusse & Sweeney, 2016). While some aspects of this process remain controversial (Houdusse & Sweeney 2010; Sweeney & Houdusse 2016; Stehle & Tesi, 2017; Robert-Paganin et al., 2020; Matusovsky et al., 2021), the initial proposition by Lymn and Taylor (Lymn & Taylor, 1971) provides the

basic template of the crossbridge cycle. Briefly, in the absence of ATP, myosin binds to actin, forming the rigor complex. Upon binding of ATP, myosin is released and the recovery stroke takes place, repriming the lever arm for the powerstroke. Subsequently, myosin hydrolyzes ATP to form a myosin-ADP-P complex. This leads to reattachment of myosin to actin, and the formation of the crossbridge. The actin-myosin interaction results in an as of yet incompletely characterized (Robert-Paganin et al., 2020) cascade of conformational changes in the motor domain of myosin, which lead to the powerstroke, the eventual release of ADP, and the formation of the rigor complex. What remains unknown is the sequence of events pertaining to the release of inorganic phosphate (Houdusse & Sweeney, 2016; Robert-Paganin et al., 2020; Matusovsky et al., 2021), namely whether phosphate is released prior to, concurrently, or following the main portion of force production and the powerstroke (Stehle & Tesi, 2017). Recent findings from Llinas and coworkers (2015) provide a theory attempting to integrate disparate findings; their work suggests that the initial interaction of myosin with actin results in an intermediate "Pi release" state, which is characterized by partial cleft closure on actin and opening of the inner cleft, which allows release of Pi (Robert-Paganin et al., 2020). Pi can then bind to another site on the release channel. Subsequently, myosin binds actin with higher affinity, full closure of the cleft is realized, and the powerstroke takes place, facilitated by conformational changes in the motor domain and accompanied by release of Pi from the second binding site, thus disallowing reversal of the cycle beyond this point (Houdusse & Sweeney, 2016; Robert-Paganin et al., 2020). In addition to the main question of Pi release timing, a number of other incompletely characterized aspects remain including the structural changes in the myosin motor domain as well as actin (reviewed in Robert-Paganin et al., 2020) throughout the cycle, and the rate-limiting transitions of the force production

process (Stehle & Tesi, 2017). In the context of this thesis, it is important to point out that as will be discussed later, posttranslational modification of the regulatory light chain by phosphorylation may directly influence the kinetics of the crossbridge cycle (Davis et al., 2002; Greenberg et al., 2009; 2010); the kinetic and structural underpinnings of these observations, however, remain largely unknown. A more complete characterization of the kinetic and structural details of the crossbridge cycle under various conditions is necessary for two main reasons; most importantly, clinical interventions targeting the crossbridge cycle would become more accurate (Stehle & Tesi, 2017); and, pertaining to this thesis, the mechanistic details of how posttranslational modifications like RLC phosphorylation affect the cycle would be better understood. Currently, findings from functional experiments including, among others, length jumps (Davis et al., 2002) and in vitro motility assays (Greenberg et al, 2009; 2010), have to be interpreted under various assumptions and levels of uncertainty regarding the kinetics and structural details of the crossbridge cycle. In turn, this hinders the characterization of the mechanism through which RLC phosphorylation modulates contraction, and makes interpretation of experimental findings from various functional models (ranging from molecular myosin to whole muscle) more difficult.

The steps of the crossbridge cycle can be modulated to facilitate the needs of each myosin class and isoform, in response to various conditions (Walklate et al., 2016; Robert-Paganin et al., 2020). For example, the duty ratio (i.e., the percentage of the crossbridge cycle spent in strongly bound, force-producing states in comparison to weakly bound and disassociated states) is increased in response to increased load through inhibition of ADP release with differing sensitivity in certain myosin classes and isoforms, although this has not been directly demonstrated in myosin II (Nyitrai & Geeves, 2004) (however see Greenberg et al., 2010). On the other hand, fatigue can

directly affect actin-myosin interactions, acting on individual steps of the crossbridge cycle (Debold et al., 2016). This combination of phenotypic, as well as conditional modulation at such a fundamental level showcases the sensitivity and complexity of the actin-myosin interaction.

IV. The Interacting Heads Motif: Implications for Thick Filament Regulation and the SRX State

Myosin heads on the thick filament exhibit an asymmetrical structural arrangement termed the "interacting heads motif" (IHM), which involves a number of intramolecular and intermolecular interactions, giving rise to the characteristic helical or pseudohelical array observed in thick filaments from a variety of models (Alamo et al., 2017; 2018). Briefly, the actin-binding site of the "blocked" head interacts with the converter site of the "free" head, and along with other inter- and intramolecular interactions, results in the helical packing of the myosin heads on the thick filament backbone characteristic of the interacting heads motif (Vandenboom, 2017). IHM appears to be conserved across a variety of different species, ranging from sponges (Lee et al., 2018) to the human myocardium (Al-Khayat et al., 2013), with slight differences potentially depending on the functional needs of each model. The most studied model of IHM to date has been the tarantula leg muscle, owing to its highly ordered structure which renders it an ideal model for this purpose (Alamo et al., 2018). Despite differences in structure and function between mammalian and tarantula muscle (Padron et al., 2020), these studies have provided important insights in regard to the functional implications of the IHM. Phosphorylation of the RLC in tarantula skeletal muscle is a main mechanism of contraction regulation, involved in what has been termed "cooperative phosphorylation activation" (CPA) (Alamo et al., 2018). In that model, constitutive phosphorylation of the RLC on Ser35 by protein kinase C allows a portion

of the “free” heads to oscillate through Brownian motion between a swaying and a docked position, while the “blocked” heads remain bound to the filament backbone. Upon activation, the swaying heads can readily interact with actin, while calcium ions can bind to calmodulin (CaM) and MLCK, subsequently catalyzing the phosphorylation of RLC on Ser45. This leads to the biphosphorylation of the “free” heads, and through structural modifications on the RLC, the perturbation of the interactions acting on the “blocked” heads, rendering their RLC open for phosphorylation. “Blocked” heads become monophosphorylated on Ser45 by MLCK, leading to the eventual full activation of the contractile apparatus (Brito et al., 2011; Padron et al., 2020). Due to the slow action of Myosin Light Chain Phosphatase (MLCP), phosphorylation of both “free” and “blocked” heads persists, providing a molecular mechanism for post-tetanic potentiation; heads would remain primed for interaction with actin, thereby leading to an enhanced contractile response upon future activation (Brito et al., 2011). This mechanism has recently been directly demonstrated in intact tarantula muscles utilizing x-ray diffraction (Padron et al., 2020).

While CPA is not present in mammalian muscle, other thick filament regulatory mechanisms have been recently elucidated and proposed to have a major role in contraction (discussed later in more detail) (Linari et al., 2015; Fusi et al., 2016). A commonality between CPA and those mechanisms appears to be the priming of the myosin heads for interaction with actin through conformational changes, facilitated by weakening of the IHM interactions, a process mediated by numerous factors including mechanical stress (Fusi et al., 2016), RLC phosphorylation (Kampourakis & Irving, 2015) and MyBP-C phosphorylation (Kensler et al., 2017). Both RLC and MyBP-C (Trivedi et al., 2018) are most likely involved in the IHM interactions, and phosphorylation-mediated disruption of the IHM may result in subtle thick filament

changes which increase the sensitivity of mechanical stress-induced recruitment of myosin motors (discussed later) (Caremani et al., 2019; Irving & Craig, 2019), and/or radially displace the myosin heads toward actin (Padron et al., 2020). In any case, these thick-filament mechanisms appear to act, at least partially, through the disruption of the IHM. Therefore, although many differences exist between tarantula and mammalian myosin, IHM appears to provide the structural basis for contraction regulation and modulation at the thick filament level, allowing muscle to adjust its activation to the imposed task. In the case of the tarantula and other arthropods (e.g., Pinto et al., 2012), IHM provides a structural basis for the main mechanism of contraction regulation. In mammals, IHM presents as a more relaxed arrangement (Jung et al., 2008), likely providing a basis for contraction regulation and modulation.

Another important aspect of the IHM is its potential role as the structural facilitator of the SRX state (discussed later in more detail). The inhibition of actin binding and ATPase activity observed with the IHM, as well as its structural effects would suggest that it is the mechanism responsible for the observed low rates of ATPase activity characterizing the SRX state. Indeed, correlations between the IHM and the SRX state have been observed (Stewart et al., 2010) as noted by Cooke in a recent review (2011); increased temperature enhances both the IHM and the SRX, substitution of GTP (guanosine triphosphate) for ATP "decreases" both, and RLC phosphorylation leads to the aforementioned conformational changes, disrupting the IHM, while it also reduces the population of SRX myosin heads. Moreover, in tarantula muscle, which exhibits an additional, very low level of ATPase activity, a well-defined model has been proposed, linking distinct structural states of the IHM to the SRX state (Alamo et al., 2016). However, as will be discussed later, recent evidence paints a more complex

picture, which requires further exploration (Caremani et al., 2019b; Nag & Trivedi, 2021).

V. Dual Filament Regulation of Contraction

Contraction has traditionally been thought to be regulated at the level of the thin actin filaments for both cardiac and skeletal muscle (Gordon et al., 2000). Thin filament regulation is described by the "Steric Blocking Model", where calcium binds to TnC, resulting in the opening of a hydrophobic cleft on its N-terminus; subsequently, the switch segment of TnI can bind to this cleft, and result in the detachment of the inhibitory segment of TnI from actin; in turn, this allows for movement of tropomyosin (Vinogradova et al., 2005; Yamada et al., 2020). This movement reveals myosin binding sites on actin, and allows actomyosin interactions to occur (Gordon et al., 2000; Geeves, 2012; Lehman, 2016). The most prominent model describing these processes, originally proposed by McKillop and Geeves (1993) and still supported (Lehman, 2017; Geeves et al., 2019), involves three states; the "blocked" state, where tropomyosin completely blocks myosin binding sites on actin, except for specific residues which allow for weak binding and are not involved in the crossbridge cycle (Lehman, 2016), the "closed" state, where calcium binding to troponin C leads to structural changes which allow the initial weak binding of myosin heads to actin, and the "open" state, where binding of myosin heads to actin leads to additional conformational changes of tropomyosin, inhibiting its return to the blocking position and fully activating the thin filament (it should be noted that as mentioned by Lehman; 2017, it has been proposed that the aforementioned terms be replaced by the terms B,C and M state). These three states do not represent static configurations of tropomyosin on actin, but instead are in constant equilibrium, with the equilibrium between states influenced by troponin, Ca^{2+} or myosin (Lehman, 2016). Thin filament activation is highly cooperative, owing to

the structural characteristics of tropomyosin and its interaction with actin and troponin (Holmes & Lehman, 2008; Lehman et al., 2020), as binding of a myosin motor can be communicated to nearby tropomyosin molecules, in turn enhancing myosin binding in an allosteric manner (Lehman, 2016). While additional sources of cooperativity exist, for example cooperative Ca^{2+} binding to the two low-affinity sites of TnC in skeletal muscle (Gordon et al., 2000), tropomyosin appears to be the most prominent, and can explain the observed Hill coefficient values (Gordon et al., 2000).

Even though the majority of research has focused on thin filament regulatory mechanisms, recent findings indicate that contraction is probably also regulated at the level of the thick filament (as pointed out and reviewed by Irving, 2017). Discussed by Linari and coworkers in their seminal 2015 work (Linari et al., 2015), the rationale for a thick filament regulation mechanism stems from studies showing that upon activation (e.g., Reconditi et al., 2011) or stretch (Reconditi et al., 2014), structural changes appear to take place in the thick filament, associated with increased length and the disruption of the axial periodicity observed in relaxation. These events precede strong myosin binding to actin and force production (Reconditi et al., 2011; Irving, 2017). As mentioned before, the interacting heads motif can act as the structural base for thick filament regulatory mechanisms, owing to its inhibiting the ATPase activity of myosin heads and their interaction with actin. The IHM has been observed in vertebrate striated muscle myosin molecules (Jung et al., 2008) and in human cardiac thick filaments (Al-Khayat et al., 2013), although up to this point only in the C-zone (Al-Khayat et al., 2013). Attempting to shed more light into the implications of this structural arrangement in skeletal muscle, Fusi and his coworkers studied demembranated fibers from rabbit psoas muscle *in situ*, utilizing fluorescence polarization after attaching bifunctional rhodamine probes on the regulatory light chain of myosin (Fusi et al.,

2015). This method allows for the detection of specific aspects of the spatial configuration of the RLC as a proxy of the orientation of the lever arm. At physiological temperatures, myosin RLC tended to adopt three orientations: two parallel to the thick filament backbone, and one perpendicular. As the authors suggest, the two parallel orientations may correspond to the "free" and "blocked" heads of the IHM, while the perpendicular heads may represent a group of constitutively ON myosin heads. This subpopulation could act to provide the initial necessary actomyosin interactions upon activation, until more myosin heads are recruited to the ON state by thick filament regulatory mechanisms. Work from the same group also demonstrated that the change in orientation of the myosin heads (i.e., turning ON of the thick filament) is a calcium-independent process, and is influenced solely by the stress imposed on the thick filament (Fusi et al., 2016). In active force production, stress would be due to the myosin motors themselves, whereas in passive stress, titin could act as the mechanosensing molecule, since it links the thick filaments to the Z-discs (Fusi et al., 2016).

A central question regarding contraction regulation is how thin and thick filaments orchestrate the response to the imposed task. Currently, the two major hypotheses involve either interfilament communication through Myosin-Binding Protein C, or mechanosensing acting in isolation from thin filament regulation, influenced only by the external load (Irving, 2017). MyBP-C is a prime candidate for interfilament communication, since it is able to bind both actin and myosin in situ (Luther et al., 2011). MyBP-C has been mostly studied in cardiac muscle (McNamara et al., 2018), where it is known to be a potential regulator of the SRX state (McNamara et al., 2016) and induce conformational changes on the thick filament through its phosphorylation (Kensler et al., 2017). Recently, Ponnam and her coworkers (2019)

have presented a detailed model of MyBP-C as a modulator of contraction through its phosphorylation at different residues, showing that it can impact both the thick and thin filaments in a complex manner, essentially acting as an "integrator of multiple signaling pathways" with a central role in contraction. Specifically, phosphorylation at different residues by Protein Kinase A (PKA), Protein Kinase Cε (PKCε) and Ribosomal S6 Kinase II (RSK2) leads to turning ON of the thick filaments, with concomitant varying effects on the activating effect of MyBP-C's N-terminus on the thin filament. The different phosphorylation sites are characterized by positive and negative regulatory coupling interactions, showcasing the versatility of MyBP-C. The authors propose a model where upon systolic activation, thin filament regulatory units opposite of the C-zone would be activated, and the initial binding of myosin heads would lead to the cooperative activation of the thick filament. While this could potentially be the answer to interfilament communication, more work is needed to better understand the complex set of interactions between thick and thin filaments and MyBP-C, as well as what the role of other modulatory mechanisms (e.g., RLC phosphorylation) would be in that model. In addition, phosphorylation sites differ between skeletal and cardiac MyBP-C paralogs (Ackermann & Kontrogianni-Konstantopoulos, 2011) and modulation of MyBP-C function by phosphorylation or other post-translational modifications in skeletal muscle has not been extensively examined.

Mechanosensing mechanisms could also explain interfilament communication (Irving, 2017). The subpopulation of constitutively ON myosin heads (Fusi et al., 2015) could act as the reserve of myosin heads necessary for low-force contractions, sensing the imposed stress in cooperation with other mechanosensing molecules like titin. Upon increased stress, additional heads would be recruited from the OFF state, essentially matching thick filament activation to the task at hand (Irving, 2017). As pointed out by

Irving (2017), evidence for mechanosensing includes the fact that thick filaments appear to be "OFF" during unloaded shortening, even at full calcium activation (Linari et al., 2015), coupled with the very low number of crossbridges necessary for unloaded shortening (Fusi et al., 2017).

Finally, as Irving (2017) suggests, interfilament communication probably involves both MyBP-C and thick filament mechanosensing, with MyBP-C modulating this process through its versatile function. However, to date, no complete model of thick filament activation or intefilament communication exists. Additionally, differences most likely exist between cardiac and skeletal muscle, owing to the distinct needs of each, and reflected in the differences between isoforms of involved molecules, like MyBP-C, as well as the functional discrepancies of the mechanosensing mechanism between the two muscle types (Park-Holohan et al., 2021).

VI. Super Relaxed State of Myosin

Only recently discovered (Stewart et al., 2010), the Super-Relaxed (SRX) state of myosin is a biochemical state of myosin heads exhibiting a very low rate of ATP turnover (>100 s, compared to <1 s in actin-bound heads and <30 s in the regular disordered relaxed state) (McNamara et al., 2014; Nag & Trivedi, 2021). Both skeletal (Stewart et al., 2010; Naber et al., 2011; Colson et al., 2015) and cardiac muscle (Hooijman et al., 2011; McNamara et al., 2016) display the SRX state, with differences between the two muscle types likely reflecting their distinct functional needs (Hooijman et al., 2011; McNamara et al., 2014). Specifically, while in skeletal muscle SRX appears to be completely abolished upon activation, cardiac muscle retains an SRX subpopulation during systolic activation (Hooijman et al., 2011, see however, Reconditi et al., 2017). In skeletal muscle, the rapid exit from the SRX state points to the existence

of potential cooperative mechanisms (Stewart et al., 2010; Moss & Fitzsimmons, 2010), addressing the need for quick activation. In contrast, the constitutively super-relaxed subpopulation in cardiac muscle may represent a reserve of myosin heads recruited only upon increased stress conditions (McNamara et al., 2014). A main question regarding the SRX state is whether it coincides with structural states of the interacting heads motif. As discussed before, the IHM appears to provide the structural configurations needed to facilitate the SRX state (Cooke, 2011). Many correlational relationships between the IHM and the SRX state have been observed (Stewart et al. 2010; Cooke, 2011), perhaps most characteristic being their positive association with temperature and their disruption by RLC phosphorylation, which is known to induce conformational changes on the thick filament (Levine et al., 1996; Kampourakis & Irving, 2015; Padron et al., 2020) presumably by weakening the IHM interactions (Irving & Craig, 2019). Given the aforementioned, it is logical to assume that the IHM could be the structural representation of the biochemically-assessed SRX state; however, diverse experimental findings have demonstrated that there is a disconnect between the two, and point towards a more complex model (reviewed in Nag & Trivedi, 2021). As a characteristic example, Caremani and his coworkers (2019b) demonstrated that low temperature can induce conformational changes in myosin heads which structurally represent the disruption of the IHM, with concomitant inhibition of actin attachment and ATPase activity, a condition which they termed the "refractory" state. Their discovery showcases an explicit disconnect between the structural IHM arrangement and the biochemical SRX state (Caremani et al., 2019b). Accordingly, it becomes apparent that additional work is necessary in order to better understand the underlying structure-function relationships, as well as how the IHM, SRX state, and thick filament regulation of contraction are integrated.

VII. Regulation of Contraction by Calcium

Both in skeletal and cardiac muscle, contraction is initiated by the influx of calcium ions from the sarcoplasmic reticulum (SR) into the cytoplasm, in response to an action potential, through the process of excitation-contraction coupling (ECC). Differences exist in certain steps of the process between the two types of muscle cells (Willegems & Efremov, 2017). This review will focus on skeletal muscle under non-pathological conditions, in accordance with the model to be utilized. A brief overview of calcium release and reuptake as well as buffering processes will be given.

Following its transmission on the plasma membrane, the action potential travels down the t-tubules, which are small invaginations of the sarcolemma; the t-tubule is positioned between terminal cisternae of the sarcoplasmic reticulum, and this junction-like formation is termed a "triad" (Shishmarev, 2020). The action potential is sensed by the $Ca_v1.1$ channels, also known as Dihydropyridine Receptors (DHPR), which interact with the Ryanodine Receptors (RyR1, the main isoform present in skeletal muscle), the calcium channels of the sarcoplasmic reticulum (Willegems & Efremov, 2017; Shishmarev, 2020), in an alternating fashion (i.e, every second RyR1 does not spatially interact with a DHPR) (Block et al., 1988), and Ca^{2+} is released in the sarcoplasm. The open probability of the RyR1 is dependent on cytoplasmic calcium concentration, decreasing at millimolar and increasing at micromolar concentrations (Chen et al. 1997), as well as a plethora of other factors which will be discussed later. In skeletal muscle, the interaction of DHPR and RyR1 involves mechanical coupling of conformational changes beginning at the DHPR, resulting in the open state of RyR1 (Willegems & Efremov, 2017). Although both DHPR and RyR1 have been characterized at near atomic resolution, their interaction has not (Rebbeck et al., 2014). Thus, only hypothetical mechanisms exist regarding their interaction, and the roles of

various residues on both proteins as well as other components in the process are currently explored through a combination of isolated protein studies and studies on intact cells from various genetically modified models (Rebbeck et al., 2014). STAC3, a junctional protein, has been found to interact with DHPR, and have essential roles in ECC (Shishmarev, 2020). It is unclear, however, whether it interacts with RyR1, and what aspects of the mechanical coupling mechanism it can explain (Shishmarev, 2020). Another protein, junctophilin, while not directly involved in the DHPR-RyR1 interaction, is necessary for calcium release to occur, through its role in maintaining the structural integrity of the junction (Shishmarev, 2020).

Calcium can also enter into the cytoplasm and the SR through other pathways. Dihydropyridine receptors, in addition to their role as voltage sensors, are also L-type Ca^{2+} channels, and upon depolarization of the t-tubule membrane, allow the entrance of t-tubule luminal Ca^{2+} into the sarcoplasm. While initially thought to play a role in calcium homeostasis, recent evidence suggests that this flux may be non-essential in skeletal muscle, both for short term contractile function, as well as overall development (Dayal et al., 2017). "Excitation-coupled calcium entry" (ECCE) describes a pathway for calcium entry upon high-frequency stimulation, which is in some, as of yet unknown manner, dependent on DHPR-RyR1 coupling (Dirksen, 2009). Although it is not clear whether ECCE is facilitated by entry through the L-type Ca^{2+} channel, the aforementioned absence of functional effects upon life-long DHPR calcium entry blockage, points towards two possibilities: either ECCE is not necessary for normal function and development (Dayal et al., 2017), or it acts through an unknown pathway, despite being functionally linked to DHPR and RyR1 (Dirksen, 2009). Another important calcium entry pathway is termed "Store-Operated Calcium Entry" (SOCE), allowing influx of Ca^{2+} from the t-tubule lumen to the SR (Dirksen, 2009). SOCE is

facilitated by ORA1, a calcium permeable channel of the plasma membrane, and STIM1 (stromal interaction molecule-1), a SR protein which acts as a Ca^{2+} sensor, forming dimers and interacting with ORA1 upon [Ca^{2+}] lowering (Protasi et al., 2020). In skeletal muscle, the STIM1L isoform forms permanent clusters with ORA1 at the junctional area, which allows for rapid initiation of SOCE (<1s) (Darbellay et al., 2011, Protasi et al., 2020). SOCE is activated with each action potential calcium release event (Koenig et al., 2018; 2019), and appears to function as a counter-flux to Ca^{2+} uptake from the t-tubular system (Koenig et al., 2018); by returning Ca^{2+} from the t-tubular lumen to the SR, it prevents the diffusion and loss of calcium outside the t-tubules (Koenig et al., 2018). SOCE activation appears to be directly dependent on localized lowering of [Ca^{2+}] near the terminal cisternae (where STIM1L is prelocalized) during RyR1 opening for its fast, phasic activation, as well as independently on total SR [Ca^{2+}] (Koenig et al., 2019). Total SR [Ca^{2+}] affects local [Ca^{2+}] near the terminal cisternae, thus indirectly influencing the extent of SOCE activation (Koenig et al., 2019). Interestingly, it has been shown that intense exercise or knockdown of calsequestrin (a calcium-buffering protein of the SR which will be discussed later), results in the formation of SR "stacks", and elongation of the t-tubules towards the longitudinal SR, forming what has been termed "Calcium Entry Units" (CEUs) (Protasi et al., 2020). While calsequestrin knockdown results in permanent formation of CEUs (Michelucci et al., 2020), these structural changes are transient following exercise (Protasi et al., 2020). These formations appear to facilitate enhanced SOCE during prolonged activity, or under conditions of reduced SR calcium content, as is the case in the absence of calsequestrin (Michelucci et al., 2020; Protasi et al., 2020).

Calcium resequestration in the SR following contraction cessation in skeletal muscle, is mainly facilitated by the Sarcoplasmic-Endoplasmic Reticulum Calcium

ATPase (SERCA) pumps, which belong to the family of P-type ATPases (Tupling, 2009). SERCA1a is the isoform found in fast skeletal muscle, while SERCA2a is predominant in slow-twitch and cardiac muscle, and SERCA2b is expressed in small amounts in all muscle cell types (Periasamy & Kalyanasundaram, 2007). Mouse muscle generally follows this pattern, but coexpression of SERCA1a and SERCA2a has been observed in type IIA fibers from both soleus and EDL (Tupling et al., 2011). The main structure of all SERCA isoforms is thought to include 3 cytoplasmic domains termed the A (actuator)-domain, P (phosphorylation)-domain and N-domain, along with 10 transmembrane helices (M1-M10) (Periasamy & Kalyanasundaram, 2007). Functionally, calcium resequestration is facilitated by the hydrolysis of ATP by SERCA, and subsequent structural changes of the cytoplasmic domains which are translated to the transmembrane helices (Møller et al., 2010). This process is characterized by autophosphorylation and dephosphorylation at Asp 351 (Møller et al., 2010). For each ATP molecule hydrolyzed, 2 Ca^{2+} are moved to the SR, while 2-3 protons are moved to the cytoplasm (Møller et al., 2010). The Ca^{2+} transport cycle is facilitated by changes between two conformational states, E1 (high affinity for calcium) and E2 (high affinity for protons), with various nucleotide intermediates (Møller et al., 2010). A brief description of the cycle, as outlined by Møller and coworkers (2010), is given below: Two cytosolic calcium ions bind to the two calcium binding sites of SERCA in the non-phosphorylated E2:ATP state, while protons are released into the cytoplasm. This leads to the Ca_2E1:ATP intermediate, with immediate subsequent autophosphorylation at Asp 315, which now results in the [Ca_2]E1~P:ADP intermediate, with Ca^{2+} occluded in the transmembrane domain. Next, ADP is exchanged with ATP and SERCA returns to the E2 state, in the form of the [Ca_2]E2P:ATP intermediate, with calcium still occluded. Subsequently, the bound

calcium ions are released in the lumen, and exchanged with 2-3 protons (H_nE2P:ATP). Those protons are then occluded in the transmembrane domain ([H_n]E2-P:ATP) and, finally, dephosphorylation occurs, with the cycle concluding at the H_nE2:ATP state.

While SERCA is responsible for returning Ca^{2+} to the SR, parvalbumin, a high-affinity calcium-binding protein, acts as a buffer and regulator of calcium kinetics in fast, but not slow mouse muscle (Schwaller et al., 1999). At rest, parvalbumin binds Mg^{2+} which, upon Ca^{2+} release from the SR, is rapidly exchanged for Ca^{2+} (Schwaller et al., 1999). Importantly, binding of Ca^{2+} to parvalbumin happens at a slower time scale than binding to troponin, thus allowing for fast thin-filament activation, and at the same time rapid buffering of cytoplasmic calcium (Schwaller et al., 1999). In turn, this facilitates the quick rate of twitch relaxation observed in fast-twitch muscle (Schwaller et al., 1999). Parvalbumin becomes increasingly saturated with extension of stimulation duration, resulting in progressive slowing of relaxation rates (Raymackers et al., 2000). Experiments utilizing parvalbumin KO mice have also demonstrated that relaxation rates were faster in wild-type mice, regardless of duration of tetanus (Raymackers et al., 2000). The authors proposed that parvalbumin could act as a shuttle, aiding in diffusion of calcium from the myofibrils to SERCA.

Mitochondria can also take up calcium following release from RyRs (Williams et al., 2013). This process is facilitated by the mitochondrial Ca^{2+} uniporter (MCU), a protein complex of the inner mitochondrial membrane, which allows influx of Ca^{2+} (Mammucari et al., 2018). In skeletal muscle, a subpopulation of mitochondria is tethered to the SR, and localized opposite of the terminal cisternae (Boncompagni et al., 2009). The low affinity of MCU for Ca^{2+} is counterbalanced by the high local calcium fluxes near the triad region, which can quickly diffuse and reach the mitochondria (Boncompagni et al., 2009). Thus, mitochondria are able to quickly take

up calcium following RyR opening (Boncompagni et al., 2009); however, the total amount and rate of Ca^{2+} influx is very low in comparison to general calcium kinetics in the cytoplasm of fast mouse skeletal muscle (Hollingworth & Baylor, 2007; Scorzeto et al., 2013; Williams et al., 2013), and unlikely to significantly impact calcium transients (Hollingworth & Baylor, 2007; Willliams et al., 2013).

Finally, Na^{2+}/Ca^{2+} (NCX) exchangers of the plasma membrane may have a minor role in calcium homeostasis. Evidence suggests that they may extrude calcium during prolonged muscular activity, when cytoplasmic [Ca^{2+}] would remain high for sufficient time for them to act, and the effects of fatigue may have hindered other mechanisms (Balnave & Allen, 1998). They may even be active during the fall phase of a tetanic Ca^{2+} transient (Calderon et al., 2014). However, their function in skeletal muscle has not been studied extensively, and current evidence is unclear on what their exact role *in vivo* may be.

VIII. Regulation and Modulation of Calcium Release

Release of calcium through the RyR1 is dependent on various mechanisms, localized at the SR, the junctional gap and the cytoplasm (Beard et al., 2008; Rebbeck et al., 2014; Willegems & Efremov, 2017; Deniss et al., 2018). These include different proteins or ligands associated with the RyR1, and post-translational modifications, namely phosphorylation and redox-related modifications (Deniss et al., 2018).

RyR activity is modulated by ATP and Mg^{2+} (Allen & Westerblad, 2008). Specifically, ATP is an agonist of RyR opening (ADP and AMP are also weaker agonists and compete with ATP for binding), while Mg^{2+} is an inhibitor (Allen & Westerblad, 2008). At resting concentrations (~1mM), Mg^{2+} acts to inhibit RyR, thus disallowing opening until mechanical coupling with the DHPR occurs (Allen &

Westerblad, 2008). Increased Mg^{2+}, reduced ATP and increased AMP and adenosine as a result of ATP hydrolysis, result in decreased Ca^{2+} release (Allen and Westerblad, 2008).

A protein with a known supporting role in RyR1 activity is FKBP12. FKBP12 is known to stabilize RyR1 function and optimize calcium release (Brillantes et al. 1994, Gaburjakova et al. 2001). It appears that it is not required for the achievement of the full conductance state, but it promotes stability once it has been achieved (Brillantes et al. 1994). In the absence of FKBP12, RyR1 displays irregular gating (Gaburjakova et al. 2001). Additionally, FKBP12 is involved in the process of coupled gating (Marx et al., 1998), facilitating the synchronized activation of release channels. Finally, FKBP12 has been proposed to be involved in the post-translational modification of RyR1 through phosphorylation by cAMP-dependent protein kinase (PKA) (Reiken et al., 2003). Specifically, phosphorylation at Ser^{2843} results in dissociation of FKBP12 from RyR1, thereby altering calcium release.

Calsequestrin, a calcium-buffering protein found in the SR, is another important regulator of calcium release in skeletal muscle (Manno et al., 2017; Rossi 2020). CSQ1, is the isoform found in fast skeletal muscle, while slow skeletal muscles express both CSQ1 and CSQ2 (Rossi, 2020). Calsequestrin buffers calcium in the SR, forming polymers localized at the terminal cisternae, which create a sort of lattice, proposed to aid in calcium movement toward the release channels (Manno et al., 2017). Its buffering capacity increases with increasing calcium levels, as polymerization creates calcium binding interfaces between monomers (Manno et al., 2017). Upon tetanic stimulation and calcium release, partial depolymerization and disturbance of the order of the lattice are observed; this results in release of Ca^{2+}, which potentially serves as the first source for release into the sarcoplasm, due to its proximal position to the release channels

(Launikonis et al. 2006; Manno et al., 2017). Calcium release from depolymerization serves to maintain SR Ca^{2+} levels during sustained stimulation, while the structural alterations in the CSQ lattice that accompany it may act as an inhibitory signal to RyR1 (Manno et al. 2017, Rossi, 2020). Inhibition of RyR1 open probability potentially happens through interactions of CSQ with Junctin (Wei et al., 2009) or Triadin (Boncompagni et al., 2012), junctional proteins which bind both to CSQ1 and RyR1. It is not yet clear, however, exactly how these proteins collectively regulate RyR1 (Rossi, 2020). It has been shown that inhibition of Triadin binding to RyR1 leads to compromised calcium release (Goonasekera et al., 2007, Wang et al., 2009). This may be due to disruptions in the structural integrity of the triad region, as exhibited in mice lacking Triadin (Oddoux et al., 2008, Boncompagni et al., 2012). Junctin's role is less clear, and findings in the literature are conflicting, proposing either a central (Wei et al., 2009) or a minor (Boncompagni et al., 2012) role in ECC coupling and QSQ-RyR1 regulation of calcium release.

In skeletal muscle, calmodulin (CaM) and S100A1 (another calcium-binding protein) appear to have a common binding domain on RyR1, and they behave in an antagonistic manner (Prosser et al., 2011). S100A1 enhances calcium release, and knockout models exhibit reduced calcium transients (Prosser et al., 2011), but no changes in resting calcium. This function of S100A1 leads to increased twitch force. Ca^{2+} free calmodulin also acts as an agonist of RyR1 activity (Prosser et al., 2011). In contrast, upon calcium release, calmodulin binds calcium and the Ca-CaM complex acts as an inhibitor of calcium release (Prosser et al., 2011). Mice with a knockout of the common S100A1 and calmodulin binding site show a steady increase in cytosolic $[Ca^{2+}]$ as a result of the impaired inactivation of calcium release, despite single calcium transients being depressed (Yamaguchi et al., 2011). Accordingly, these fibers also

present with increased force summation during high frequency stimulation (Yamaguchi et al., 2011).

Redox post-translational modifications also regulate calcium release in a complex manner. (Moore et al., 1999; Sun et al., 2001; 2003; 2011; 2013; Aracena et al., 2003; 2005; 2006) At low PO_2 (partial pressure of oxygen), S-nitrosylation of Cys-3635 and potentially other cysteines, enhances the open probability of RyR1 (Sun et al., 2003; Aracena et al. 2003; 2005; 2006), while at high PO_2, oxidation through the production of ROS by NADPH Oxidase 4 again increases calcium release, while also preventing S-nitrosylation (Sun et al., 2011). Together, those two mechanisms appear to modulate calcium release in the range of possible in vivo PO_2 (Sun et al., 2011). Additionally, calcium release appears to be indirectly modulated by S-glutathionylation, through decrease of RyR1 inhibition by Mg^{2+} (Aracena et al., 2003).

IX. Regulation and Modulation of Calcium Reuptake

SERCA function is mainly regulated by phospholamban (PLB) and sarcolipin (SLN), two transmembrane proteins, with cytosolic N-terminal domains, and, in the case of SLN, a luminal C-terminal domain, with distinct structural and functional characteristics (Shaikh et al., 2016). In mice, soleus muscles express both PLB and SLN (Tupling et al., 2011; Fajardo et al., 2013), while EDL appear to only express SLN, at lower levels than soleus (Tupling et al., 2011; Gamu et al., 2019). Unfortunately, expression in lumbrical muscles has not been explored.

Both PLB and SLN regulate SERCA calcium uptake, but through different, as of yet not completely characterized mechanisms (Shaikh et al., 2016). Briefly, PLB inhibits Ca^{2+} uptake by decreasing the affinity of SERCA for Ca^{2+}, and this inhibition is relieved by high cytosolic Ca^{2+} levels, or phosphorylation at cytosolic Ser16 and

Thr17 by PKA and Ca^{2+}/calmodulin-dependent protein kinase (Ca^{2+}/CaM kinase) respectively (MacLennan & Kranias, 2003; Shaikh et al., 2016). Two different structural mechanisms have been proposed for PLB function: either it inhibits SERCA as a monomer, with phosphorylation or high Ca^{2+} resulting in detachment from SERCA and formation of pentamers, or it remains bound to SERCA, and its inhibitory effect, or lack thereof, is mediated through conformational changes of its cytoplasmic domain, again due to the aforementioned factors (Shaikh et al., 2016). SLN decreases the V_{max} of calcium uptake, and can uncouple SERCA function from calcium transport, thus leading to futile ATP consumption and production of heat (Shaikh et al., 2016). While PLB can only bind to SERCA in the calcium-free E2 state, SLN binds to SERCA in the E2 state and can remain bound during the calcium transport cycle, and at high [Ca^{2+}], factors which can explain its ability to induce calcium slippage back into the cytoplasm (Shaikh et al., 2016).

A newly discovered micropeptide, myoregulin (MLN), exhibits structural and functional similarities with SLN and PLB, but is expressed in all types of skeletal muscle in mice (Anderson et al., 2015). Importantly, it is highly expressed in fast skeletal muscles like the quadriceps, gastrocnemius and EDL, thus providing a new aspect of calcium regulation in these phenotypes (Anderson et al., 2015). Functionally, MLN appears to reduce the rate of calcium uptake, and MLN KO mice exhibit significantly enhanced endurance performance. Additionally, peak Ca^{2+} release in the presence of an RyR agonist was markedly higher in myoblasts from MLN KO mice, compared to wild type counterparts (Anderson et al., 2015). These findings are indicative of the central role of MLN in SERCA regulation in skeletal muscle, but more details about its function and potential post-translational modification sites are currently lacking.

Another recently discovered micropeptide, dwarf open reading frame (DWORF), is expressed in mice soleus muscles, but not quadriceps (Nelson et al., 2016). DWORF acts to displace SLN, PLB and MLN, thus enhancing SERCA activity (Nelson et al., 2016). Characteristically, isolated soleus muscles from DWORF KO mice exhibited similar peak force and twitch kinetics, but impaired tetanic relaxation, in comparison to wild types (Nelson et al., 2016). These findings indicate that DWORF may have a central role in calcium reuptake regulation, and may become more important at higher stimulation frequencies (Nelson et al., 2016).

Small Ankyrin 1 (sAnk1) is a protein localized at the non-junctional SR, which has recently been shown to be able to inhibit SERCA1 activity in rabbit fast-twitch muscle (Desmond et al., 2015). Interestingly, sAnk1 also appears to interact with SLN, and in fact acts to reduce the latter's inhibitory effect on SERCA (Desmond et al., 2017). However, an exact role of sAnk1 in calcium regulation, as well as a detailed description of how it interacts with SLN or potentially other proteins is currently lacking.

X. Calcium Kinetics

Calcium release and reuptake exhibit kinetic characteristics which differ across the fiber type continuum (Calderon et al., 2010; Baylor and Hollingworth, 2012), and under different contractile conditions, and have been studied utilizing a variety of methods (Baylor & Hollingworth, 2011; Barclay, 2012). Here, focus will be given on experiments using mouse skeletal muscle tissue.

Irrespective of methodology, fast twitch mouse muscles exhibit calcium transients of larger amplitude than slow twitch muscles (~x2 or more) following a single twitch (Baylor & Hollingworth 2003; 2012; Calderon et al., 2009). Additionally, the

amount of calcium released also appears to be greater in fast fibers, when calculated based either on computational modeling (Baylor & Hollingworth, 2003; 2012), or on SERCA ATP consumption (Barclay, 2012). Although there is relatively good agreement on the aforementioned relationships, findings regarding the kinetics of the twitch transients are more controversial. Specifically, while there appears to be an agreement on the fact that slow and fast twitch fibers present with distinct transient decay temporal characteristics (with slow fibers exhibiting slower decay), transient rise rates have been shown to either be essentially the same (Baylor & Hollingworth, 2003), or faster in fast fibers (Calderon et al., 2009; 2010; 2014) (see discussion in Hollingworth et al., 2012). Calcium release rates, as calculated by computational modeling, seem to be faster in fast fibers (Baylor & Hollingworth, 2003; Hollingworth et al., 2012). However, the half-duration (time from half-rise to half-decay) of the calcium flux event is similar between muscle types, suggesting that flux rate and total calcium released is possibly dependent on the quantitative fiber-type differences in the calcium release machinery (i.e., larger RyR1 concentration in fast-twitch fibers, and other potential differences) (Baylor & Hollingworth, 2003; Hollingworth et al., 2012).

Ca^{2+} transients following short tetanic stimulation (5 shocks at 67 Hz or 350 ms simulation at 100 Hz) are also indicative of the distinct function of slow and fast phenotypes (Baylor & Hollingworth 2003; Calderon et al., 2010, 2014). In both types of muscle, the calcium transient of the second stimulus is smaller than that of the first (e.g., Baylor & Hollingworth, 2003). Subsequently, transients from slow fibers exhibit a characteristic staircase pattern, thought to arise from the inferior buffering capacity compared to fast fibers (Baylor & Hollingworth, 2003; Calderon et al., 2014). This difference is potentially due to the lower, or nonexistent concentration of parvalbumin, and the lower concentration of SERCA in slow fibers (Baylor & Hollingworth, 2003).

This results in latter twitches beginning with residual, unbuffered cytoplasmic calcium (Baylor & Hollingworth, 2003). In contrast, transients from fast fibers exhibit similar amplitudes, which demonstrates the ability of the fast phenotype to rapidly buffer calcium, allowing fast relaxation and contractile function. Relevant to this observation is the fact that cytoplasmic calcium leads to calcium-induced inactivation of calcium release, which in mouse muscles has been demonstrated using both computational simulation (Baylor & Hollingworth, 2003), and heat release measurements (Barclay, 2012). Calcium release is reduced by the second pulse (Baylor & Hollingworth, 2003; Barclay, 2012), and it is unclear whether it keeps getting lower (Baylor & Hollingworth, 2003) or remains fairly stable (Barclay, 2012). In addition, transient decay rates appear to decrease both in fast and slow fibers following the first stimulus, with the effect being much more pronounced in fast fibers. As Baylor & Hollingworth (2003) mention, the larger initial decay rates, as well as the aforementioned difference in their decrease, possibly reflect the presence of parvalbumin, the two calcium binding sites of the fast troponin isoform in comparison to the one of the slow, and the larger concentration of SERCA in fast fibers. Finally, return to baseline levels of cytoplasmic calcium is markedly slower in fast than in slow muscles (Hollingworth & Baylor, 2013), which Baylor and Hollingworth attribute to parvalbumin, due to the slow release of buffered Ca^{2+}.

2.2 Activity-Dependent Potentiation

I. What is Activity-Dependent Potentiation?

Activity-dependent potentiation is the contractile history-dependent increase in force, rate of force development, work and power, observed in fast-twitch skeletal

muscle (MacIntosh, 2010; Stull et al., 2011; Vandenboom et al., 2013; Vandenboom, 2017). Activity-dependent potentiation is typically quantified through isometric twitch responses, but it can also be seen in isometric, submaximal tetanic contractions (MacIntosh, 2010) and dynamic contractions (e.g., Xeni et al., 2011). When observed following a tetanic contraction, it is referred to as post-tetanic potentiation. The incremental increase in force during low-frequency stimulation is called staircase. Finally, *in vivo*, potentiation observed following a voluntary contraction is referred to as post-activation potentiation (MacIntosh, 2010). Activity-dependent potentiation is a well-characterized phenomenon, with a multitude of studies utilizing various stimulation and evaluation protocols; different experimental models ranging from *in vitro* motility assays (e.g., Greenberg et al., 2009) to humans *in vivo* (e.g., Baudry & Duchateau, 2004); and with strong evidence for its underlying mechanisms (e.g., Zhi et al., 2005). However, despite considerable progress, its exact role in skeletal muscle function in vivo, as well as its mechanisms at the molecular level, are still under investigation.

II. RLC Phosphorylation and Activity-Dependent Potentiation

The main mechanism of potentiation appears to be phosphorylation of the regulatory light chain of myosin (Vandenboom, 2017). In skeletal muscle, RLC phosphorylation is catalyzed by the enzyme skMLCK (skeletal myosin light chain kinase), and its dephosphorylation by MLCP (myosin light chain phosphatase) (Stull et al., 2011). The signaling cascade leading to RLC phosphorylation is, briefly, as follows: Ca^{2+} released from the SR during ECC binds to calmodulin, a cytoplasmic protein, in a 4:1 stoichiometry. In turn, the Ca^{2+}- calmodulin complex binds to the calmodulin-binding site of skMLCK, which results in conformational changes and lifting of the autoinhibition of the enzyme, binding to the RLC, and eventual phosphorylation

utilizing ATP (Stull et al., 2011). RLC phosphorylation occurs on a slower timescale than contraction; while Ca^{2+} binds to calmodulin and troponin at a similar rate, the subsequent events resulting in phosphorylation are slower than contraction regulatory processes (Stull et al., 2011). On the other hand, upon cessation of stimulation and lowering of cytoplasmic Ca^{2+} concentration, dissociation of Ca^{2+} from the skMLCK/calmodulin/Ca^{2+} complex is slow, as is the rate of dephosphorylation by MLCP; thus, RLC phosphorylation acts as a "molecular memory" mechanism, with cumulative increases in phosphate content over multiple Ca^{2+} release events, and after relaxation (Stull et al., 2011). RLC phosphorylation is quantitatively dependent on stimulation frequency (Moore & Stull, 1984).

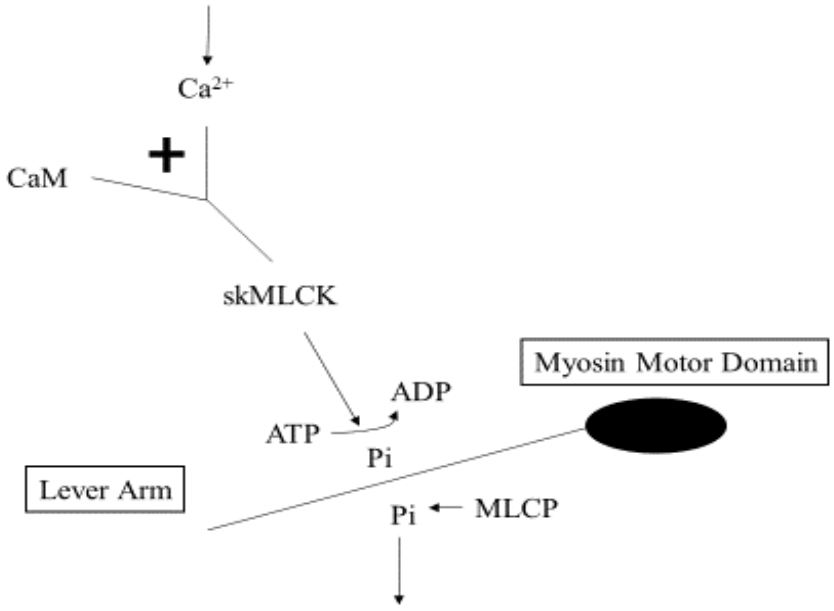

Figure 1. Overview of the biochemical signaling cascade of RLC phosphorylation - dephosphorylation. Ca^{2+} enters the cytoplasm from the sarcoplasmic reticulum and binds to calmodulin (CaM) in a 4:1 stoichiometry. Subsequently the

Ca^{2+}-CaM complex binds to skMLCK, which can then phosphorylate the RLC by hydrolyzing ATP. MLCP acts to dephosphorylate the RLC on a considerably slower timescale. Based on Stull et al., 2011.

Initially, RLC phosphorylation was proposed as a potential mechanism underlying potentiation due to the strong temporal correlations that had been observed between RLC phosphate content following a tetanus or with continuous low-frequency stimulation, and twitch force potentiation, in rat fast twitch muscle (Manning & Stull, 1979; 1982, Klug et al., 1982; Moore & Stull, 1984). Subsequent permeabilized fiber studies, the first being the work of Persechini and coworkers (1985), provided more convincing evidence for a causal link between potentiation and RLC phosphorylation; in the aforementioned paper, permeabilized rabbit psoas fibers exhibited enhanced isometric tension (50% increase) at 0.6 μM Ca^{2+}, but not 10 μM Ca^{2+}, upon addition of calmodulin and skMLCK which resulted in a robust increase in RLC phosphate content. The added control over the intracellular environment in comparison to whole-muscle studies provided more direct evidence for a causal link between RLC phosphorylation and potentiation (Persechini et al., 1985). Other studies over the following years provided similar results (Sweeney & Stull, 1986; 1990; Metzger et al., 1989; Stephenson & Stephenson, 1993; Szczesna et al., 2002). More recently, the central role of RLC phosphorylation in potentiation has been more directly validated: Zhi and coworkers (2005) utilized transgenic mice which did not express skMLCK, thus being unable to exhibit normal RLC phosphorylation function. EDL muscles from these mice did not exhibit post-tetanic potentiation, although staircase was still present but substantially reduced. These experiments directly demonstrated the causative

relationship of RLC phosphorylation and potentiation, while later works also reproduced similar findings under various conditions (e.g., Gittings et al., 2011). Interestingly, skMLCK knockout mice exhibited a basal level of RLC monophosphorylation, adjacent to the residue phosphorylated by skMLCK (Zhi et al., 2005). The authors suggested that another, activation-independent kinase, may contribute to RLC phosphorylation. Unfortunately, up until the time of this writing, this has not been further examined. The findings discussed above, provide a brief overview of current available evidence, implicating RLC phosphorylation as the main mechanism of activity-dependent potentiation. The work of Zhi and coworkers, however, points towards some important issues (discussed in Vandenboom, 2017); primarily, it becomes clear that RLC phosphorylation cannot, as an isolated mechanism, explain potentiation (this had also become apparent before and will be discussed later); secondarily, the nature of the signaling cascade and kinase responsible for basal RLC phosphorylation upon skMLCK ablation need to be investigated. As will be discussed later, the strong evidence for the existence of alternative or complementary potentiation mechanisms, the not as of yet completely characterized molecular mechanisms of RLC phosphorylation discussed in the subsequent section and the emerging findings in contraction regulation (especially thick filament-based regulation) discussed in the previous chapter, complicate the characterization of the mechanistic aspects of potentiation.

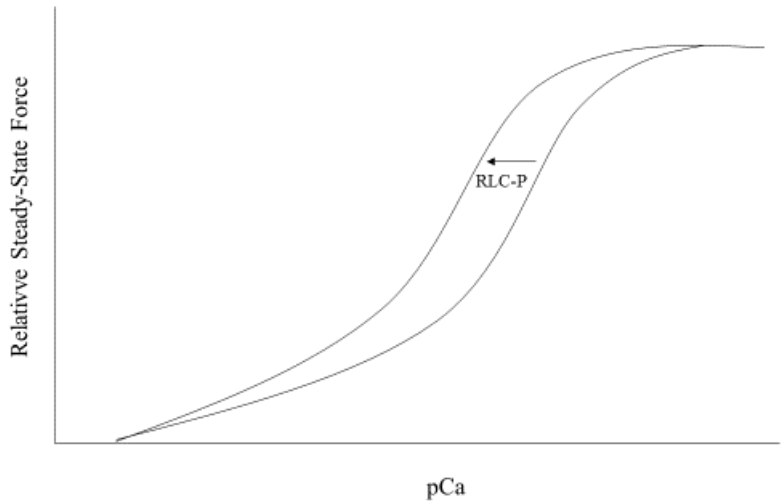

Fig. 2. Effects of RLC phosphorylation on the Ca^{2+} sensitivity of steady-state force production in permeabilized fibers. RLC phosphorylation results in a leftward shift of the force-Ca^{2+} relationship and enhances submaximal force production, but has no effects on maximal force. Based on Vandenboom, 2017.

III. Structural and Functional Implications of RLC Phosphorylation

While the findings discussed above clearly indicate that RLC phosphorylation is a central mechanism of potentiation, the molecular underpinnings of this process are not completely understood. Although significant work was carried out two decades ago (Sweeney et al., 1994; Levine et al., 1996; Levine et al., 1998; Yang et al., 1998), focus regarding the molecular mechanisms of RLC phosphorylation has shifted towards cardiac, and arthropod (mainly tarantula) skeletal muscle. In the former, RLC phosphorylation is an integral part of function and is implicated in various pathological conditions (e.g., Toepfer et al., 2013); in the latter, it is directly involved in contraction regulation through the Cooperative Phosphorylation Activation (CPA) mechanism,

discussed in the previous chapter. The well-characterized thick filament surface of tarantula thick filaments allows for a more nuanced characterization of RLC phosphorylation, as well as of the IHM discussed above (Vandenboom, 2017). Findings from both muscle types can provide useful insights into potential characteristics of RLC phosphorylation in mammalian skeletal muscle.

The work of Levine and coworkers (1996) directly demonstrated the structural effects of RLC phosphorylation in isolated rabbit psoas thick filaments, utilizing electron microscopy and optical diffraction. Incubation of thick filaments in solution containing skMLCK resulted in disruption of the organized array of myosin heads on the thick filament backbone, which was apparent in electron micrographs as well as through diffraction patterns. Parallel experiments on permeabilized fibers were carried out to confirm the correlation of disorder, RLC phosphorylation and potentiation of force response. The authors calculated the radial displacement of the myosin heads relative to the center of the thick filament backbone; in the absence of RLC phosphorylation it was approximately 13.4 nm, while upon disorder, it varied between 16.1 to 19 nm. It was hypothesized that this disorder would result in greater probability of actin-myosin interaction due to the increased proximity of myosin heads to actin (although effects of RLC phosphorylation on the nucleotide state of the active domain of myosin were also considered). Subsequent findings from the same group (Yang et al., 1998) further supported this hypothesis; the effects of RLC phosphorylation in permeabilized rabbit psoas fibers were mimicked by interventions which resulted in decreased interfilament lattice spacing, namely osmotic compression by dextran, or longer sarcomere length. RLC phosphorylation did not further enhance Ca^{2+} sensitivity under these conditions. Finally, a more recent X-ray diffraction study in permeabilized rabbit psoas fibers has recapitulated these results (Yamaguchi et al., 2016); RLC

phosphorylation was associated with structural changes indicating disruption of the helical arrangement of the myosin heads, as well as radial movement toward the thin filament. At longer sarcomere lengths, the order-to-disorder transition was still evident upon phosphorylation. However, radial movement of the heads was not detected. Recent advances using other experimental models, and findings in other areas of muscle physiology may provide some additional insights.

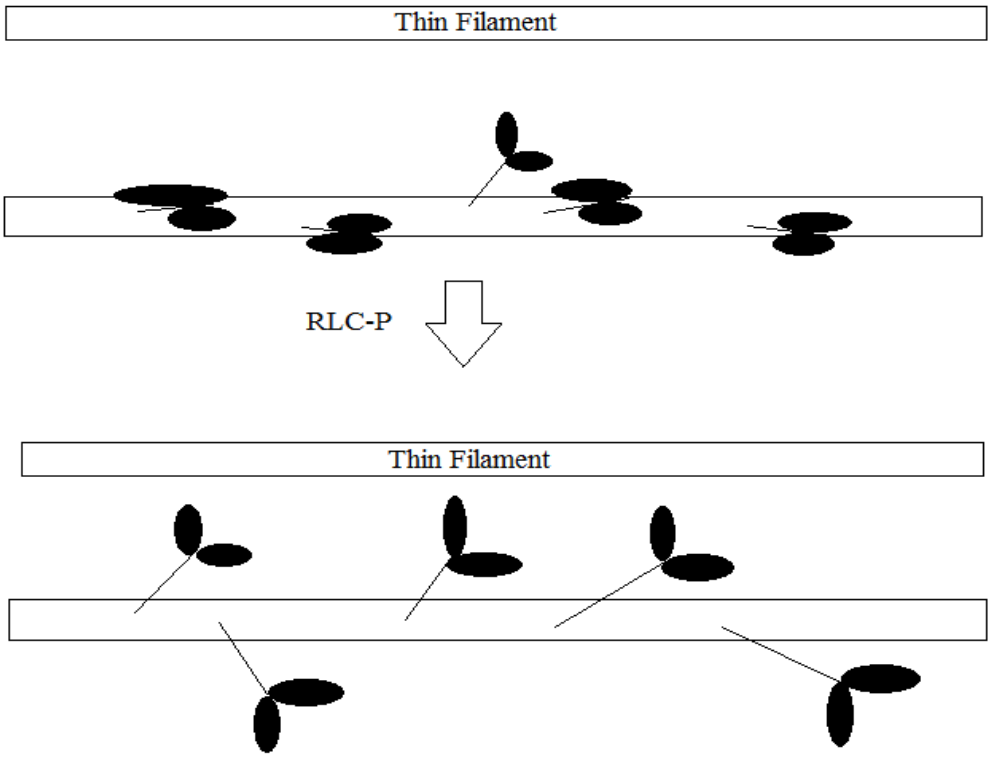

Fig. 3. Simplified representation of the structural effects of RLC phosphorylation in skeletal muscle. Top: Myosin heads are folded back on the thick filament backbone, in the IHM or other partially inhibited conformations. Note that a subset of heads is constitutively "ON". Bottom: Following RLC phosphorylation, the helical arrangement of the myosin heads on the filament backbone is disrupted, and heads are radially displaced/in disorder. Based on Sweeney et al., 1993; Fusi et al., 2016; Irving, 2017.

Research in cardiac muscle has provided unprecedented details on the structural changes following RLC phosphorylation (Kampourakis et al., 2016), as well as MyBP-C phosphorylation, and, importantly for this thesis, increased sarcomere length (i.e., length-dependent activation, which will be discussed later in more detail). While there are many differences between cardiac and skeletal muscle, which preclude immediate translation of these findings to skeletal muscle models (Martyn and Gordon, 2001; ter Keurs, 2012; Park-Holohan et al., 2021), they nevertheless lead to some questions regarding the molecular mechanisms of potentiation. In addition, most of the findings in regard to potentiation in skeletal muscle have not been examined in the context of thick-filament regulation mechanisms, which open up new possibilities for interpretation.

Perhaps most important in regard to earlier findings, recent research has showcased the fact that results from intact muscle x-ray diffraction studies and skinned-fiber and electron microscopy assays do not necessarily lead to the same conclusions (see discussion in Irving & Craig, 2019 and Caremani et al., 2019b). Conformational changes observed in skinned fibers or isolated filaments as a result of length change or MyBP-C phosphorylation were not observable in intact mouse cardiac muscle (Caremani et al., 2019). In addition, RLC phosphorylation did not significantly alter myosin head orientation under diastolic (i.e., resting but with a low calcium concentration) conditions, in permeabilized cardiac fibers treated with dextran, to restore normal dimensions, at close to physiological temperature (Park-Holohan et al., 2021); as pointed out by the authors, this was in stark contrast to previous findings where dextran was not utilized and temperature was lower than physiological (Kampourakis et al., 2016). In addition, Caremani and coworkers (2019b) demonstrated the differential response in intact mouse EDL thick filament structure and function upon

temperature lowering, in comparison to previous findings in rabbit skinned fibers (discussed in chapter 1). Permeabilization attenuates the effects of temperature on force, and does not result in the refractory state of a population of myosin heads observed in intact muscle. These realizations lead to the following conclusion: while the findings from the earlier studies discussed above provide the essence of how RLC phosphorylation potentiates contraction, the proposed model could be slightly different; instead of inducing conformational changes (which could exist but be a lot smaller in the intact filament), phosphorylation would instead solely disrupt or weaken IHM bonds, resulting in enhanced thick-filament based activation (Caremani et al., 2019; Irving & Craig, 2019; Park-Holohan et al., 2021). In essence, thick filament mechanosensing mechanisms would be more sensitive to the imposed stress stimuli (Caremani et al., 2019; Irving & Craig, 2019; Park-Holohan et al., 2021). On the other hand, the recent demonstration (Padron et al., 2020) of radial displacement of myosin heads in intact tarantula muscle at rest, following a tetanic stimulus and increased RLC phosphorylation, supports the original proposition. It is unclear which of the two observations would be present in intact mammalian muscle. Tarantula skeletal muscle does not exhibit the same thick filament structural changes (increased length and alteration of axial periodicity) observed in vertebrate muscle upon activation, probably owing to the presence of paramyosin and the consequent higher thick filament stiffness (Padron et al., 2020). As Padron and coworkers state, tarantula skeletal muscle activation probably does not depend on mechanosensing mechanisms, or at least it does to a significantly smaller extent than vertebrate skeletal muscle (Padron et al., 2020). Regardless of the actual structural changes, in both cases RLC phosphorylation would increase thick filament activation, resulting in the observed functional characteristics of potentiation.

Specific work on RLC phosphorylation in cardiac muscle has also provided interesting insights regarding its function, as well as its potential interaction with other factors in contraction regulation (Kampourakis et al., 2016; Park-Holohan et al., 2021). RLC phosphorylation appears to disrupt the IHM interactions on the thick filament (observed as a more perpendicular in respect to the thick filament average position of myosin heads in permeabilized trabeculae), with high cooperativity across myosin heads (Kampourakis et al., 2016). Interestingly, this effect of RLC phosphorylation appears to be accompanied by concomitant changes in the Ca^{2+} sensitivity of thin filament structural changes (observed by bifunctional rhodamine probes on TnC) (Kampourakis et al., 2016). Additionally, this effect is not mediated by crossbridge binding, since it appeared even in the presence of blebbistatin (Kampourakis et al., 2016). While in a more recent study, the myosin head conformational changes at rest observed by Kampourakis and coworkers were not present under more physiological conditions, as discussed above (Park-Holohan et al., 2021), RLC phosphorylation was still observed to enhance thick filament conformational changes upon Ca^{2+} activation. These findings, as well as others discussed later (e.g., Ait-Mou et al 2016), point strongly towards the possibility of an interfilament communication mechanism (discussed in the previous chapter). Corresponding work regarding interfilament communication has not been undertaken in skeletal muscle. However, the possibility of a similar mechanism facilitating potentiation at the molecular level is intriguing, especially given the discovery of thick filament mechanosensing (see Irving, 2017), and the increasingly understood function of MyBP-C (Harris, 2020; Heling et al., 2020; Song et al., 2021).

Another question that needs to be addressed in skeletal muscle, is to what extent MyBP-C phosphorylation or other post-translational modifications may influence

potentiation. While RLC phosphorylation appears to be almost exclusively responsible for post-tetanic potentiation (Zhi et al., 2005), MyBP-C phosphorylation may mediate the staircase response, reduced posttetanic potentiation observed in the absence of skMLCK activity, or have a role in the length-dependence of potentiation. It is currently unknown whether the fast isoform of MyBP-C (fMyBP-C) can be phosphorylated, or what the functional implications of its post-translational modification would be (Robinett et al., 2019). However, mouse EDL and gastrocnemius muscles express variants of the slow isoform of MyBP-C (sMyBP-C), which can be phosphorylated by PKA and PKC (Ackermann & Kontrogianni-Konstantopoulos, 2011). In mouse soleus fibers, MyBP-C phosphorylation by PKA results in increased transient force overshoot at low [Ca^{2+}] and rate of force development at all [Ca^{2+}], as well as enhanced loaded shortening. In contrast, fast twitch psoas fibers were not affected by PKA (Robinett et al., 2019). However, this does not mean that the specific variants expressed in psoas are not able to be phosphorylated by other kinases, or otherwise affect contraction and potentiation. Given its ability to interact with both thin and thick filaments, its central role in cardiac contraction regulation (Heling et al., 2020), and these early results in slow mammalian fibers, it seems possible that MyBP-C may interact with RLC phosphorylation and potentiation in fast twitch skeletal muscle. Both native thick filaments and monomeric myosin from rat EDL and soleus have been shown to be regulated by MyBP-C, in a manner similar to cardiac muscle, using motility assays (Li et al., 2019). While soleus expressed three sMyBP-C isoforms, EDL was shown to express the same three isoforms, while additionally exhibiting an isoform of fMyBP-C. Importantly, the precise modulation of thin filament calcium sensitivity and sliding velocity was dependent on both the myosin isoform (EDL- or soleus-derived) and the variant of the N-terminal fragment introduced (in each case representative of one of the

aforementioned isoforms) (Li et al., 2019). Thus, these experiments clearly demonstrated that MyBP-C can regulate contraction in skeletal muscle, in a manner similar to that observed in cardiac preparations. Additionally, this process can be finely tuned through concomitant expression of multiple isoforms in, and differential combined function with, each fiber phenotype. (Li et al., 2019). Unfortunately, more research is necessary in order to understand exactly how MyBP-C regulates contraction; until more details are available, it remains unclear exactly how these observations can be temporally incorporated in a working model of contraction. Finally, as recently shown, fast MyBP-C appears to be essential for normal contractile function in fast skeletal muscle, demonstrated by functional deficits of homozygous knockout models, in vivo, in whole EDL muscles in vitro, as well as in skinned EDL fibers (Song et al., 2021); while these observations do not necessarily implicate MyBP-C as a locus of potentiation mechanisms, they point to the need to interpret experimental findings in the context of its functions.

Finally, before discussing the mechanical aspects of contraction modulation by potentiation in the next section, it should be noted that the effects of RLC phosphorylation on contraction and crossbridge cycling kinetics. have been interpreted using the framework proposed by Brenner (1988). Briefly, crossbridge turnover between force producing and non- force producing states is described by two apparent rate constants, f_{app} (non-force generating to force generating) and g_{app} (force generating to non-force generating), which can then be extended to the following:

1) the fraction of crossbridges in force generating states $\alpha_{Fs} = f_{app}/(f_{app}+g_{app})$

2) the rate of force redevelopment $k_{redev} = f_{app}+g_{app}$

3) isometric force $F = n\,F'\,f_{app}/(f_{app}+g_{app})$

4) isometric stiffness $S = n\ S'\ f_{app}/(f_{app}+g_{app})$

5) isometric ATPase, ATPase = $(n\ b\ f_{app}\ g_{app})/(f_{app}+g_{app})$

Where n = number of turning-over crossbridges per half sarcomere, F', S' = mean force or stiffness of the crossbridge in the force-generating states, and b = number of half sarcomeres within the fiber. ATPase is calculated under the assumption of hydrolysis of one ATP molecule per cycle (Brenner, 1988).

Interpreting their findings using this framework, Sweeney and Stull (1990) showed that RLC phosphorylation increases f_{app}, without an effect on $g_{app,}$ force per crossbridge, or number of cycling crossbridges. Independent of this observation, work by Greenberg and coworkers (2009; 2010) directly demonstrated the distinct effects of RLC phosphorylation on unitary myosin. They utilized the in vitro motility assay, and found that RLC phosphorylation increases the duty cycle and step size of unitary myosin interactions with thin filaments, with a concomitant reduction in myosin velocity (Greenberg et al., 2009). In addition, RLC phosphorylation in this preparation did not increase Ca^{2+} sensitivity of interactions with either regulated or unregulated thin filaments. These findings, in combination with the demonstration of increased actomyosin affinity for ADP upon phosphorylation (Greenberg et al., 2010), indicate a kinetic role of RLC phosphorylation in the crossbridge cycle, which would be interpreted as a decrease in g_{app}. This has also been suggested by Patel and coworkers (1998) (discussed in the next section). In combination, as Greenberg and coworkers (2009; 2010) suggest, it appears that RLC phosphorylation acts both at the level of a single myosin head, and has effects that are only observable with an intact thick filament. The structural changes upon RLC phosphorylation (Levine et al., 1996) discussed above, in combination with other potential thick filament regulatory

mechanisms, and the effects on ADP affinity of unitary myosin, would result in the observed functional effects in physiological studies (Greenberg et al., 2009). In turn, consideration of these distinct mechanisms should be given when interpreting studies in whole muscle or fiber preparations, as the combined effects on f_{app} and g_{app} would influence the findings (Greenberg et al., 2010). In addition, it becomes apparent that caution should be taken when looking at findings in cardiac muscle, as the potential distinct kinetic effects of RLC phosphorylation in different myosin isoforms, as well as differences in the structural effects between muscle types, may result in different functional outcomes, especially regarding crossbridge cycling kinetics. Finally, the uncertainty surrounding the kinetic and structural details of the crossbridge cycle discussed above, and the resulting limitations regarding interpretation of functional studies, is an additional barrier towards understanding how RLC phosphorylation acts at the molecular level to influence potentiation.

IV. Modulation of Contraction by Activity-Dependent Potentiation

As discussed above, the mechanical effects of potentiation have been extensively investigated using various experimental models (see Vandenboom, 2017). Here, focus will be given to permeabilized fiber studies, and intact mouse and rat muscle studies. The functional effects of potentiation will be further discussed in the context of RLC phosphorylation and other potential mechanisms.

Both in permeabilized fibers (e.g., Persechini et al., 1985) and intact muscle (e.g., Manning & Stull, 1979), potentiation enhances isometric force production, mainly at low [Ca^{2+}] (for permeabilized fibers) and low-frequencies of stimulation (for intact muscle) (Vandenboom et al., 1993). The increase in force production is also present during repeated, incompletely fused tetani (MacIntosh & Willis, 2000) and very high

frequency, very brief contractions (MacIntosh et al., 2008). Additionally, concentric force appears to be enhanced to a greater extent than isometric (Xeni et al., 2011), and this effect is contractile speed dependent (Gittings et al., 2012); at moderate shortening speeds (0.50 V_{max} and 0.30 V_{max}), force is enhanced more than at a low speed (0.10 V_{max}), while in addition, the frequency domain over which potentiation is present appears to increase, and maximum potentiation appears at higher frequencies (Gittings et al., 2012).

In addition to its effects on force, potentiation enhances rate of force development, and this is apparent both in permeabilized fiber studies (where this aspect of contraction is assessed through the rate of force redevelopment following a slack-restretch maneuver) (Metzger et al., 1989; Sweeney and Stull, 1990) and intact muscle preparations (e.g., Vandenboom et al., 1995; MacIntosh et al., 2008). Increases in RFD are observable both in post-tetanic and staircase potentiation (Vandenboom, 2017). Importantly, in intact muscle, the effect of potentiation on rate of force development appears to be present even in tetanic contractions, where peak force is not enhanced, or is even depressed (Vandenboom et al., 1995), and at very short contractions at very high stimulation frequencies (MacIntosh et al., 2008). In contrast to force development, force relaxation is differentially modulated in twitch and tetanic contractions, as pointed out by Vandenboom (2017): twitch contractions exhibit accelerated relaxation, but this effect appears to not be related to RLC phosphorylation, as it is present in skMLCK$^{-/-}$ mice, lumbrical muscle, and soleus muscle following conditioning stimuli; tetanic contractions on the other hand display slowed relaxation, and this effect is contractile speed-dependent. A clear mechanistic explanation for these observations is currently unavailable (Vandenboom, 2017). In this regard, Patel and coworkers (1998) demonstrated that RLC phosphorylation slows the rate of relaxation from low levels of

force (~50% max and below) in permeabilized rabbit psoas fiber bundles, utilizing a photosensitive Ca^{2+} chelator, thus attempting to eliminate the effects of Ca^{2+} on relaxation kinetics. Their findings suggested that RLC phosphorylation results in slowed relaxation kinetics, an effect that they explained on the basis of an increased tendency of crossbridges to occupy strongly bound states, which would result in longer strong attachment of crossbridges after Ca^{2+} removal, and longer thin filament activation through the effect of strong attachment on tropomyosin. In addition to this, Greenberg and coworkers demonstrated that RLC phosphorylation increases the affinity of myosin for ADP (Greenberg et al., 2010); this biochemical effect was readily apparent in isolated myosin in the in vitro motility assay in the form of reduced velocity and an increased duty cycle (Greenberg et al., 2010). In combination, the aforementioned findings and others (e.g., Karatzaferi et al., 2007) demonstrate that RLC phosphorylation may conditionally affect g_{app} (fatigue vs non-fatigue, filamentous vs monomeric myosin) (Vandenboom, 2017). It becomes apparent then, that the effects of RLC phosphorylation on relaxation in permeabilized fibers or whole muscles is a complex combination of altered unitary myosin properties, sarcomere level mechanisms (the structural mechanism of RLC phosphorylation discussed above, potential interfilament communication mechanisms) as well as the other mechanisms facilitating relaxation, most prominent being SERCA pump activity. Of course, alternative mechanisms of potentiation (discussed later) may also interact with RLC phosphorylation and calcium resequestration mechanisms, thus further complicating any attempts for a mechanistic explanation of these observations.

A similar situation arises regarding the effects of potentiation on unloaded and loaded shortening velocity. For example, Roger Cooke's group has observed in a series of papers that RLC phosphorylation appears to inhibit shortening velocity of

permeabilized fibers under conditions that directly mimic fatigue (Karatzaferi et al., 2007), or utilizing phosphate analogs and blebbistatin, thus trapping myosin in pre-powerstroke states (Franks-Skiba et al., 2007; Stewart et al., 2009). Different phosphate analogs and temperature conditions resulted in differential effects of RLC phosphorylation (Franks-Skiba et al., 2007; Stewart et al., 2009). Earlier experiments at 12 ^{o} C (Sweeney & Kushmerick, 1985) and 25 ^{o} C (Persechini et al., 1985) in permeabilized fibers did not indicate any changes in maximum shortening velocity upon RLC phosphorylation, under normal conditions. In contrast to the above, Greenberg and coworkers demonstrated that RLC phosphorylated monomeric myosin in vitro exhibits decreased velocity of actin translocation in a non-fatigue-like environment, but decreased attenuation of velocity under conditions of fatigue, when compared to non-phosphorylated myosin (Greenberg et al., 2010). To add another layer of complexity, Gittings and coworkers (2011) utilized mouse EDL muscles in vitro at 25 ^{o} C, from wild type and skMLCK$^{-/-}$ mice, and tested them before, during and following a fatiguing protocol, to try and replicate the aforementioned permeabilized fiber findings in a whole muscle model. Unloaded shortening velocity as measured through a slack test (V_o), was not different between genotypes before stimulation, and, surprisingly, exhibited a similar pattern over the course of, and following the imposed protocol. As in the case of relaxation kinetics, these seemingly different findings can be reconciled when different levels of organization and other model-dependent differences are taken into account. Effects of RLC phosphorylation appear to act on two levels; modulation of single molecule properties (Greenberg et al., 2009; 2010), and structural mechanisms at the sarcomere level (Levine et al., 1996). The increased ADP affinity and increased duty cycle observed in monomeric phosphorylated myosin would coexist with thin and thick filament activation mechanisms, interfilament

communication, and the effect of RLC phosphorylation on those mechanisms (including potential cooperative effects as those observed by Kampourakis et al., [2016] in cardiac muscle). The observation that unloaded shortening can be facilitated by as little as 1-4 myosin motors per half thick filament (Fusi et al., 2017) and the possibility of RLC phosphorylation acting to sensitize thick filament mechanosensing as discussed above, could account for the absence of any effects on this parameter. Future studies are required in order to clarify exactly how RLC phosphorylation interacts with different shortening speeds at the molecular level, as well as what the role of other potentiation mechanisms is in this process.

In addition to the above, indicative of the potential functional importance of potentiation in vivo are the observations that it may act to attenuate aspects of fatigue (e.g., Gittings et al., 2011; 2017) and that it may enhance power and work production (Caterini et al., 2011; Xeni et al., 2011; Bowslaugh et al., 2016). Potentiation also increases loaded shortening speed, as indicated by increased displacement during isotonic twitch contractions, with no increase in time to maximal displacement (Grange et al., 1995). These findings, in combination with the fact that concentric force is potentiated to a greater extent and at a higher frequency range (as discussed above) than isometric force, the increased rate of force development even in tetanic contractions, the presence of potentiation in very high frequency contractions (MacIntosh et al., 2008) and the fact that potentiation appears to be greater with increasing temperature (Moore et al., 1990), collectively make a strong case for a role of potentiation in in vivo muscular function. Despite all these findings, the function of potentiation in living humans and animals remains unclear (Vandenboom, 2017). The limited knowledge regarding the interaction of potentiation with nervous system regulation of contraction,

as well as other possible upstream factors (e.g., estrogen) does not allow, up to this point, for a clear understanding to be formulated (Vandenboom et al., 2017).

V. Additional Mechanisms of Potentiation

While the central role of RLC phosphorylation in potentiation has been established through experiments with skMLCK $^{-/-}$ mice, the initial work of Zhi and coworkers (2005), as well as previous (Rassier et al., 1999b) and later (Gittings et al., 2017) findings, clearly demonstrate that potentiation involves additional mechanisms. In the experiments of Zhi and coworkers (2005), skMLCK $^{-/-}$ mice exhibited staircase potentiation, albeit attenuated in comparison to their wild-type counterparts. Even more convincingly, Gittings and coworkers (2017) demonstrated that the velocity-dependent enhancement of post-tetanic concentric twitch force was present in skMLCK $^{-/-}$ mice, again to a reduced extent in comparison to wild-types.

Despite these findings, not much focus has been given on exploring what the additional mechanisms of potentiation may be (MacIntosh, 2010; Vandenboom, 2017). Interesting work has demonstrated a redox-based mechanism involving S-glutathionylation of troponin I, which could have a role in potentiation, and appeared to be fast-fiber specific (Lamb & Posterino, 2003; Posterino et al., 2003; Mollica et al., 2012). While quantitatively able to account for RLC phosphorylation-independent potentiation, this mechanism has not been extensively explored in that context (see also Dutka et al., 2017). On the other hand, work by Smith and coworkers (Smith et al., 2013; 2014) has provided interesting insights into the potential role of Ca^{2+} related mechanisms in potentiation. They utilized mouse lumbrical muscles, which exhibit high levels of fast-twitch fiber expression (mostly IIX and not IIB, however, in contrast with the IIB dominant EDL) (Smith et al., 2013), and, concomitantly, low levels of

skMLCK, and high levels of MYPT2 (myosin phosphatase targeting subunit 2). Lumbrical muscle displays potentiation despite the absence of RLC phosphorylation, and thus provides a useful model for the study of other potentiation mechanisms.

Post-tetanic potentiation of twitch force and rate of force development in lumbricals is temporally correlated with an increased basal level of Ca^{2+}, without any apparent changes in Ca^{2+} transient kinetics, at 37 ^{o}C (Smith et al., 2013). In addition, at 37 ^{o}C (but not 30 ^{o}C), staircase potentiation of force and rate of force development is exhibited, and is again correlated with elevated basal Ca^{2+}, but changes are also evident in the Ca^{2+} transient; at 37 ^{o}C, the amplitude of the calcium transient appears to steadily decrease, concomitantly with the increase in basal Ca^{2+} (Smith et al., 2014). Interestingly, as noted by the authors, while twitch relaxation was enhanced for the first 2 s of stimulation, transient decay was slowed, and both factors were further slowed after the 2 s mark, showing a disconnect between Ca^{2+} removal and relaxation (Smith et al., 2014). At 30 ^{o}C, twitch force exhibited depression instead of potentiation, but the rate of force development was enhanced. Therefore, it appears that the elevation of basal Ca^{2+} following a tetanic stimulus or during low-frequency stimulation is temporally correlated with enhanced rate of force development at both temperatures, and twitch force at 37 ^{0}C only, at least for the stimulation protocols utilized (Smith et al., 2013; 2014). Additionally, during staircase, prolongation of the Ca^{2+} transient may also have a role in the observed outcomes (Smith et al., 2014). It is currently unclear, however, whether these alterations in Ca^{2+} kinetics are causative of the observed potentiation, or simply temporally coincident. The main potential mechanism that the authors proposed is that the increased basal Ca^{2+} may act to saturate parvalbumin buffering capacity (they detected parvalbumin in lumbricals), thus allowing for enhanced troponin Ca^{2+} binding, and explaining the increased Ca^{2+} sensitivity (Smith

et al., 2013; 2014). The mechanism responsible for the prolongation of the transient during staircase but not following tetanic stimulation is unclear (Smith et al., 2014).

It becomes apparent from the aforementioned findings, that the additional mechanisms of potentiation are not well understood. Despite the promising findings regarding redox-related mechanisms, and the strong temporal correlations observed in the works of Smith and coworkers, no clear causative relationships have been observed. In addition, potential muscle type differences (e.g., EDL vs lumbrical), as well as the vast number of factors concurrently regulating and modulating contraction, make it extremely difficult to understand exactly which mechanism, or mechanisms, and to what extent, complement RLC phosphorylation. Despite this lack of clarity, the lumbrical muscle as an experimental model can aid in further exploring certain aspects of potentiation due to its lack of RLC phosphorylation, and complement experiments in skMLCK $^{-/-}$ mice. One such example is the length-dependence of potentiation, which is the subject of this thesis and will be discussed in the next chapter.

2.3 Length-Dependence of Activity-Dependent Potentiation

I. Brief Background

Up to this point, the basic mechanisms of contraction and activity-dependent potentiation have been discussed. However, in vivo, muscle function is also affected by a variety of factors, including and not limited to; temperature (e.g., Caremani et al., 2019b), sarcomere or muscle length (de Tombe et al., 2010; MacIntosh, 2017), interconnection with elastic or viscoelastic components, whether in series or parallel (e.g., MacIntosh & MacNaughton, 2005; de Tombe & ter Keurs, 2016) etc. All these

factors influence contraction outcomes, and have been studied extensively using various experimental models. Such a relationship is observed regarding activity-dependent potentiation, with potentiation magnitude being inversely related to musculotendinous unit, or sarcomere, length (e.g., Rassier & MacIntosh, 2002). This is not an exclusive attribute of potentiation; contraction in general is characterized by the force-length relationship and the phenomenon of length-dependent activation (LDA) (Rassier et al., 1999; de Tombe et al., 2010; Campbell, 2011; MacIntosh, 2017). The force-length relationship refers to the influence of muscle or sarcomere length on maximal force production, whereas length-dependent activation refers to the fact that maximal twitch, or otherwise submaximal force, is observed at longer muscle or sarcomere lengths than maximal tetanic force (Rassier et al., 1999; MacIntosh & MacNaughton, 2005), at least in skeletal muscle. Cardiac muscle operates on the ascending part of the force-length relationship (de Tombe & ter Keurs, 2016), so LDA is typically observed at sarcomere length ranges where maximal force is also increasing (Martyn & Gordon, 2001). While cardiac and skeletal muscle exhibit multiple differences in their contractile protein isoforms (Gordon et al., 2000) as well as their function (e.g., Park-Holohan et al., 2021), research regarding LDA has almost exclusively focused on cardiac muscle, since it is the cellular facilitator of the Frank-Starling mechanism, a central aspect of cardiac function (reviewed by de Tombe et al., 2010; Campbell, 2011). Consequently, the following sections will include multiple findings from cardiac muscle. Despite the fact that the mechanisms of LDA in cardiac muscle may not directly correspond to skeletal muscle, they nevertheless provide interesting perspectives and facilitate rethinking and discussion of past interpretations of findings from skeletal muscle experiments. In the case of the length-dependence of potentiation, an examination of the molecular mechanisms of LDA (and of course other

areas where substantial progress has been made, notably thick filament regulation and MyBP-C function) is of high importance, since the majority of research on the topic was carried out approximately two decades ago, and interpreted based on contemporary views of length-dependent sarcomere function. Most notably, the length-dependence of potentiation has been attributed to the structural effects of RLC phosphorylation, as well as the effect of decreased interfilament lattice spacing on Ca^{2+} sensitivity (e.g., Yang et al., 1998); both of these areas have seen considerable progress over the past two decades (e.g., de Tombe et al., 2010; Reconditi et al., 2014; Ait-Mou et al., 2016; Li et al., 2016; Yamaguchi et al., 2016; Caremani et al., 2019; Irving & Craig, 2019; Padron et al., 2020), while it has additionally become increasingly apparent that potentiation involves additional mechanisms (Zhi et al., 2005; Smith et al., 2013; 2014). In the following sections, the influence of muscle/sarcomere length on contraction will be discussed, followed by research regarding the length-dependence of potentiation.

II. Length-Dependence of Contraction

The length dependence of contraction has been extensively researched both in skeletal (Rassier et al., 1999; MacIntosh, 2017) and cardiac (de Tombe et al., 2010) muscle. At a quantitative level, the force-length relationship and LDA have been well characterized in a variety of models, ranging from sarcomeres to whole muscles (Rassier et al., 1999; Rassier, 2017). In skeletal muscle, the force-length relationship is characterized by a plateau of maximal force production, which is thought to correspond to optimal filament overlap and maximum capacity of actin-myosin interactions (Rassier et al., 1999). On the left of the plateau, the ascending part of the relationship represents shorter sarcomere lengths, where various factors (spatial constraints on the filaments, resisting internal forces) may hinder force production (see discussion in Rassier et al., 1999). To the right of the plateau, the descending part of the relationship

represents reduced filament overlap with increasing sarcomere lengths (Rassier et al., 1999).

LDA, as mentioned previously, likely differs between skeletal and cardiac muscle (e.g., Martyn & Gordon, 2001). In skeletal muscle, at longer sarcomere lengths, submaximal contractions appear to be enhanced, but maximal activation is not affected; this generally becomes apparent as a shift to the left of the force-pCa relationship (Rassier et al., 1999). Essentially, at longer sarcomere lengths, despite the decrease in filament overlap and the consequent reduced maximal force, the increased force response for a given level of submaximal intracellular Ca^{2+} (i.e., calcium sensitivity) allows for higher submaximal forces to be achieved. Conceptually, calcium sensitivity becomes less important at higher Ca^{2+} concentrations, since both the thin and thick filaments would be maximally activated, therefore making the number of possible actomyosin interactions (determined mainly by thin-thick filament overlap) the limiting factor for force production. This has been observed in both steady state force measurements in permeabilized fiber preparations (e.g., Martyn and Gordon, 2001), as well as whole muscle contractility experiments (where submaximal Ca^{2+} corresponds to low stimulation frequencies) (e.g., Rassier and MacIntosh, 2002b). On the other hand, in cardiac muscle, the enhanced Ca^{2+} sensitivity is typically observed across lengths where maximal force production is also increasing (e.g., Martyn & Gordon, 2001). This is related to the fact that cardiac muscle normally operates on the ascending part of the force-length relationship (de Tombe & ter Keurs, 2016); functional sarcomere length ranges are typically ~1.5 μm to ~2.3 μm for cardiac (ter Keurs, 2012), and ~1.8 μm to ~3.6 μm (Rassier et al., 1999) for skeletal muscle, with slight differences depending on the species and muscle type. Interestingly, this narrower range of sarcomere lengths does not allow for passive force (at the level of the sarcomere, not

higher levels of organization where extrasarcomeric passive elements contribute) to develop to the point where activation of the thick filament becomes possible (Park-Holohan et al., 2021), in contrast to what has been observed in skeletal muscle (Fusi et al., 2016). A relevant finding is that while both cardiac (Reconditi et al., 2017) and skeletal (Linari et al., 2015) muscle exhibit the mechanosensing thick filament activation mechanism, there appear to be important functional differences between them. Specifically, in cardiac muscle, while the response of the thick filament to passive stress appears to be similar to that observed in skeletal muscle (while in turn skeletal muscle exhibits a relatively similar response to both passive and active filament stress) (Fusi et al., 2016), active tension generation appears to activate the thick filament with an approximately 8-fold greater sensitivity (Park-Holohan et al., 2021). These discrepancies, along with the different isoforms of contractile proteins (most notably troponin I and MyBP-C) (Gordon et al., 2000; Heling et al., 2020) may explain the differences in LDA observed between cardiac and skeletal muscle.

A major experimental issue regarding the length-dependence of contraction is the potential influence of compliance (whether due to the tissue itself, or the experimental apparatus), as well as sarcomere inhomogeneities, in the measured active force, and on the interpretation of results. Any form of in series compliance would result in sarcomeres shortening (along with existing potential sarcomere inhomogeneities) across the muscle or fiber examined, despite the length of the preparation remaining seemingly unchanged. In turn, this would lead to a change of passive force at the peak of force production, relative to the one observed at rest, at the same preparation length. This can lead to misinterpretation of active force, since active force is derived by subtracting passive force from the total observed force. In addition, other factors like crossbridge cycling kinetics measurements may be influenced (Pavlov & Landesberg,

2016). This issue has been separately pointed out regarding skeletal (Rassier et al., 1999, MacIntosh & MacNaughton, 2005; MacIntosh, 2017) and cardiac (de Tombe & ter Keurs, 2016) muscle, and is readily countered through sarcomere length tracking (de Tombe & ter Keurs, 2016) or may be partially attenuated by using an approximation of passive force at the fascicle length attained at the peak of the measured contraction, instead of the one measured prior to its beginning (as described in MacIntosh & MacNaughton, 2005), in skeletal muscle. As pointed out by MacIntosh (2017), experiments addressing force at long muscle lengths in skeletal muscle, where passive force would be substantial, are prone to this kind of experimental error, but he suggests that experiments with minimal tendon may still be fairly accurate. De Tombe and ter Keurs (2016) on the other hand, consider sarcomere length tracking essential in order to study cardiac mechanics, as in cardiac preparations, the in-series compliance would be due to damaged cardiomyocytes (which could be in various contractile states) and not exclusively connective tissue, thus exhibiting unpredictable passive behaviors. It becomes obvious from the above that care should be taken when interpreting findings regarding the length dependence of contraction and potentiation.

In addition to intra-contraction changes in passive force, another complication arises when working with skeletal muscle preparations which allow significant internal shortening (MacIntosh, 2017; Holt & Williams, 2018); since sarcomeres actively shorten against resistance before isometrically producing force, shortening-induced force depression may alter force production in comparison to a purely isometric contraction, and potentially influence optimal length (Holt & Williams, 2018). Briefly, shortening-induced force depression refers to the decrease in steady-state isometric force observed following loaded shortening, in comparison to the force produced at the same final length without prior shortening (Joumaa et al., 2012). Force depression is

positively related to increased shortening amplitude, force for a given constant speed, and decreasing speed (Rassier & Herzog, 2004). The mechanism responsible for shortening-induced force depression is thought to be related to deformations of the thin filament during active shortening, which affect subsequent crossbridge binding at the final sarcomere length, in an as of yet unknown manner (Pun et al., 2010; Joumaa & Herzog, 2010; Joumaa et al., 2012; Joumaa et al., 2018). Sarcomere or half-sarcomere inhomogeneities may also play a role at the whole muscle level, but since isolated myofibrils present with depression that cannot be explained by variations in sarcomere length (Pun et al. 2010; Joumaa & Herzog, 2010), the aforementioned thin filament mechanism appears to form the basis of the phenomenon (Joumaa & Herzog, 2010). Through this mechanism, a part of the shift of optimal length towards longer lengths at lower forces may be explained (Holt & Williams, 2018), acting concurrently with the mechanisms of LDA at the sarcomere level. Although a recent study (MacDougall, Kristensen & MacIntosh, 2020) failed to recapitulate the hypothesis of Holt & Williams (2018), the potential role of shortening-induced force depression, as well as the change in passive force when internal shortening is allowed, as discussed above, must be taken into account when interpreting length-dependent force findings, as is the case for this thesis. Nevertheless, the exact methodological and interpretative implications of these observations are currently unclear (MacDougall et al., 2020),

III. Molecular Mechanisms of Length-Dependent Activation

As mentioned earlier, the majority of mechanistic LDA research has been undertaken in cardiac preparations. Thus, in the following section, the molecular mechanisms of LDA in cardiac muscle will be discussed, while simultaneously discussing similar findings in skeletal muscle where available, or addressing potential knowledge gaps. The rationale for discussing cardiac findings is not to directly correlate

them to skeletal muscle, but instead provide an overview of emerging concepts in LDA which may be transferable to varying degrees to skeletal muscle, and facilitate discussion.

Historically, researchers have focused on three prominent potential mechanisms for LDA (reviewed by de Tombe et al., 2010; Campbell 2011): i) reduction of myofilament lattice spacing at longer muscle lengths, facilitating actin-myosin interactions through proximity of thin and thick filaments ii) effects of muscle length on thin filament function, namely enhanced Ca^{2+} activation/cooperativity of activation and iii) potential effects on thick filament activation. Furthermore, specific sarcomere proteins appear to be necessary for LDA, as has become apparent from various studies utilizing transgenic animals or recombinant protein models. Primarily, titin seems to have a central role, as a transgenic rat model expressing a more compliant titin isoform displays severely attenuated LDA in both cardiac (e.g., Ait-Mou et al., 2016) and skeletal (Mateja et al., 2013) muscle. MyBP-C ablation/expression, as well as phosphorylation, has been shown to modulate LDA in cardiac muscle (Mamidi, Gresham & Stelzer, 2014; 2016; Hanft et al., 2021), but, unfortunately, similar data are lacking in skeletal muscle. Given its probable role in interfilament communication in both muscle types (Reconditi et al., 2014; Irving, 2017; Brunello et al., 2020; Solis & Solaro, 2021), the paucity of data regarding MyBP-C in skeletal muscle is a major limitation in interpreting length-dependent contractile characteristics in that muscle type. Thus far, only preliminary structural data exist in support of a potential MyBP-C interfilament communication mechanism (Luther et al., 2011; Reconditi et al., 2014), which may have length-dependent characteristics, owing to MyBP-C's exclusive localization to the C-zone (Reconditi et al., 2014). Troponin also appears to be important for LDA, but again, data are only available for cardiac muscle. It has been

demonstrated that troponin undergoes conformational changes during stretch, which appear to be unrelated to the ones during Ca^{2+} activation, and are attenuated in compliant titin models, concomitant with the reduction of LDA (Ait-Mou et al., 2016; Zhang et al., 2017) (c.f. Caremani et al., 2019). Additionally, threonine 144 of the inhibitory domain of cardiac TnI (cTnI) appears to be an integral part of the LDA signaling mechanism (Tachampa et al., 2007), as discussed by de Tombe and coworkers (2010); slow skeletal TnI (ssTnI) differs in its inhibitory domain only in regard to the aforementioned residue (Tachampa et al., 2007), and slow skeletal muscle additionally exhibits attenuated LDA in comparison to cardiac muscle (Konhilas et al., 2002; Tachampa et al., 2007). Exchange of native cTnI with recombinant ssTnI in permeabilized cardiac preparations is sufficient to induce LDA characteristics similar to those of slow skeletal muscle (Tachampa et al., 2007). Even more convincingly, preparations in which recombinant TnIs with single-residue substitutions (proline 121 to threonine for ssTnI, threonine 144 to proline for cTnI) were introduced, displayed LDA characteristics corresponding to each respective residue (Tachampa et al., 2007). Finally, TnI can be phosphorylated in cardiac muscle, and its phosphorylation modulates LDA (e.g., Kumar et al., 2015). Data regarding the role of troponin in skeletal muscle LDA are sparse. Findings from an early study indicated that LDA in permeabilized skeletal fibers does not depend on changes in the Ca^{2+} sensitivity of Ca^{2+}-induced conformational changes of TnC, in contrast to cardiac fibers (Martyn & Gordon, 2001). In addition, while the length-dependent changes in the Ca^{2+} sensitivity of TnC conformational changes were dependent on strong crossbridge binding in the cardiac preparations, as has also been recently demonstrated using more sensitive methods (Li et al., 2019), skeletal fibers exhibited a complete absence of an effect of strong-binding crossbridges in TnC structure, independent of length or activation level

(Martyn & Gordon, 2001). Given these findings, and the numerous differences between skeletal and cardiac troponin isoforms (Gordon et al., 2000), it is currently unknown whether troponin could have a role in LDA in skeletal muscle.

Regarding the lattice spacing hypothesis, while initially being the prominent theory, evidence has accumulated questioning its central role both in cardiac (see discussion in de Tombe, 2010; Ait-Mou. 2016), as well as skeletal muscle (Li et al., 2016). As discussed by de Tombe and coworkers in their review (de Tombe et al., 2010), they managed to directly demonstrate a disconnect between interfilament lattice spacing and length-dependent activation. Initially, they showed that changes in interfilament lattice spacing are not proportionately related to fiber diameter, under various conditions of osmotic compression with dextran, utilizing direct measurements of lattice spacing through x-ray diffraction (Konhilas, Irving & de Tombe, 2002b); fiber diameter has been traditionally used as a proxy for lattice spacing in experiments where dextran was utilized to osmotically compress permeabilized fiber preparations in an attempt to simulate lattice spacing at longer lengths (de Tombe et al., 2010). In contrast to those findings, in skeletal muscle, the relationship between fiber diameter and lattice spacing appears to be linear upon dextran compression, at least for rabbit psoas fibers (Kawai, Wray & Zhao, 1993). Subsequently, they found that when dextran compression is graded to accurately mimic interfilament lattice spacing changes between lengths, again directly assessed through x-ray diffraction, length-dependent Ca^{2+} sensitivity changes are not recapitulated; namely, the increase in Ca^{2+} sensitivity is directly related to greater sarcomere length, and not necessarily the concomitant reduction in interfilament lattice spacing (Konhilas et al., 2002b). In addition to the above, they carried out experiments using rat cardiac, fast and slow skeletal muscle, and demonstrated that despite their different LDA responses (as assessed by the difference

in [Ca^{2+}] required for half-maximal activation between a short and a long sarcomere length), the slopes of their interfilament lattice spacing-sarcomere length relationships were not significantly different (Konhilas et al., 2002). Finally, in a more recent work, they utilized x-ray diffraction and studied myocardium from wildtype rats, as well as a transgenic rat model displaying a compliant titin isoform (Ait-Mou et al., 2016). In those experiments, the relationship between sarcomere length and interfilament lattice spacing was quantitatively similar between the two muscle types, despite the marked difference in length-dependent contractile characteristics. In skeletal muscle, recent work has also questioned whether lattice spacing per se can completely explain LDA. Tibialis anterior fiber bundles from the same rat transgenic model mentioned above, expressing a more compliant titin isoform, were studied, and their length-dependent contractile characteristics were compared to those of respective bundles from wild-type rats (Mateja, Greaser & de Tombe, 2013). The length-dependent increase in calcium sensitivity and maximal force production observed in wild-type skinned fiber bundles was significantly attenuated by transgenic titin expression (sarcomere length change 2,8 μm to 3,2 μm), indicating that in the same manner as in cardiac muscle, titin-mediated passive force signaling has a central role in LDA. It should be noted that those experiments were carried out at 20 ºC, in the absence of osmotic compression. These conditions are known to induce structural changes of the thick filaments of mammalian skinned fibers, which correspond to partial activation at rest (Caremani et al., 2021). The implications for the above findings are currently unknown. In another recent study, Li and coworkers investigated whether differences in titin stiffness between isoforms are related to proportional changes in the lattice spacing-sarcomere length relationship (Li, Lang & Linke, 2016). Specifically, they compared myofibrils of rabbit psoas (stiff titin isoform) and diaphragm (compliant titin isoform) muscles,

and examined their sarcomere strain-lattice spacing relationships, under normal conditions, as well as under osmotic compression using 5% dextran. Surprisingly, despite the marked difference in titin stiffness between their respective isoforms, both types of myofibrils exhibited similar relationships, especially under osmotic compression. With 5% dextran, there was no significant difference in the slope describing the two regressions. In stark contrast, A-band lateral stiffness, as assessed by atomic force microscopy, appeared to be directly related to the titin isoform. Both with and without dextran, A-band stiffness exhibited a more pronounced dependence on strain in psoas fibers. In combination with the work of Mateja and coworkers, these findings indicate that LDA in skeletal muscle is mediated through titin passive tension, and this effect may involve strain induced interactions in the A-band, instead of solely differential reduction of lattice spacing (Li et al., 2016). As will be discussed later, this increased A-band stiffness is potentially indicative (Li et al., 2016) of the molecular mechanisms underpinning LDA, which may include conformational changes of both the thin and thick filaments (e.g., Ait-Mou et al., 2016), as well as changes in interactions between both filaments and MyBP-C (Reconditi et al., 2014). However, further work is required in skeletal muscle, specifically comparing strain-lattice spacing and strain-A band stiffness relationships utilizing the same muscle type, and comparing between wildtype and either transgenic models, or models where titin stiffness is changed in vivo or in situ by different means. In total, as becomes apparent from the above, the role of interfilament lattice spacing in mediating LDA is controversial. While it probably cannot explain the main mechanisms, however, its role should not be underestimated, especially considering its potential effects on spatially-determined parameters of the myosin-actin interaction (discussed in Campbell, 2011; Williams et al., 2013). Among others, these include effects of lattice spacing on unitary force

production itself, as well as potential thin filament deformation-related mechanisms of cooperative activation (Campbell et al., 2011).

The utilization of transgenic models with giant titin isoforms (e.g., Mateja et al., 2013; Ait-Mou et al., 2016), in combination with the realization that striated muscle contraction is regulated at the level of the thick filament (Linari et al., 2015; Reconditi et al., 2017) have provided new insights into LDA. As mentioned above, it is becoming increasingly apparent that titin-based passive stiffness may mediate the signaling cascade of LDA (Ait-Mou et al., 2016). Using x-ray diffraction, Ait-Mou and coworkers (2016) found that intact wild-type rat myocardium in diastole exhibited conformational changes of troponin, which were different than those observed during activation. They confirmed this observation utilizing fluorescent probe measurements in permeabilized cardiomyocytes with recombinant fluorescent troponin C in the presence of 2,3 butanedione monoxime, to block actin-myosin interactions. In that preparation, it was also apparent that the Ca^{2+} sensitivity of troponin fluorescence changes during activation (which indicate binding of Ca^{2+} to troponin and thin filament activation) was not influenced by sarcomere length, as was also the case with the Hill coefficient. In addition to thin filament structural changes, they also observed thick filament conformational changes, which were, however, not related to increased activation. In fact, myosin heads were interpreted to be radially closer to the thick filament backbone upon stretch (Ait-Mou et al., 2016). All the above changes were absent in myocardium from transgenic rats expressing compliant titin, concomitantly with severely attenuated LDA (Ait-Mou et al., 2016). Zhang and coworkers (2017) reached similar conclusions through fluorescence polarization measurements of troponin C and myosin RLC structural changes in permeabilized trabeculae. Specifically, they demonstrated that troponin C undergoes structural changes during

stretch that do not correspond to Ca^{2+} activation. In addition, the magnitude of change in troponin fluorescence during activation (which, as mentioned above, corresponds to binding of Ca^{2+} to troponin and thin filament activation) was independent of length, but the Ca^{2+} sensitivity of those changes was increased in proportion to the increases in Ca^{2+} sensitivity of force production. These observations were independent of strongly-bound myosin heads, since they were similar in the presence of blebbistatin. The authors interpreted these findings as indicating that increases in calcium sensitivity with LDA are related to conformational changes of troponin, but maximal force production increase in not, since thin filament activation (assessed through total change in fluorescence during maximum activation) appears to be maximal at both, and does not differ between, short and long lengths. On the other hand, fluorescence measurements using bifunctional rhodamine probes on the RLC, indicated that fluorescence increases during Ca^{2+} activation, and that this effect is enhanced at long sarcomere lengths, concomitantly with the increase in maximal force. In total, their findings indicated that LDA is a combination of structural thin filament changes leading to enhanced calcium sensitivity, while in turn the increased force can be attributed to enhanced thick filament mechanosensing activation mediated by stretch (Zhang et al., 2017). As the authors noted, structural studies of troponin using other techniques and detecting movements of other parts of the molecule may provide additional insights (Zhang et al., 2017), and indeed, it has been shown using FRET (Förster Resonance Energy Transfer) that strong myosin binding-dependent effects on troponin, modulated by sarcomere length, are also related to LDA and mediated by titin (Li et al., 2019). Nevertheless, the exact role of cycling crossbridges in thin filament regulation in cardiac muscle is unclear (Solis & Solaro, 2021). These findings provided a useful framework for understanding LDA, which was also supported by computational modeling (Campbell, Jannsen & Campbell,

2018). However, as discussed in the previous chapter, it became apparent that findings from permeabilized fiber or isolated filament preparations do not necessarily correspond to the native filament lattice of intact muscle, due to the effect of the permeabilization or isolation process to weaken the inter- and intramolecular interactions characterizing the filaments (Caremani et al., 2019; Irving & Craig, 2019; Caremani et al., 2021). This is true both for skeletal (Caremani et al., 2021) and cardiac muscle experiments (Caremani et al., 2019). Specifically, Caremani and coworkers (2019) showed that both increased length, as well as PKA-mediated phosphorylation of MyBP-C and TnI, did not result in conformational changes of the thick filament corresponding to activation, during diastole, as indicated by the meridional and layer line reflections characterizing the thick filament (see also Reconditi et al., 2017). Brunello and coworkers (2020) reached the same conclusion regarding length increase, again using x-ray diffraction of intact trabeculae. As discussed by Caremani and coworkers, as well as Irving and Craig (2019), this was an unexpected finding, considering the effect of MyBP-C phosphorylation to radially displace the myosin heads as shown through x-ray diffraction of permeabilized cardiac preparations (Colson et al., 2012), as well as through electron microscopy of isolated cardiac thick filaments (Kensler et al., 2017). Similar findings were recently reported by Park-Holohan and coworkers (2021), who used permeabilized cardiac preparations, but under more physiological conditions (higher temperature and dextran compression). In their experiments, both passive thick filament stress through stretch, as well as RLC phosphorylation, did not significantly activate the thick filament under diastolic conditions, in contrast to previous findings under less physiological temperature and lattice spacing (Kampourakis et al., 2016). During submaximal activation, however, both interventions enhanced thick filament activation and calcium sensitivity.

Importantly, they demonstrated that in contrast to skeletal muscle (Fusi et al., 2016), stretch through the functional sarcomere range of cardiac muscle is not sufficient to induce thick filament activation. Collectively, all the aforementioned findings suggest that cardiac LDA is facilitated by a complex signaling cascade, involving both filaments, which appears to function downstream of Ca^{2+} thin filament activation (Reconditi et al., 2017; Caremani et al., 2019; Irving & Craig, 2019; Brunello et al., 2020; Park-Holohan et al., 2021). While it is still debated whether stretch-induced structural changes of the thick filament at rest mediate increased thick filament activation upon Ca^{2+} activation of the thin filament, (Irving & Craig, 2019; Caremani et al., 2019), it seems fairly certain that they would not be related to the ones observed upon thick filament activation (Reconditi et al,, 2017; Caremani et al., 2019; Park-Holohan et al., 2021), but may, however, weaken some of the numerous interactions regulating the filament off state (Irving & Craig, 2019). The actual signaling mechanism following length change remains to be elucidated, but current consensus suggests that it probably involves interfilament signaling through MyBP-C, in an as of yet unspecified manner (Caremani et al., 2019; Irving & Craig, 2019; Brunello et al., 2020; Park-Holohan et al., 2021). In that scenario, MyBP-C interactions with the thin filament (Inchingolo et al., 2019) would be enhanced by increased sarcomere length, and this could explain the increased calcium sensitivity. In turn this effect would be modulated by numerous post-translational modifications of MyBP-C, troponin, and other sarcomeric components (Ponnam et al., 2019; Solis & Solaro, 2021). The realization of the central role of MyBP-C in cardiac contraction regulation (Ponnam et al., 2019; Brunello et al., 2020; Solis & Solaro, 2021) makes the elucidation of this signaling complex necessary in order to understand LDA. Finally, it should be mentioned that as most researchers conclude (de Tombe et al, 2010; Campbell, 2011;

Sequeira & Van den Velden, 2017; Park-Holohan et al., 2021), LDA probably involves numerous mechanisms (including interactions of titin with the thin filament, structural mechanisms related to interfilament spacing etc.), and converging pathways (which possibly include common pathways with posttranslational modifications like RLC phosphorylation, as suggested by Park-Holohan and coworkers [2021]) thus further complicating its characterization. All these mechanisms would also be integrated with the mechanosensing mechanism of the thick filament, and the role of constitutively activated myosin heads to initiate contraction (Irving, 2017). Such heads may be increased by inotropic mechanisms to a small extent, even in the absence of large-scale thick filament changes (Park-Holohan et al., 2021).

How the above findings can be related to skeletal muscle LDA is currently not well understood. In skeletal muscle, the situation is further complicated by the small amount of information available regarding the function of MyBP-C, as well as the less extensive interest for length-dependent activation in general (at least not at the molecular level, however see MacIntosh, 2017). In mouse EDL muscle, structural changes signaling thick filament activation are slower than those related to thin filament activation (Hill et al., 2021), and it remains an open question as to how the thick filament can "sense" Ca^{2+} activation of the thin filament and transition to the "ON" state (Irving, 2017). As discussed previously, current theories include, similar to cardiac muscle, constitutively "ON" myosin heads binding and increasing thick filament stress, i.e., the mechanosensing mechanism, and/or interfilament communication through MyBP-C (Irving, 2017). The larger functional range of sarcomere lengths in skeletal muscle results in a submaximal force peak to the right of the force-length relationship maximum (e.g., Rassier and MacIntosh, 2002b), which however drops as filament overlap is further reduced (Rassier & MacIntosh, 2002b). This greater range allows for

sufficient passive tension to be developed in the thick filaments, to allow for partial activation independent of [Ca^{2+}], as indicated by fluorescence measurements in permeabilized fibers, at 25 ^{o} C and 5% dextran, in the presence of blebbistatin, which abolishes active force production (Fusi et al., 2016). This can also be seen in frog tibialis anterior fiber bundles, where stretching to long sarcomere lengths (over 3 μm in that muscle type) can induce a partial "ON" state of the thick filament, characterized by disruption of the helical array of the myosin heads on the backbone (associated with decreased intensity of the first myosin layer line reflection, ML1) and increased thick filament periodicity (indicated primarily by increased spacing of the M6 meridional reflection), while the folded conformation of the heads is thought to be retained (as interpreted by the constancy of the intensity and interference fine structure of the M3 meridional reflection) (Reconditi et al., 2014). Therefore, it is possible that skeletal muscle thick filaments, in contrast to cardiac muscle (Caremani et al., 2019), may indeed be partially activated at rest, as sarcomere length is increased. This partial activation may underpin the increased submaximal force production under incomplete thin filament activation and temporal constraints, as expected during a twitch or low Ca^{2+} steady state force. This idea is further supported by the observation of Linari and coworkers (2015); force redevelopment following unloaded shortening (which rapidly induces the filament "OFF" state) from a tetanic plateau was inversely related to shortening duration (Linari et al., 2015); thus, although possibly not directly corresponding to the resting state at longer sarcomere lengths, it appears that initiation of force production from an incompletely inactivated state may indeed allow for more rapid force production, and can at least partially explain the increased submaximal force. The interaction of this partial activation with the increasingly reduced filament overlap as sarcomere length is increased, as well as the effects of lattice spacing on

crossbridge function (e.g., Williams et al., 2013) would result in the observed maximal and submaximal force-length relationships. In addition to the thick filament, cooperative activation of the thin filament through distal tropomyosin translation in the cooperative unit could also be enhanced, either by an unknown interfilament communication mechanism likely involving MyBP-C, or directly through the enhanced crossbridge binding facilitated by thick filament mechanosensing. In support of a MyBP-C mediated mechanism, the aforementioned changes indicating partial thick filament activation, observed by Reconditi and coworkers (2014), became apparent at a sarcomere length of ~2,6 μm, and were maximal at 3 μm, while remaining fairly constant at greater lengths. As the authors point out, these lengths correspond to steady loss of overlap with the C-zone (in the muscle type utilized) where MyBP-C is localized. Concomitantly, the intensity of the M1 meridional reflection (corresponding to MyBP-C related periodic mass distribution) was markedly reduced over that range (Reconditi et al., 2014). As the authors pointed out, this indicates that when thin filaments overlap the C-zone, MyBP-C binds to actin, and this interaction may in part stabilize thick filament structure (Reconditi et al., 2014). Furthermore, a homozygous MyBP-C KO mouse model exhibited expansion of the filament lattice (Song et al., 2021), indicating that MyBP-C may both facilitate interfilament communication, and influence changes in lattice spacing at different sarcomere lengths, as well as spatial modulation of force in general (Williams, Regnier & Daniel, 2010). In contrast to these potential mechanisms, in skeletal muscle, sarcomere length does not appear to influence Ca^{2+} binding to troponin (Fuchs and Wang, 1991; Patel et al., 1997; Martyn & Gordon, 2001) (c.f. Vandenboom, Claflin & Julian, 1998), which could also explain the increased calcium sensitivity (Gordon et al., 2000). As Martyn and Gordon suggest, it is likely that LDA in skeletal muscle is the result of enhanced crossbridge binding

probability, which conceivably also increases tropomyosin translation (Martyn & Gordon, 2001). This effect would be apparent in submaximal conditions, where increased crossbridge binding could aid in fully activating the thin filament, but would be redundant at high [Ca^{2+}], where the thin filament would already be maximally activated (Martyn & Gordon, 2001). A major question is to what extent decreased interfilament spacing facilitates this enhanced binding probability, as previously suggested (Gordon et al., 2000). As discussed above, it has become apparent that it can probably explain part, but not the totality of the observed LDA effects (de Tombe et al., 2010; Ait-Mou et al., 2016). As a relevant example, a recent computational study demonstrated how both changes in lattice spacing and sarcomere length are necessary in order to recapitulate the experimentally observed force-length relationship in their model (Williams et al., 2013), while other modeling work from the same group has shown how lattice spacing can influence axial and radial myosin force production, unitary step size, alter the probability of actin-myosin interactions, and modulate the effect of crossbridge binding on lattice spacing (Williams et al., 2010). A complete characterization of the spatial mechanisms of LDA in the intact filament lattice will be very challenging, and will have to include other sarcomeric components like titin and MyBP-C, describe the role of filament deformation and realignment mechanisms, and interpret past findings in the light of new developments. The fact that crossbridge cycling (and potentially MyBP-C) can dynamically influence lattice spacing during contraction in and of its own (e.g., Kawai et al., 1993), further complicates the situation. Progress in eludicating structural and functional differences between intact muscle preparations and permeabilized fibers (see for example Caremani et al., 2021) will aid in answering this question and better understanding how findings from different experimental models can be integrated. In turn, a more nuanced consensus on the

complex interplay between the filament-based mechanisms of LDA with lattice geometry-related influence on myosin-actin interaction (Williams et al., 2010) will help in better interpreting experimental findings, like the length-dependence of potentiation, which will be discussed below.

IV. Length-Dependence of Activity-Dependent Potentiation

Activity-dependent potentiation, whether staircase or post-tetanic, has been observed to be negatively related to resting sarcomere (Rassier & MacIntosh, 2002), or muscle length (Rassier et al., 1997; 1998; Rassier & MacIntosh; 2000; Rassier & Herzog, 2002) in skeletal muscle. When optimal length (L_o) of force production is assessed with doublet stimulation (which has been shown to closely correlate with L_o attained with tetanic stimulation but differ significantly with the one obtained with twitch contractions, see Rassier & MacIntosh, 2002b), potentiation is diminished with increasing muscle lengths, and enhanced at lower lengths relative to L_o, in rat gastrocnemius muscle in situ, at 37 ^{o}C (Rassier et al., 1997; 1998; Rassier & MacIntosh; 2000). A similar relationship has also been observed in mouse EDL fiber bundles at 25 ^{o} C (Rassier & Herzog, 2002). Additionally, in mouse EDL fiber bundles, where sarcomere lengths were assessed at rest and following, but not during activation, both staircase at 35 ^{o} C and 22 ^{o} C, and post-tetanic potentiation at 22 ^{o} C decrease with increasing resting sarcomere lengths (Rassier & MacIntosh, 2002). Importantly, the magnitude of RLC phosphorylation is similar between conditioning stimuli delivered at different muscle lengths, at least for staircase potentiation (Rassier et al., 1997). Finally, while an earlier study (Moore & Persechini, 1990) found a positive relationship of muscle length with post-tetanic potentiation, the consistent findings described above, under different conditions, indicate that this discrepancy may have been due to some effect of the experimental procedures, which, however, is not known.

The current mechanistic explanation of this relationship is based on the proposed structural effects of RLC phosphorylation (Levine et al., 1996). Specifically, since RLC phosphorylation is thought to increase actin-myosin interaction probability by inducing radial displacement/disorder of the myosin heads (Levine et al., 1996; Gordon et al., 2000), it is thought that increased sarcomere length, and thus decreased interfilament lattice spacing, may render this structural change redundant (MacIntosh, 2010). The already increased Ca^{2+} sensitivity at longer muscle lengths, earlier thought to be caused by the aforementioned lattice compression, would have a ceiling effect in combination with thick filament radial disorder, thus resulting in reduced potentiation at longer sarcomere lengths. This theory was further supported by the finding that osmotic compression induced by dextran, reduced interfilament lattice spacing and mimicked the effect of longer lengths on potentiation, at L_o (Yang et al., 1998). Moreover, as discussed in the previous chapter, an x-ray diffraction study in permeabilized rabbit psoas fibers (Yamaguchi et al., 2016) showed that at longer sarcomere lengths, RLC phosphorylation disrupted the helical arrangement of myosin heads, but did not result in radial head movement, as in shorter lengths. In addition, other factors which are known to ablate LDA in skeletal muscle (lowered pH, caffeine), were shown to also abolish the length-dependence of potentiation (Rassier et al., 1998; Rassier & Herzog, 2002). Even more convincingly, when caffeine (which increases both Ca^{2+} release and Ca^{2+} sensitivity) was combined with dantrolene sodium (which acts to decrease Ca^{2+} release but has no effect on Ca^{2+} sensitivity), the length-dependence of potentiation was not restored, despite the inhibition of Ca^{2+} release, further supporting the role of a potential ceiling effect of Ca^{2+} sensitivity as the main factor responsible for the length-dependence of potentiation (Rassier & MacIntosh, 2000).

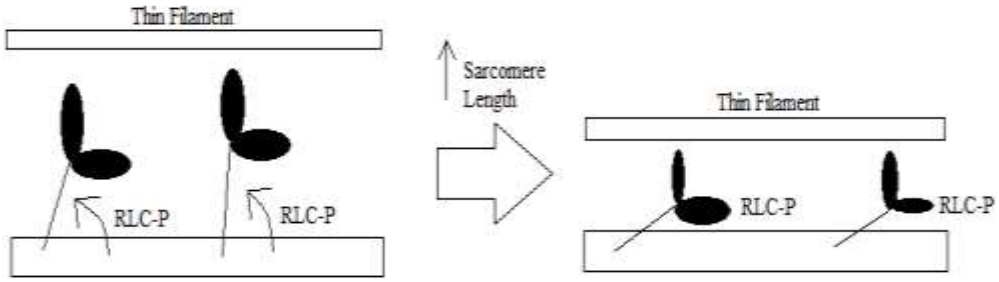

Fig. 4. Simplified representation of the proposed mechanistic model of potentiation length-dependence. At short sarcomere lengths where interfilament lattice spacing is sufficient, RLC phosphorylation radially displaces/disorders the myosin heads, positioning them closer to the thin filament and increasing myosin-actin interaction probability. At longer lengths, interfilament lattice spacing is reduced, and the structural effects of RLC phosphorylation become redundant. Based on Yang et al., 1998; Rassier et al., 1998; Rassier & MacIntosh, 2000, MacIntosh, 2010; Yamaguchi et al., 2016. RLC-P = RLC phosphorylation

While these results provide a framework to understand why potentiation is influenced by sarcomere length, certain findings from physiological studies, as well as recent progress in regard to the molecular mechanisms of contraction in skeletal muscle, indicate that it may not be completely characterized. Initially, Rassier and coworkers (1998) found that when caffeine was used to abolish LDA and the length dependence of potentiation, potentiation magnitude was enhanced at longer muscle lengths. Essentially, instead of potentiation magnitude being moved towards lower values across all lengths, it seemed to decrease at shorter, and simultaneously increase at longer lengths, in contrast to what would be expected by a combined ceiling effect of length and caffeine on calcium sensitivity. Similarly, Rassier and Herzog (2002)

showed that when pH was lowered, thus abolishing LDA, potentiation was again independent of length and increased at longer lengths, while decreasing at shorter lengths. In that case, increased potentiation at longer lengths would be expected, given the fact that force was reduced at all lengths, but why potentiation decreased at short lengths (L_o was the lowest length used) is not clear. Notably, caffeine and pH affect Ca^{2+} sensitivity in an opposite manner, with caffeine enhancing, and pH decreasing it. Both of these observations point towards a more complex model, which necessitates incorporating both the mechanisms of LDA itself, as well as the exact molecular effects of caffeine and pH, which are unfortunately not well understood, more so for caffeine. Lowered pH is thought to decrease calcium sensitivity by inhibiting calcium binding to troponin C in a competitive manner, and potentially influencing the structural changes of troponin upon calcium binding, thus inhibiting actin-myosin interactions (Unger & Debold, 2019). Potential effects on interfilament interactions or thick filaments have not been studied extensively. As mentioned above, when combined with dantrolene, caffeine still abolishes the length-dependence of potentiation, but as the authors point out, this does not necessarily mean that this effect is solely mediated by its influence on Ca^{2+} sensitivity; different modulation of Ca^{2+} release across lengths might additionally affect the findings (Rassier & MacIntosh, 1999). In regard to that, it has been recently demonstrated in intact flexor digitorum brevis (a fast muscle) mouse fibers, that calcium release during tetanic contractions is inhibited at lengths corresponding to the ascending limb of the force-length relationship (sarcomere lengths lower than ~1.9 μm) (Rassier & Minozzo, 2016). This inhibition was reversed by caffeine, resulting in both higher force production and calcium release similar to that observed at longer muscle lengths (Rassier & Minozzo, 2016). In addition, it has also been shown that caffeine may inhibit the phenomenon of calcium-induced calcium

release characterizing repeated submaximal contractions (Smith et al., 2019), in that way facilitating continuous flow of Ca^{2+}. Thus, while it is not clear whether inhibition of calcium release at short lengths would have any meaningful effect in twitches, it is possible that such an effect, as well as the increased calcium release during the staircase owing to the effects of caffeine, would influence the findings of Rassier and coworkers. Conceivably, caffeine may differentially affect the Ca^{2+}-related mechanisms of potentiation and RLC phosphorylation. For example, increased calcium release during the staircase could result in enhanced RLC phosphorylation (Stull et al., 2011), specifically for the caffeine conditions, while both dantrolene and caffeine could affect calcium release in a different manner at short and long lengths (Rassier et al., 1998; Rassier & MacIntosh, 1999; Rassier & Minozzo, 2016).

A separate issue is the central question of whether RLC phosphorylation in mammalian skeletal muscle radially displaces the myosin heads, results in a partially "ON" state, or alternatively, follows the findings in cardiac muscle (Park-Holohan et al., 2021) and does not greatly affect thick filament structure at rest. As mentioned previously, it has become apparent that findings in permeabilized fibers or isolated thick filaments, particularly at low temperatures, cannot necessarily be extrapolated to the intact muscle environment (Irving & Craig, 2019; Caremani et al., 2019; 2019b; 2021). The experiments of Levine and coworkers (1996) utilized isolated thick filaments, while Yang and coworkers (1998) used isolated thick filaments, and permeabilized fibers at 23 ^{o}C. Similarly, Yamaguchi and coworkers (2016) used permeabilized rabbit psoas fibers at a low temperature (20 ^{o} C), in the absence of osmotic compression. All these conditions result in not-well characterized effects on thick filament structure (Irving & Craig, 2019; Caremani et al., 2021), and thus preclude direct extrapolation to the muscle native environment. This does not necessarily mean that findings would be

different in a whole muscle model; in intact tarantula skeletal muscle, RLC phosphorylation at rest, following a tetanus, results in radial displacement of the myosin heads (Padron et al., 2020). However, thick filament structure in tarantulas is different than in mammals, most notably displaying absence of MyBP-C and a paramyosin core (Padron et al., 2020). Additionally, as previously mentioned, the markedly smaller changes in thick filament length upon contraction, a structural change associated with activation in mammals and amphibians (related to increased M6 spacing), is almost completely absent in tarantulas, indicating that thick filament mechanosensing has at most a secondary role (Padron et al., 2020). Thus, it remains unclear whether in mouse or rat muscle, RLC phosphorylation would radially displace the myosin heads towards the thin filament. Considering the above, and the fact that LDA may not be mediated by lattice spacing to the extent that was initially thought, as discussed in the previous section, it becomes apparent that the interaction between RLC phosphorylation and lattice spacing may be more complex than previously thought. Outstanding questions include how the partial thick filament activation observed during stretch in frog muscle (Reconditi et al., 2014) and permeabilized rabbit psoas fibers under physiological conditions (Fusi et al., 2016), would interact with RLC phosphorylation and potentiation, and to what extent it can explain LDA; how MyBP-C influences LDA and by extension potentiation, in and out of the C-zone, based on the findings of Reconditi and coworkers (2014) discussed above; what could the role of alternative potentiation mechanisms be in determining its length-dependence, especially considering the recent findings of asymmetrical calcium release inhibition in mammalian fibers (Rassier & Minozzo, 2016); and how potentiation would be structurally manifested in intact muscle during physiological activation. In regard to the last point, it must be considered that steady-state potentiation experiments in permeabilized fibers cannot be directly

extrapolated to physiological activation, where calcium kinetics are rapid (Metzger & Moss, 1989; Irving et al., 2017; Hill et al., 2021). Finally, while not extensively discussed above, another incompletely characterized aspect of the length-dependence of contraction is the alteration of force kinetics with length, and the mechanisms underlying them, which may involve calcium and crossbridge cycling kinetics. Time to peak tension (time from the initiation of contraction to peak force) and time to half relaxation are increased for twitch contractions at lengths longer than optimal, while at the same time rates of force development and relaxation are reduced (Rassier & MacIntosh, 2002). These findings may be partially explained by the observed discrepancies in crossbridge cycling kinetics at different sarcomere lengths in permeabilized fibers (MacDonald, Wolff & Moss, 1997; Fenwick, Leighton & Tanner, 2016) and whole muscle (Fenwick, Lin & Tanner, 2021). MacDonald and coworkers (1997) showed that rate of force redevelopment was increased at 2,3 μm compared to 2 μm in permeabilized rabbit psoas fibers, a range over which submaximal force and calcium sensitivity were enhanced. Fenwick and coworkers have additionally demonstrated that ADP release and crossbridge cycling kinetics might be slowed at long sarcomere lengths, in slow rat soleus permeabilized fibers (Fenwick et al., 2016) and whole mouse soleus muscles (Fenwick et al., 2021). However, how these findings would translate to fast mammalian muscle, which exhibits potentiation (in contrast to slow muscle, Vandenboom, 2017) is unknown. Nevertheless, the fact that RLC phosphorylation appears to have kinetic effects on the crossbridge cycle (Davis et al., 2002; Greenberg et al., 2009; 2010) indicates that the length-dependence of potentiation must be interpreted both at the level of structural mechanisms influencing thick filament activation, as well as kinetic effects at and downstream of crossbridge attachment.

In sum, length-dependence of potentiation, much like LDA, appears to be a complex phenomenon involving multiple sarcomeric components. Combining findings from different methodologies will likely be necessary to understand exactly how potentiation interacts with sarcomere length at the molecular level. Lattice spacing (Williams et al., 2010; 2013), thick filament activation with stretch (Reconditi et al., 2014; Fusi et al., 2016), MyBP-C (Li et al., 2019; Song et al., 2021), crossbridge cycling kinetics (Greenberg et al., 2009; 2010), Ca^{2+} kinetics (Smith et al., 2013; 2014; Rassier & Minozzo, 2016) and other potential mechanisms all likely contribute to the observed relationship. The initial proposition that increased length and the concomitant decrease in lattice spacing may interact with the radial displacement/disorder of the myosin heads (MacIntosh, 2010) forms the basis of current understanding and future findings will continue to add to this model and better explain why potentiation is length-dependent.

Chapter Three: Statement of the Problem

Activity-dependent potentiation is an integral characteristic of mammalian muscle physiology, with a central role in modulating skeletal muscle contraction. While the physiological aspects of RLC phosphorylation, the main mechanism of potentiation, have been extensively studied and characterized (Vandenboom et al., 2013; 2017), recent progress has highlighted the existence of additional potentiation mechanisms (e.g., Zhi et al., 2005; Smith et al., 2013; 2014) in different skeletal muscle models. A distinct characteristic of potentiation in skeletal muscle is its negative dependency on muscle (Rassier et al., 1997) or sarcomere (Rassier & MacIntosh, 2002) length, which has been mainly attributed to the effects of RLC phosphorylation on thick filament

structure and function (Levine et al., 1996; Yang et al., 1998; Yamaguchi et al., 2016). This relationship has not been explored in skMLCK$^{-/-}$ mouse EDL muscles, which display potentiation in the absence of RLC phosphorylation.

Investigating the length-dependence of potentiation in the aforementioned model will allow for an additional, indirect validation of its primary proposed mechanism in a whole muscle model. Additionally, new insights into the RLC-phosphorylation independent mechanisms can be potentially discovered, by exploring the extent to which they are influenced by muscle length.

3.1 Purpose and Hypotheses

The purpose of this study was to determine the effects of muscle length on post-tetanic potentiation in vitro. This relationship was investigated in wildtype and skMLCK $^{-/-}$ mouse fast twitch EDL muscles, at 25 ^{o} C. It was originally hypothesized that the length-dependence of potentiation would be attenuated in skMLCK$^{-/-}$ compared to WT EDL muscles. This would be initially apparent as a statistically significant interaction between the effects of genotype and muscle length on potentiation, and subsequently as a difference between the trends characterizing the length-potentiation relationship in each genotype, and/or the amount of variance they can explain. In the alternative case, a robust length-dependence of potentiation in this model, similar to what has been traditionally observed in WT mice, would provide novel insights into the additional mechanisms of potentiation.

Chapter Four: Methodology

I. Mouse Models and Housing

This study was approved by the Animal Care Committee of Brock University: AUP # 20–04–02.

The wild type (WT) models (C57BL/6) used in this experiment were purchased from Charles River Laboratories and then transported to Brock University for housing. The skMLCK $^{-/-}$ mice were selected from our breeding colony kept on site. All test animals were kept in the Comparative Bioscience Facility (CBF) at Brock University, according to CCAC guidelines and the following SOPs:

• HUSB04 - Care and Maintenance of Mice

• EE02 – Environmental Enrichment for Mice

Animals Approved for Study:

• 20 WT C57BL/6 Mice (10M and 10F)

• 28 skMLCK$^{-/-}$ Mice (14M and 14F)

All mice used were aged 10-24 weeks. In addition, as shown in Table 1 weight was not significantly different between WT and skMLCK$^{-/-}$ mice ($p > .05$).

Genotype	Mean Weight	n
WT	22.7 ± 1.1	8
skMLCK$^{-/-}$	23.9 ± 0.6	10

Table 1. Mean mouse weight in grams, not significantly different between genotypes ($p > .05$) (see "Statistical Analysis" section). Note that n indicates mouse and not muscle number. Values are mean ± SEM.

II. Surgical Protocol

All procedures were done at Brock University's Center for Bone and Muscle Health (CRN431). Prior to experimentation, mice of either genotype were selected and transported to the lab from the CBF in a covered container (SOP #SAFE06 – Transportation of Laboratory Rodents within the University). Subsequently, mice were fully anaesthetized via inhalation of isoflurane gas (SOP #HEAL25 – Use of Isoflurane in Rodent Surgeries Using a Vaporizer) and euthanized by means of cervical dislocation (SOP #-EUTH04 – Methods of Euthanasia for Various Animals). Following euthanasia, both EDL muscles were excised from the mouse's hindlimbs. During the procedure, surgical silk suture was tied around the distal and proximal EDL tendons, and subsequently used for mounting on the experimental apparatus.

III. Preliminary Experimental Protocol

Immediately following excision, EDL muscles were mounted vertically in a jacketed organ bath, between a catch in the bath and a steel hook attached to a servomotor (Model 305B, Aurora Scientific Inc., Aurora, ON), in continuously oxygenated Tyrode's solution with controlled temperature (25 ^{o} C). While one of the muscles was mounted on the experimental apparatus, the other was placed in a resting bath with the same solution, stretched slightly beyond taught length. Muscle stimulation was provided through flanking platinum electrodes (Model 701B biphasic stimulator, Aurora Scientific Inc., Aurora, ON). Following suspension, the muscle was adjusted to 5 mN passive tension (a value corresponding to slightly above the average for optimal length for force production for mouse EDL in our laboratory) and underwent a brief, high frequency tetanic contraction (100 Hz, 100 ms) to remove any slack in the preparation and ensure the integrity of the silk suture. Subsequently, the muscle

underwent at least 30 min of equilibration (one twitch every 3 minutes), whereafter twitch force becomes stable. Following equilibration, the voltage required for maximal activation of the muscle was found, and voltage was set to 125% of this value for the rest of the experiment. Then, doublet stimulation was used to approximate optimal length for tetanic force production, as described by Rassier and Macintosh (2002b). Stimulation initially took place at 5 mN passive tension and force was then assessed at approximately 0.5 mN intervals above and below this value, with at least 20 seconds between successive doublets. After locating the passive tension value that corresponded to the highest active force (peak force attained during the doublet minus passive force immediately before), muscle length was measured using digital vernier calipers, and defined as optimal length (L_o) for the rest of the experiment. Finally, twitch force at L_o was assessed prior to initiating the main experimental process (mean of two twitches). Muscle length and contractile data were monitored using Aurora Scientific's 600A software (Aurora Scientific Inc., Aurora, ON), with data collection taking place at 1000 Hz.

Fig. 5. Mouse EDL in vitro, at 25 ^{o} C.

IV. Main Experiments and Mechanical Data

The main experimental process involved paired isometric twitch measurements at five different muscle lengths, interspersed by an isometric conditioning stimulus (CS). Prior to the conditioning stimulus (Pre), the muscle underwent 10 twitch contractions in a 200 second period (pacing), at one of the following lengths: 0.90 $L_{o,}$ 0.95 $L_{o,}$ L_{o}, 1.05 L_{o} or 1.10 L_{o}. In each case, the conditioning stimulus was administered 30 seconds after the 200 second period, and consisted of four, 100 Hz, 400 ms tetani in a 20 second window. The conditioning stimulus was carried out at the same muscle length as the prior and following twitches. This was done to avoid complications arising due to the insufficient time for passive force stabilization following ramps to long

muscle lengths (1.05 and 1.10 L_o). This has been a consistent observation in our lab in the mouse EDL in vitro at 25 ^{o} C, and is possibly related to the specific viscoelastic properties of this preparation. Peak tetanic force (P_o, peak total force minus passive force prior to stimulation) was assessed during each conditioning stimulus, by comparing the peak values of the four tetani. 10 (Post 10) and 30 (Post 30) seconds after the conditioning stimulus period, twitches were elicited to examine force potentiation. Potentiation at each time point was calculated as peak twitch force (P_t) after the CS divided by the average of the peak forces of the last three twitches of the prior pacing period (representing Pre-CS P_t), and expressed as a normalized value (e.g., 1.10 of initial twitch force). In turn, these normalized values could also be expressed as percentages (e.g., 1.10 = 10% potentiation). Following the completion of the aforementioned protocol at a given length, a 20 min rest period was undertaken to allow for dissipation of fatigue and potentiation effects. During this resting period the muscle remained at the length of the preceding stimulation. Each muscle underwent the described protocol at all five experimental lengths, in a randomized order. Previous work using this experimental model and conditions has demonstrated that repetitive application of conditioning stimuli in a timescale similar to the one described above (i.e., 3-5 experimental conditions interspersed with 20 minutes of rest) results in both stable and repeatable force values, as well as RLC phosphate incorporation (see discussion in Gittings et al., 2015). It should be noted, however, that in previous experiments, conditioning stimuli were always administered at L_o.

Following the end of the main experiment, the muscle was taken to L_o and a 30-minute rest period was undertaken, with a twitch elicited every 3 minutes. Afterwards, twitch force was assessed at L_o (mean of two twitches), and compared with the value measured prior to the start of the main experiment, in order to check for potential

damage caused by the experimental sequence. Muscles were excluded from analysis if twitch active force was decreased by more than 5% of the pre-experiment value.

In addition to force measurements, force kinetics were assessed through the first derivatives of force increase and decrease (+*d*F/*d*t and -*d*F/*d*t respectively, directly provided by the 600A software analysis function), time to peak tension (TPT) and half-relaxation time (½ RT) (derived through the raw data files using Excel [Microsoft Corporation, 2016]). +*d*F/*d*t and -*d*F/*d*t are instantaneous values of force change representing rate of force development or relaxation, and their peaks were collected for each twitch. For the rest of this thesis, +*d*F/*d*t and -*d*F/*d*t will refer to peak values. TPT was quantified by subtracting the time (in milliseconds) of stimulation initiation from the time when P_t was achieved. In a similar manner, ½ RT was calculated by finding the time point after P_t where force was half of the maximal value and subtracting the time of P_t. Potentiation of +*d*F/*d*t and -*d*F/*d*t was determined in the same manner as for force, i.e., by dividing Post 10 or Post 30 by Pre values (with Pre for all force kinetics measures again consisting of the mean value of the last three twitches of the pacing period in each case), and expressed as a relative value (e.g., 1.10), which, again, can also be thought of as % increase or decrease (e.g. 1.10 = 10% increase post to pre).

Finally, the change in force between the first and the fourth tetanus of the CS (i.e., fatigue) was measured at each length and expressed as % change. The following formula was used to calculate these values: 100 - [(Force of tetanus 4/Force of tetanus 1) * 100]. Potentiation can occur concomitantly with fatigue (Rassier & MacIntosh, 2000b), and this measure can be used to at least partially assess any length-dependent confounding effects of the latter on the observed values of the former.

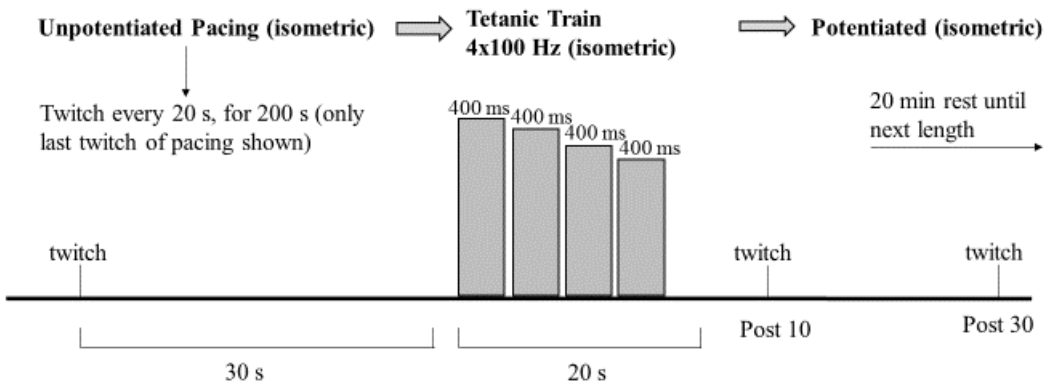

Fig. 6. Overview of the main experimental process. Thirty seconds after the final twitch of the pacing period (200 s, one twitch every 20 s), a 4x100 Hz, 400 ms tetanic train (CS), within a 20 s window was elicited. Potentiated twitch responses were measured at 10 and 30 s post-CS. Each muscle underwent this protocol at all five experimental lengths (0.90 L_o, 0.95 L_o, L_o, 1.05 L_o, 1.10 L_o) in a randomized order, with 20 min rest between protocols.

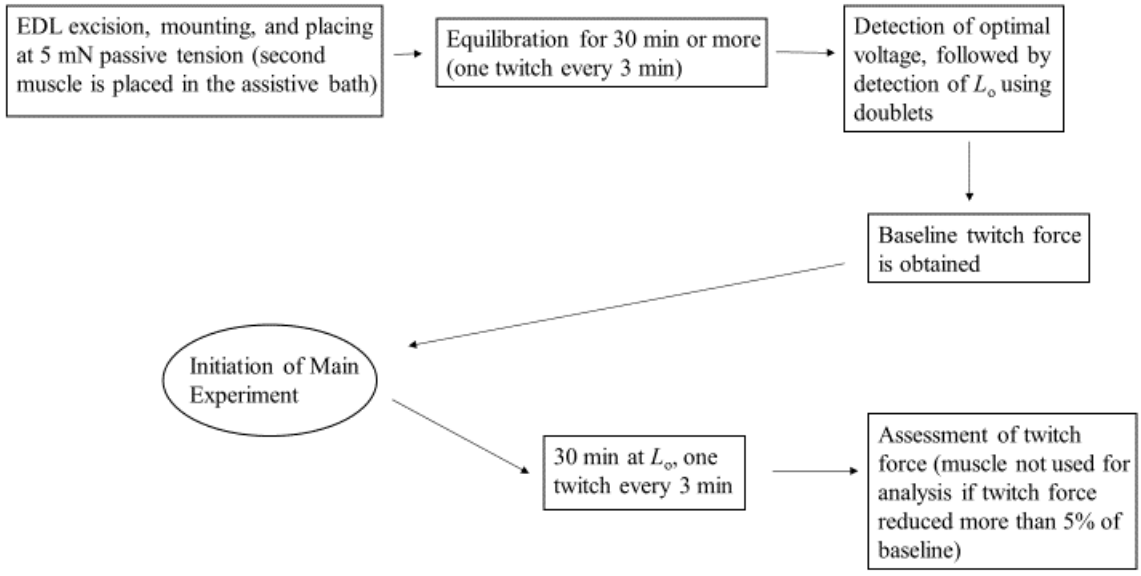

Fig. 7. Experimental design flow chart.

V. Statistical Analysis

Mouse weight was compared between genotypes using an independent samples t-test. The effects of muscle length and genotype on P_o were evaluated through a two-way mixed Analysis of Variance (ANOVA). For the two-way mixed ANOVA, the assumption of homogeneity of covariances was assessed through Box's test. To assess the effects of genotype, muscle length and time on each of the mechanical measurements (P_t, +*d*F/*d*t, -*d*F/*d*t, TPT, ½ RT) and the potentiation values of P_t, +*d*F/*d*t and -*d*F/*d*t, three-way mixed ANOVAs with one between- (genotype) and two within- (muscle length, time) subjects factors were utilized. In each case, the existence of outliers was determined through boxplot inspection. When outliers were present, the test was carried out with and without including them, and the results were compared. In all cases, no differences were observed in the statistical significance of interactions and main effects, and the decision was made to include outliers in the final analysis. To evaluate normality, Shapiro-Wilk's test was used. Homogeneity of variance for the between-subjects factor was evaluated through Levene's test in each case, while Mauchly's test was used to assess sphericity where necessary. When the assumption of sphericity was violated, a Greenhouse-Geisser correction was applied. Finally, it should be noted that there was a missing data point (Post 30 twitch in a WT muscle), owing to a malfunction of the bath. This has to be taken into account in regard to the ANOVAs, as a missing data point results in the corresponding subject not being considered in the test calculations.

Significant simple main effects or main effects were further analyzed using post-hoc pairwise comparisons with Bonferroni corrections, or polynomial contrasts for trend analysis. When a significant trend was detected (linear, quadratic, cubic or higher order), the percentage of variance of the total observed trend it could explain was

calculated by dividing its sum of squares by the sum of squares of the total observed trend. Bonferroni corrections were additionally used to control for multiple simple main effect testing within a given interaction. All the above analyses were carried out in IBM SPSS Statistics for Windows, versions 27 and 28 (IBM Corp., Armonk, NY, USA).

Fatigue data were not normally distributed at any cell of the design; thus, a robust mixed ANOVA on the 20% trimmed means was utilized. This test was carried out through the *bwtrim* function of the WRS2 package (Mair & Wilcox, 2019) in R (R Core Team, 2021), using RStudio (RStudio Team, 2016). To further examine the main effect of the within-subjects factor (i.e., muscle length), multiple dependent-samples post-hoc robust t-tests with Bonferroni corrections (again on the 20% trimmed means) were used (*yuend* function of the WRS2 package, Mair & Wilcox, 2019).

Significance was set at $\alpha = .05$ and all data are reported as mean ± SEM, unless otherwise indicated. All graphs were created using OriginPro (Version 2021, OriginLab Corporation, Northampton, MA, USA).

Chapter Five: Results

I. Tetanic Force

Figure 8 depicts representative tetanic force records of EDL muscles from wildtype and skMLCK$^{-/-}$ mice obtained during experiments. Tetanic force at each length was defined as the highest value recorded during the four tetani of the conditioning stimulus (CS) (4 x 100 Hz, 100 ms within a 20-second window). A tetanic force-length relationship was produced by these values.

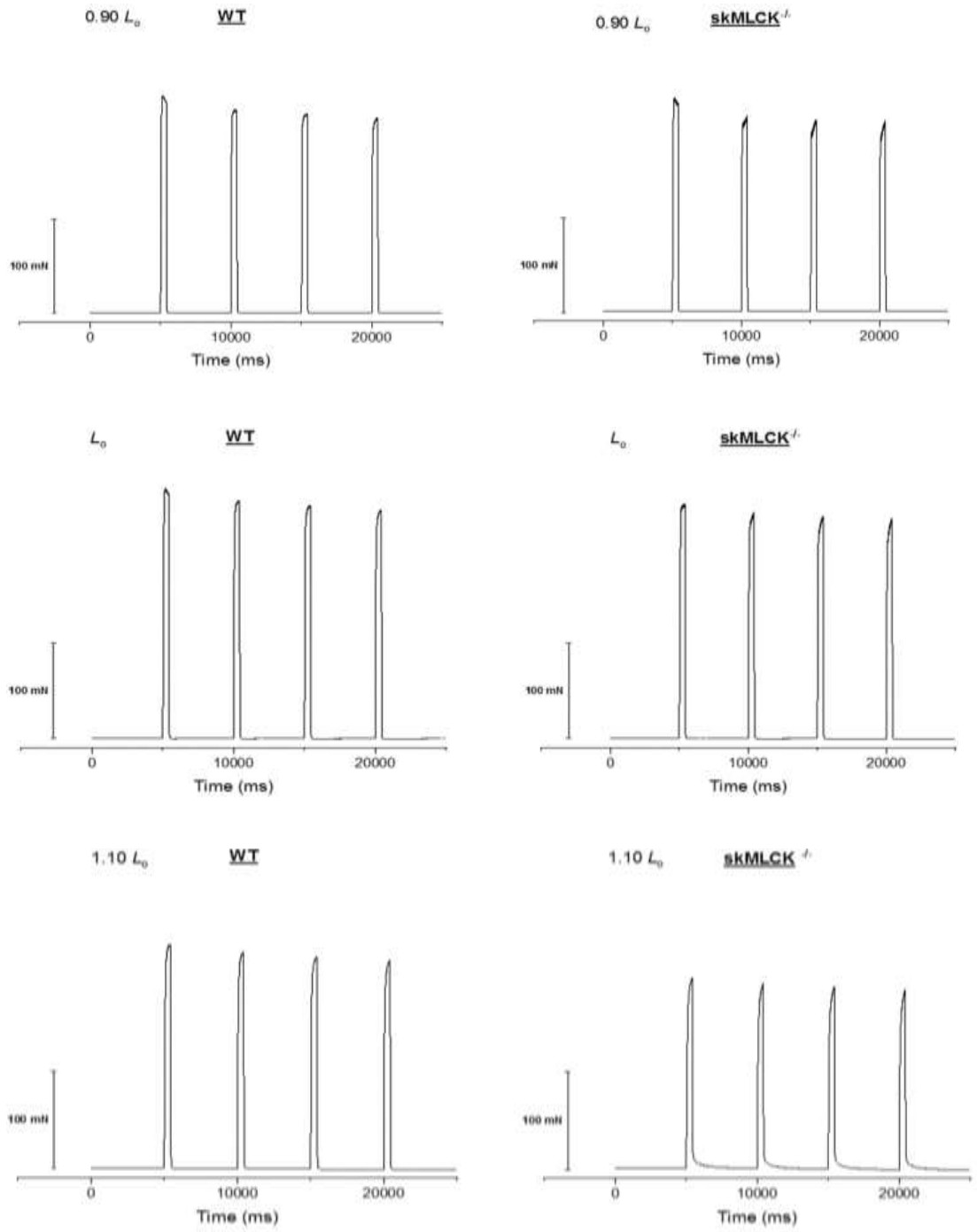

Fig. 8. Representative force traces of the conditioning stimuli (4 x 100 Hz, 100 ms tetani within a 20-second window) at 0.90 L_o, L_o and 1.10 L_o for a typical WT (left) and a typical skMLCK $^{-/-}$ (right) mouse EDL muscle. Y-axis scale bar represents 100 mN.

As summarized in Table 2, tetanic force was not different between genotypes at any length ($p < .05$). For example, at L_o WT tetanic force was 211.7 ± 13.1 mN, while skMLCK $^{-/-}$ tetanic force was 224.1 ± 20.4 mN.

WT

Relative Muscle Length (L/Lo)	0.90	0.95	1	1.05	1.10
Tetanic Force	180.3 ± 12.1	198.7 ± 12.7	211.7 ± 13.1	199.2 ± 12.9	179.1 ± 12.9

skMLCK$^{-/-}$

Relative Muscle Length (L/Lo)	0.90	0.95	1	1.05	1.10
Tetanic Force	180.3 ± 17.8	210.8 ± 18.5	224.1 ± 20.4	217.1 ± 20.3	187.1 ± 18.8

Table 2. Mean tetanic force (mN) for WT (top, n=12) and skMLCK$^{-/-}$ (bottom, n=12) mouse EDL muscles at all experimental muscle lengths. No significant differences between genotypes at any length ($p > .05$). Values are mean ± SEM.

Tetanic force was dependent on muscle length but this relationship was not different between genotypes, as indicated by the non-significant muscle length x genotype interaction ($p > .05$) (Figure 9).

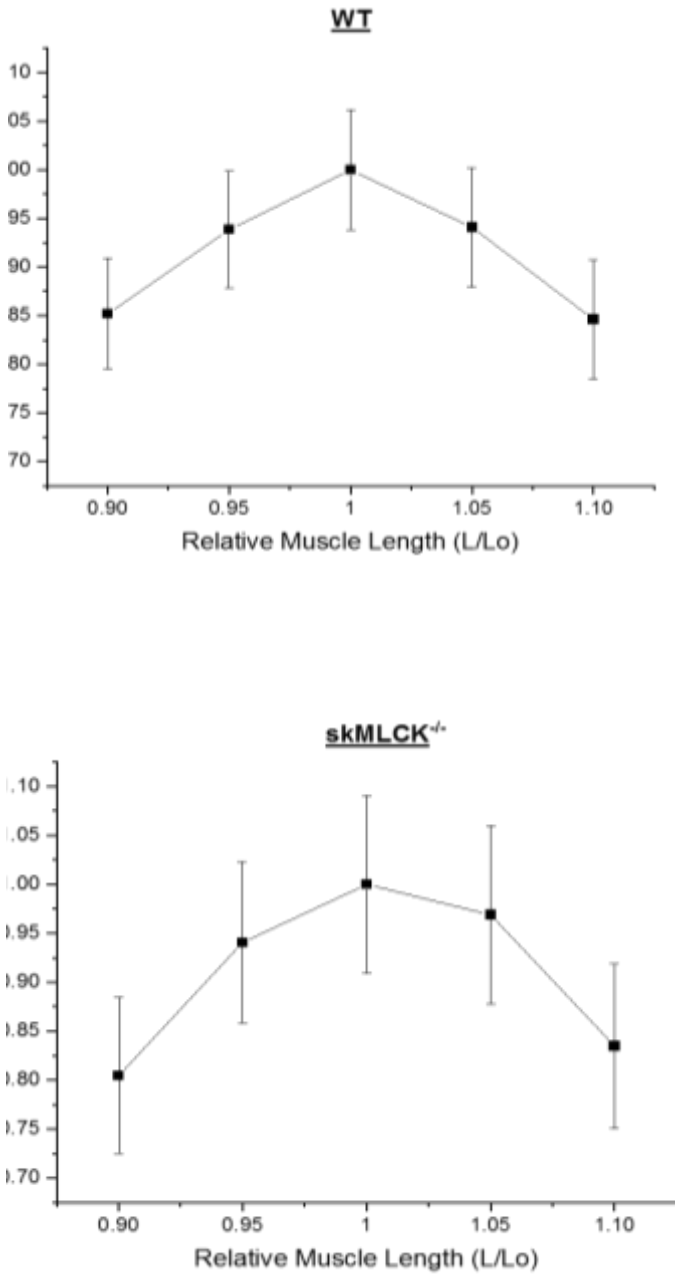

Fig. 9. Relative force-length relationship for WT (top, n=12) and skMLCK$^{-/-}$ (bottom, n=12) mouse EDL muscles. Force values were normalized to the L_o value for each genotype. Tetanic force production was not significantly different between genotypes at any length. Error bars represent SEM.

To further assess the length-dependence of tetanic force, polynomial contrasts were used for trend analysis. Specifically, there was a significant quadratic trend ($p < .001$), which could explain 98.46% of the variance of the observed relationship, reflecting the curvilinear dependence of P_o on length observed graphically. These findings are shown in Table 3.

Tetanic Force	
Main Effect: Muscle Length	F: 38.181*
% Variance Accounted	
Linear: NS Quadratic: 98.46%* Cubic: NS 4th Order: NS	

Table 3. Trend components of the polynomial contrast analysis for the main effect of muscle length. The ANOVA F-value for the main effect of muscle length is presented (Muscle length x Genotype interaction was not significant), along with the percent variance explained by each significant trend component. * $p < .001$, NS = non-significant

II. Tetanic Fatigue

In addition to P_o, the degree of force decline, or fatigue, displayed by each muscle during each experiment was assessed. Fatigue was quantified as % change in tetanic force between the first and last tetanus of the CS, and this was done for all lengths. These data are summarized in Table 4. Fatigue was not different between WT

and skMLCK$^{-/-}$ muscles ($p > .05$). Additionally, there was not a significant muscle length x genotype interaction ($p > .05$). There was, however, a significant main effect of muscle length ($p < .05$), with % change in tetanic force being lower at 1.05 L_o and 1.10 L_o compared to 0.9 L_o, 0.95 L_o and L_o. Moreover, values were not significantly different between 1.05 L_o and 1.10 L_o, as well as between 0.9 L_o, 0.95 L_o and L_o.

Fatigue

Relative Muscle Length (L/Lo)	0.90	0.95	1	1.05	1.10
Mean Fatigue (% Change in Tetanic Force)	-7.6 ± 1.4	-8 ± 1.2	-6.7 ± 0.9	-4.4 ± 0.6*	-2.6 ± 0.7*

Table 4. Decline in tetanic force (i.e., fatigue) displayed from tetanus 1 to 4 during the CS, collapsed across genotypes (values were not significantly different between WT and skMLCK$^{-/-}$ muscles). Fatigue was calculated using the following formula: 100 - [(Force of tetanus 4/Force of tetanus 1) * 100]. Values are 20% trimmed mean ± SEM. * significantly different than L_o ($p < .001$)

III. Twitch Force and Twitch Force Potentiation

Both for WT and skMLCK$^{-/-}$ muscles, twitch force (Pt) was evaluated prior to the CS (Pre) and both 10 (Post 10) and 30 (Post 30) seconds after the CS, at all five

experimental lengths. As shown in Table 5, unpotentiated twitch force obtained prior to the CS was not different between genotypes at any length.

WT

Relative Muscle Length (L/Lo)	0.90	0.95	1	1.05	1.10
Pt (Pre)	36.7 ± 3.3	47.6 ± 3.6	51.3 ± 3.4	49.3 ± 3.5	45 ± 3.3

skMLCK$^{-/-}$

Relative Muscle Length (L/Lo)	0.90	0.95	1	1.05	1.10
Pt (Pre)	32.9 ± 3.1	45.2 ± 3.3	48.9 ± 3.7	47.4 ± 3.9	41.1 ± 4.1

Table 5. Mean unpotentiated twitch force (mN) of WT (top, n=12) and skMLCK $^{-/-}$ (bottom, n=12) mouse EDL muscles at all experimental lengths. No significant differences between genotypes at any length ($p > .05$). Values are mean ± SEM.

In contrast, as expected by the presence of RLC phosphorylation, twitch force was significantly greater in WT compared to skMLCK$^{-/-}$ muscles both at 10 and 30 seconds following the CS across lengths. These observations were reflected in the significant time x genotype interaction ($p < .001$), and the significant simple main effects of genotype at Post 10 and Post 30 (both $p < .001$), but not at Pre ($p > .05$). Despite the different potentiation mechanisms, twitch force in both genotypes was highest 10 seconds after the CS and had declined by the 30-second mark, but was still higher than pre-CS values at that point (i.e., Post 10 > Post 30 > Pre). This relationship was observed at all muscle lengths (all $p < .001$). All the above data are summarized in Table 6.

WT

Relative Muscle Length (L/Lo)	0.90	0.95	1	1.05	1.10
Post 10 Pt	52 ± 3.7*†	56.8 ± 3.9*†	59.8 ± 3.8*†	58 ± 3.9*†	52.5 ± 3.8*†
Post 30 Pt	49.5 ± 3.6*	55 ± 3.8*	58.3 ± 3.7*	56.8 ± 3.8*	51.7 ± 3.7*

skMLCK$^{-/-}$

Relative Muscle Length (L/Lo)	0.90	0.95	1	1.05	1.10
Post 10 Pt	42.1 ± 3.2†	49.9 ± 3.1†	52 ± 3.5 †	51.5 ± 3.7 †	44.3 ± 4†
Post 30 Pt	38.9 ± 3.1	47.4 ± 3.1	49.9 ± 3.4	49.3 ± 3.7	42.8 ± 3.9

Table 6. Mean twitch force of WT (top, n=12) and skMLCK $^{-/-}$ (bottom, n=12) mouse EDL muscles at Post 10 and Post 30, at all experimental lengths. Values are mean ± SEM. * significantly different than skMLCK$^{-/-}$ at the same time point and length ($p < .001$), † significantly different than Post 30 within genotype ($p < .001$)

Twitch force was dependent on muscle length ($p < .001$), and this relationship was similar between WT and skMLCK$^{-/-}$ muscles both prior to and following the CS, as indicated by the absence of significant time x muscle length x genotype, and muscle length x genotype interactions (both $p > 0.5$) (Figure 10).

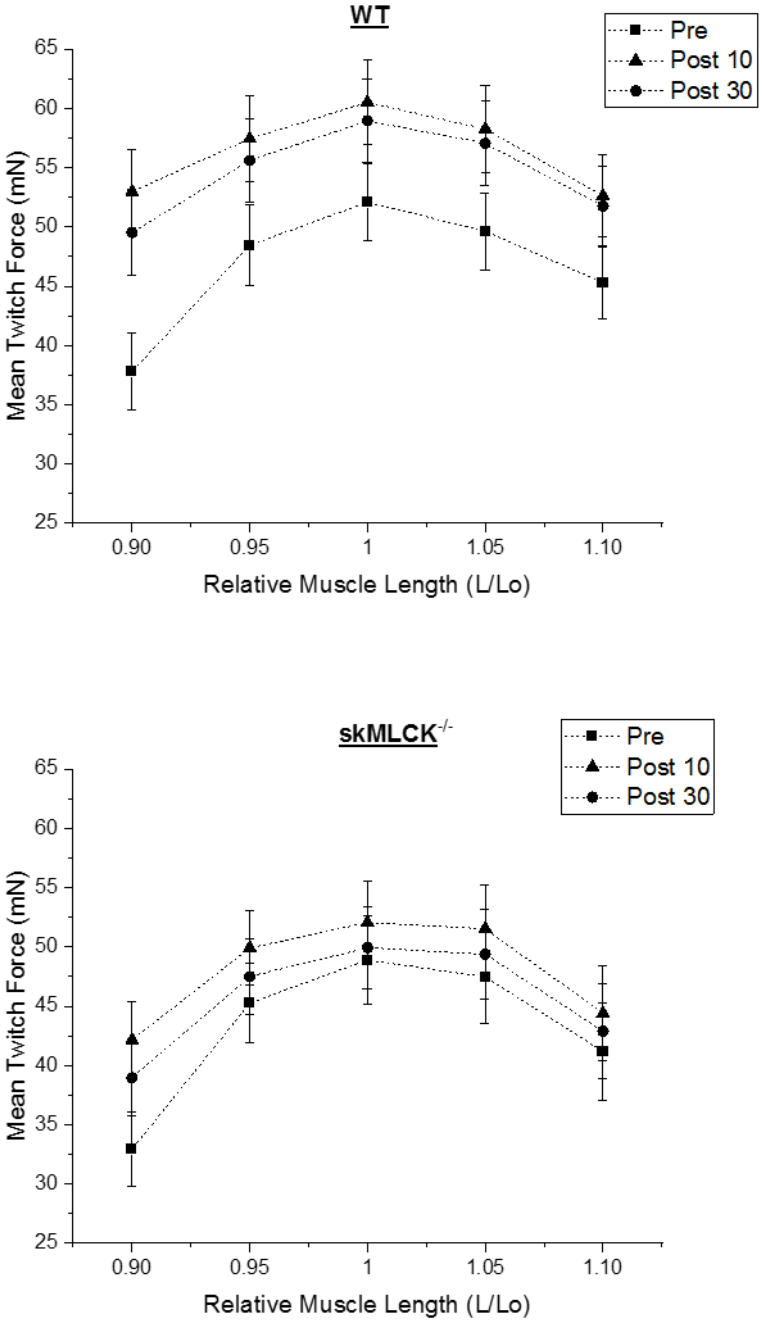

Fig. 10. Mean twitch force (Pt) – muscle length relationship for WT (top, n=12) and skMLCK$^{-/-}$ (bottom, n=12) mouse EDL muscles. Pre Pt was not different between genotypes but at Post 10 and Post 30, Pt was greater for WT across lengths. Note that for both genotypes at all lengths, Post 10 Pt > Post 30 Pt > Pre Pt. Error bars represent SEM.

Trend analysis revealed a different pattern of length-dependence of twitch force at Pre compared to Post 10 and Post 30. At Pre, there were significant linear, quadratic and cubic trends (all $p < .001$), which could explain 14.02%, 50% and 0.9% of the variance respectively. In contrast, at Post 10 and Post 30, only quadratic trends were significant ($p < .001$), and could explain 98.06% and 90.64% of the variance respectively (Table 7). Graphically, this became apparent as a more "level" and distinctly curvilinear length-Pt relationship at 10- and 30-seconds post-CS, owing to the disproportionately greater increase of force at 0.90 L_o following the CS compared to other lengths. In comparison, at Pre, the ascending part of the relationship was characterized by low forces at 0.9 L_o, as expected by earlier force-length studies (e.g., Rassier & MacIntosh, 2002b), resulting in a steep increase in force with length and potentially explaining the observed linear trend.

Twitch Force			
Time x Muscle Length - F: 54.190*	Pre – F: 51.124*	Post 10 - F: 30.573*	Post 30 - F: 33.44*
% Variance Accounted	Pre	Post 10	Post 30
Linear:	14.02%*	NS	NS
Quadratic:	50%*	98.06%*	90.64%*
Cubic:	0.9%*	NS	NS
4th Order:	NS	NS	NS

Table 7. Trend components of the polynomial contrast analysis for the simple main effects of muscle length at each time point. The ANOVA F-values for the Time x Muscle Length interaction, as well as the simple main effects of length at each time point are presented. At the bottom of the table, the percent variance explained by each significant trend component for each simple main effect can be found. * $p < .001$, NS = non-significant

Potentiation of force (as well as $+dF/dt$ and $-dF/dt$) was characterized as a relative value, by dividing post by pre force (defined as the mean value of the last three twitches of the pacing period) at each time point, thus providing potentiation values for Post 10 and Post 30. Figure 11 shows representative twitch force traces from muscles of both genotypes, with Post 10 and Post 30 traces superimposed on Pre traces to demonstrate the effects of potentiation. Potentiation was greater in WT than skMLCK$^{-/-}$ muscles both at 10 ($p = .001$) and 30 ($p < .001$) seconds following the CS, at all lengths. For both genotypes at all lengths, potentiation was greater at 10 compared to 30 seconds after the CS (all $p < .001$). These data are summarized in Table 8.

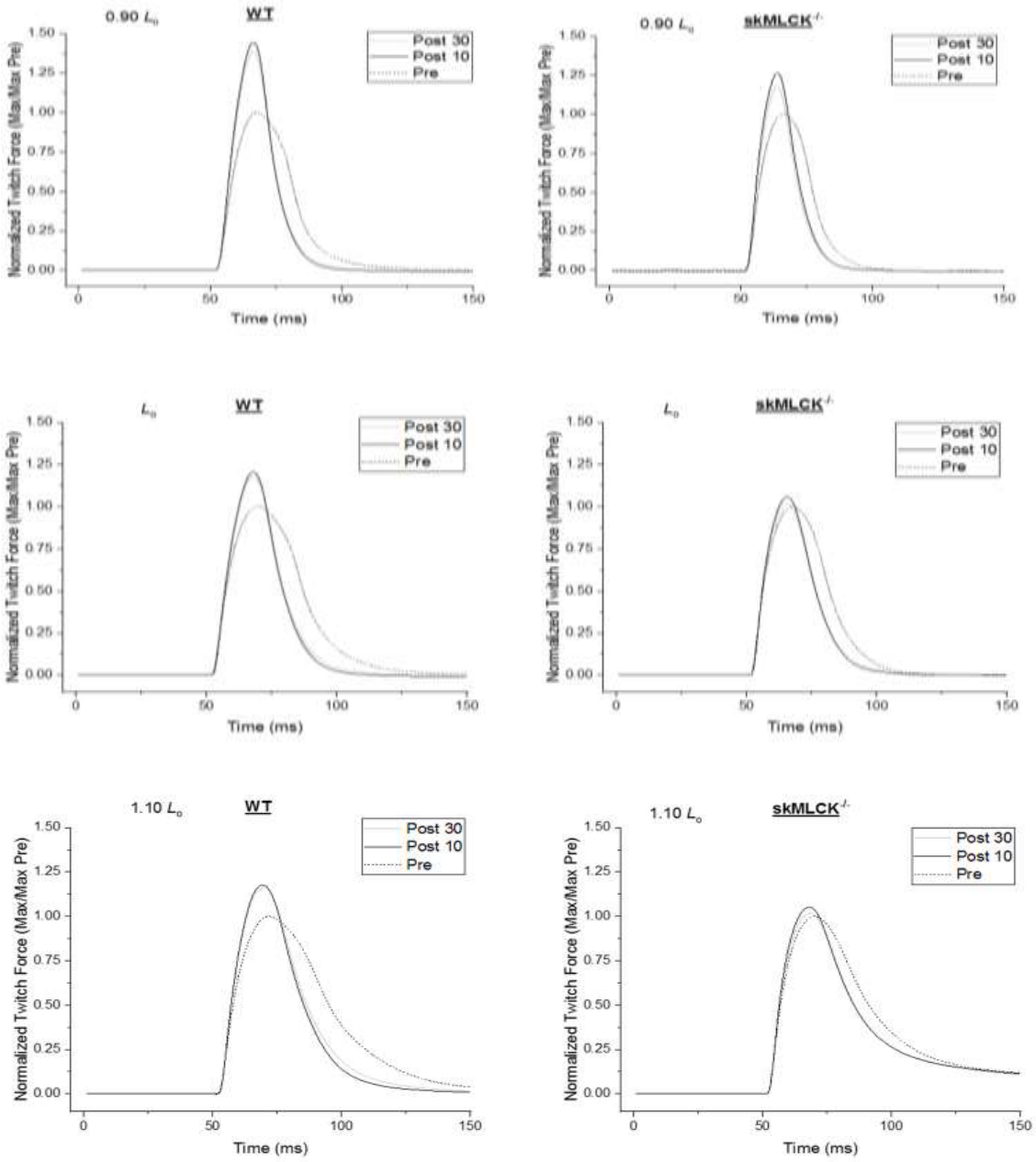

Fig. 11. Representative twitch force traces for a typical WT (left) and a typical skMLCK $^{-/-}$ (right) mouse EDL muscle, at 0.90 L_o (top), L_o (middle) and 1.10 L_o (bottom). Force is normalized to the maximum value of Pre twitch force (mean of last three twitches of pacing period) in each case. Note that potentiation appears markedly enhanced at 0.90 L_o for both genotypes. Potentiation is greater in the WT muscle at all lengths shown.

WT

Relative Muscle Length (L/Lo)	0.90	0.95	1	1.05	1.10
Potentiation (% Pre P_t) at Post 10	44.31 ± 4.6*†	19.99 ± 1.7*†	16.95 ± 1.6*†	17.85 ± 1.5*†	16.92 ± 1.3*†
Potentiation (% Pre P_t) at Post 30	37.2 ± 4.3**	16.07 ± 1.5**	13.92 ± 1.4**	15.45 ± 1.6**	14.99 ± 1.2**

skMLCK$^{-/-}$

Relative Muscle Length (L/Lo)	0.90	0.95	1	1.05	1.10
Potentiation (% Pre P_t) at Post 10	33.55 ± 6.2†	11.89 ± 1.6†	7.35 ± 1.5†	9.64 ± 1.6†	9.14 ± 1.8†
Potentiation (% Pre P_t) at Post 30	21.99 ± 4.2	5.65 ± 1.1	2.77 ± 1.2	4.64 ± 0.9	5.18 ± 1.4

Table 8. Mean potentiation (+ % Pre) values at Post 10 and Post 30, for WT (top, n=12) and skMLCK$^{-/-}$ (bottom, n=12) EDL muscles. Values are mean ± SEM. * significantly different than skMLCK $^{-/-}$ at the same time point and length ($p < .05$), ** significantly different than skMLCK $^{-/-}$ at the same time point and length ($p < .001$), † significantly different than Post 30 within genotype ($p < .001$)

Potentiation was dependent on muscle length in both genotypes, both at 10 ($p < .001$) and 30 ($p < .001$) seconds after the CS. Importantly, the pattern of length-dependence was similar between WT and skMLCK$^{-/-}$ muscles, as shown by the non-significant time x muscle length x genotype, and muscle length x genotype interactions (both $p > .05$) (Figure 12).

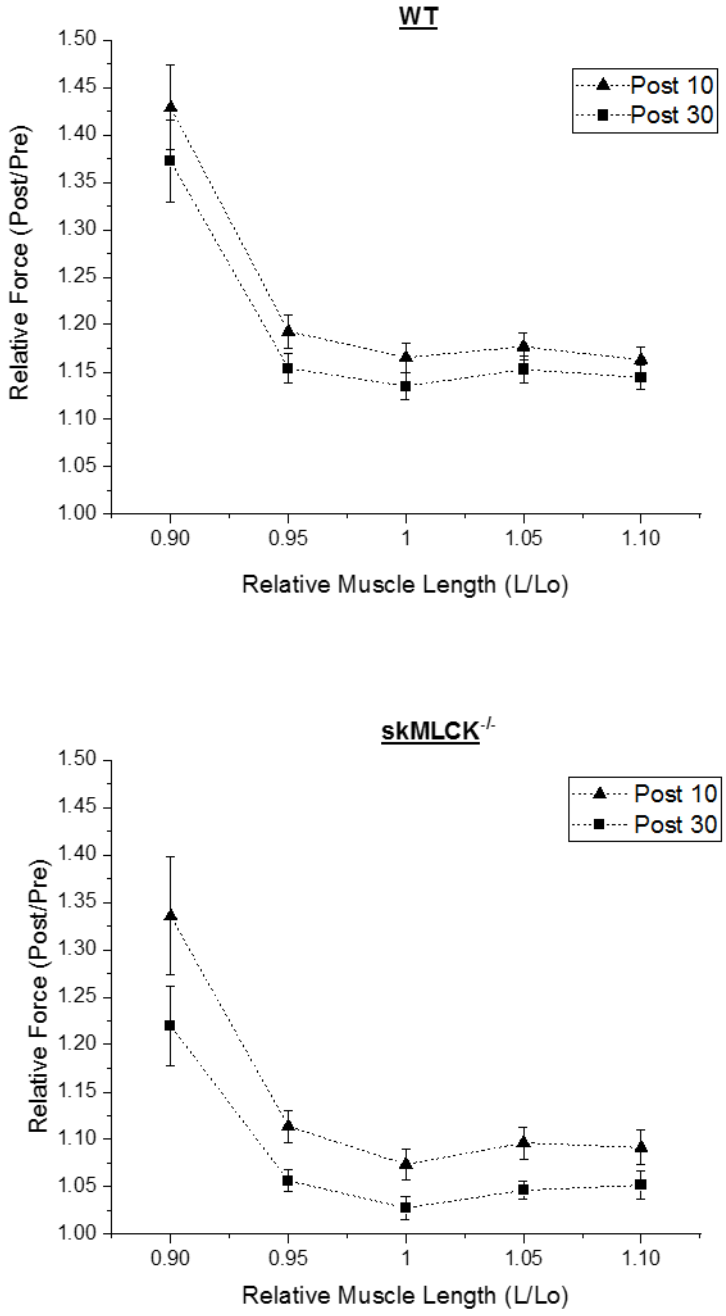

Fig. 12. Relative force (i.e., potentiation) – muscle length relationship for WT (top, n=12) and skMLCK$^{-/-}$ (bottom, n=12) EDL mouse muscles. Note that at both Post 10 and Post 30, WT > skMLCK$^{-/-}$ at all lengths. Additionally, in all cases Post 10 > Post 30. Error bars represent SEM.

Furthermore, trend analysis revealed that the length-dependence of potentiation was similar between Post 10 and Post 30, with both exhibiting significant linear, quadratic and cubic trends (all $p < .001$), which explained comparable total trend portions. Specifically at Post 10 and Post 30, linear trends explained 55.62% and 50.18% respectively, quadratic trends 34.40% and 39.61%, and cubic trends 9.85% and 10% (Table 9).

Relative Force (Post/Pre)		
Time x Muscle Length - F: 22.646*	Post 10 - F: 47.503*	Post 30 - F: 44.893*
% Variance Accounted	Post 10	Post 30
Linear: Quadratic: Cubic: 4th Order:	55.62%* 34.40%* 9.85%* NS	50.18%* 39.61%* 10%* NS

Table 9. Trend components of the polynomial contrast analysis for the simple main effects of muscle length at each time point. The ANOVA F-values for the Time x Muscle Length interaction, as well as the simple main effects of length at each time point are presented. At the bottom of the table, the percent variance explained by each significant trend component for each simple main effect can be found. * $p < .001$, NS = non-significant

In total, these findings suggest that: i) the pattern of the length-potentiation relationship was independent of genotype ii) it did not meaningfully differ between the 10- and 30-second timepoint after the CS iii) potentiation magnitude was greater in WT than skMLCK$^{-/-}$ muscles at all times and muscle lengths iv) Post 10 potentiation > Post 30 potentiation for both genotypes in all cases. Thus, while skMLCK ablation attenuated potentiation magnitude, it did not appear to influence the pattern of dependence of potentiation on muscle length, contrary to the initial hypothesis.

Summary of Force and Force Potentiation Data

WT

	Relative Muscle Length				
Condition	0.90	0.95	1.00	1.05	1.10
Pre (mN)	36.7 ± 3.3	47.6 ± 3.6	51.3 ± 3.4	49.3 ± 3.5	45 ± 3.3
Post 10 (mN)	52 ± 3.7*†	56.8 ± 3.9*†	59.8 ± 3.8*†	58 ± 3.9*†	52.5 ± 3.8*†
Post 30 (mN)	49.5 ± 3.6*	55 ± 3.8*	58.3 ± 3.7*	56.8 ± 3.8*	51.7 ± 3.7*
Pot 10 (% change vs Pre)	44.31 ± 4.6*†	19.99 ± 1.7*†	16.95 ± 1.6*†	17.85 ± 1.5*†	16.92 ± 1.3*†
Pot 30 (% change vs Pre)	37.2 ± 4.3*	16.07 ± 1.5*	13.92 ± 1.4*	15.45 ± 1.6*	14.99 ± 1.2*
Po (Tetanic Force, in mN)	180.3 ± 12.1	198.7 ± 12.7	211.7 ± 13.1	199.2 ± 12.9	179.2 ± 12.9

skMLCK$^{-/-}$

	Relative Muscle Length				
Condition	0.90	0.95	1.00	1.05	1.10
Pre (mN)	32.9 ± 3.1	45.2 ± 3.3	48.9 ± 3.7	47.4 ± 3.9	41.1 ± 4.1
Post 10 (mN)	42.1 ± 3.2†	49.9 ± 3.1†	52 ± 3.5†	51.5 ± 3.7†	44.3 ± 4†
Post 30 (mN)	38.9 ± 3.1	47.4 ± 3.1	49.9 ± 3.4	49.3 ± 3.7	42.8 ± 3.9
Pot 10 (% change vs Pre)	33.55 ± 6.2†	11.89 ± 1.6†	7.35 ± 1.5†	9.64 ± 1.6†	9.14 ± 1.8†
Pot 30 (% change vs Pre)	21.99 ± 4.2	5.65 ± 1.1	2.77 ± 1.2	4.64 ± 0.9	5.18 ± 1.4
Po (Tetanic Force, in mN)	180.3 ± 17.8	210.8 ± 18.5	224.1 ± 20.4	217.2 ± 20.3	187.1 ± 18.8

Table 10. Summary of force (mN) and force potentiation (Pot) (+ % Pre) data for WT (top, n=12) and skMLCK $^{-/-}$ (bottom, n=12) mouse EDL muscles at all experimental relative muscle lengths (L/L_o). Values are mean ± SEM. *significantly different than skMLCK$^{-/-}$ at the same time point and muscle length ($p < .05$), † significantly different than corresponding value at Post 30 within genotype ($p < .05$)

IV. +dF/dt and +dF/dt Potentiation

+*d*F/*d*t displayed qualitatively similar results to force, as expected by the well-established effects of potentiation on RFD (e.g., Vandenboom et al., 1995). Unpotentiated +*d*F/*d*t was similar between genotypes at all lengths ($p > .05$), as summarized in Table 11.

WT

Relative Muscle Length (L/Lo)	0.90	0.95	1	1.05	1.10
+*d*F/*d*t (Pre)	4.6 ± 0.4	6 ± 0.4	6.3 ± 0.4	5.9 ± 0.4	5.2 ± 0.4

skMLCK$^{-/-}$

Relative Muscle Length (L/Lo)	0.90	0.95	1	1.05	1.10
+*d*F/*d*t (Pre)	4.4 ± 0.3	6 ± 0.3	6.3 ± 0.3	5.8 ± 0.4	4.8 ± 0.4

Table 11. Mean +*d*F/*d*t (mN/ms) values at Pre for WT (top, n=12) and skMLCK$^{-/-}$ (bottom, n=12) mouse EDL muscles. Values are mean ± SEM. No significant differences between genotypes at any length ($p > .05$).

Following the CS, +*d*F/*d*t was significantly greater in WT when compared to skMLCK$^{-/-}$ muscles at both 10 ($p = .014$) and 30 ($p = .007$) seconds, at all lengths. For both genotypes at all lengths (all $p < .001$), +*d*f/*d*t was greatest at Post 10, while at Post 30 +*d*F/*d*t magnitude had declined but was still elevated in comparison to Pre (i.e., Post 10 > Post 30 > Pre). These observations are summarized in Table 12.

WT

Relative Muscle Length (L/Lo)	0.90	0.95	1	1.05	1.10
+*d*F/*d*t Post 10	6.6 ± 0.4*†	7.1 ± 0.4*†	7.4 ± 0.4*†	7.2 ± 0.5*†	6.5 ± 0.4*†
+*d*F/*d*t Post 30	6.3 ± 0.4**	6.9 ± 0.4**	7.3 ± 0.4**	7.1 ± 0.5**	6.4 ± 0.4**

skMLCK $^{-/-}$

Relative Muscle Length (L/Lo)	0.90	0.95	1	1.05	1.10
+*d*F/*d*t Post 10	5.9 ± 0.3†	6.8 ± 0.3†	6.9 ± 0.3†	6.7 ± 0.4†	5.6 ± 0.4†
+*d*F/*d*t Post 30	5.5 ± 0.3	6.6 ± 0.3	6.7 ± 0.3	6.5 ± 0.4	5.4 ± 0.4

Table 12. Mean +*d*F/*d*t (mN/ms) values at Post 10 and Post 30 for WT (top, n=12) and skMLCK $^{-/-}$ (bottom, n=12) mouse EDL muscles. Values are mean ± SEM. * significantly different than skMLCK $^{-/-}$ at the same time point and length ($p < .05$), ** significantly different than skMLCK $^{-/-}$ at the same time point and length ($p < .05$), † significantly different than Post 30 within genotype ($p < .001$)

+*d*F/*d*f was dependent on muscle length at all time points (all $p < .001$), but the pattern of length-dependence was again not different between genotypes, as evident by the non-significant time x muscle length x genotype ($p > .05$) and muscle length x genotype ($p > .05$) interactions (Figure 13).

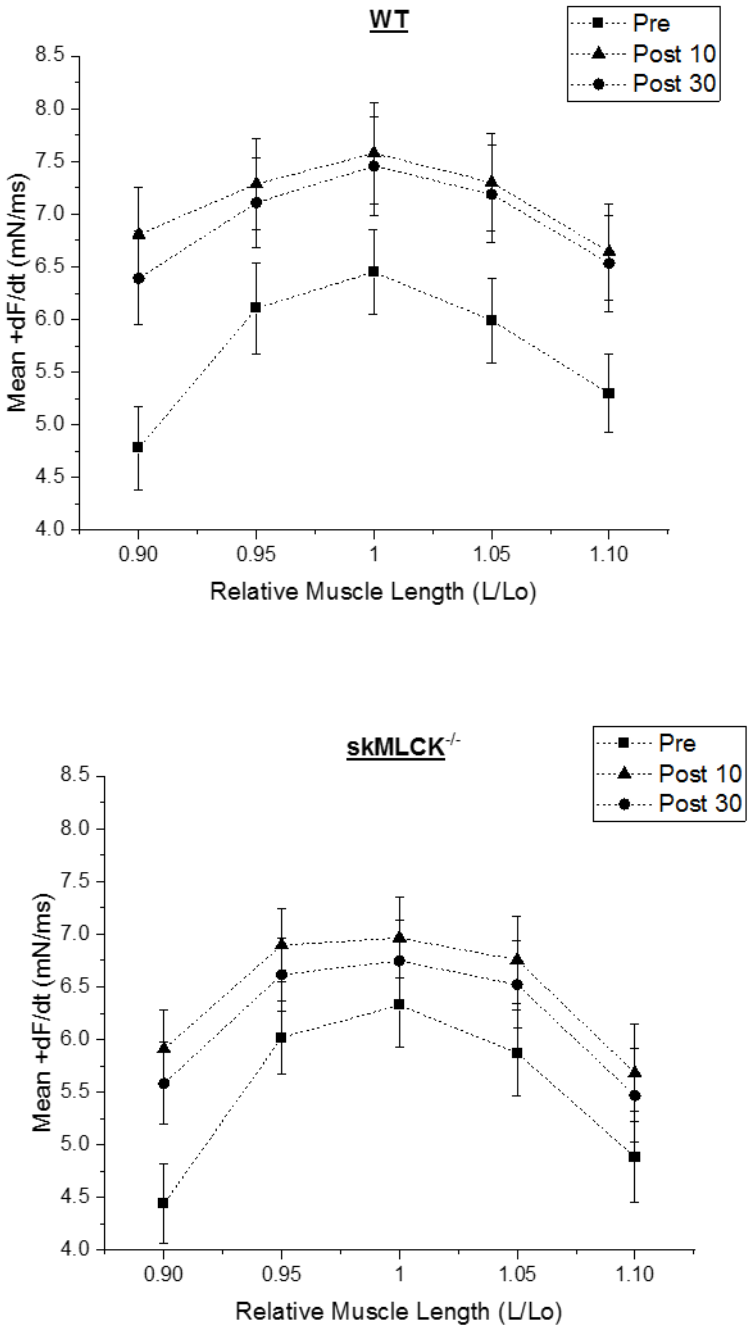

Fig. 13. +*d*F/*d*t – muscle length relationship for WT (top, n=12) and skMLCK $^{-/-}$ (bottom, n=12) mouse EDL muscles. Pre +*d*F/*d*t was not different between genotypes, but at Post 10 and Post 30, +*d*F/*d*t was greater for WT across lengths. Note that for both genotypes at all lengths, Pre < Post 30 < Post 10. Error bars represent SEM.

Moreover, while the pattern of length-dependence was largely similar pre- and post-CS, there were small differences, as indicated by trend analysis. At Pre, there was a significant quadratic trend ($p < .001$) which could explain 94.31% of the overall trend, as well as a significant cubic trend ($p < .001$), explaining 2.5% of the overall trend. In contrast, at Post 10 and Post 30, only the quadratic trend was significant ($p < .001$), explaining 97.57% and 99.76% of the observed variance respectively (Table 13). While these differences are not as pronounced as the ones observed for Pt, they again appear to represent the relatively greater increase of $+dF/dt$ at 0.9 L_o following the CS, as can be observed graphically.

+dF/dt			
Time x Muscle Length - F: 29.359*	Pre – F: 47.694*	Post 10 - F: 23.817*	Post 30 - F: 24.138*
% Variance Accounted	Pre	Post 10	Post 30
Linear:	NS	NS	NS
Quadratic:	94.31%*	97.57%*	99.76%*
Cubic:	2.5%*	NS	NS
4th Order:	NS	NS	NS

Table 13. Trend components of the polynomial contrast analysis for the simple main effects of muscle length at each time point. The ANOVA F-values for the Time x Muscle Length interaction, as well as the simple main effects of length at each time point are presented. At the bottom of the table, the percent variance explained by each significant trend component for each simple main effect can be found. * $p < .001$, NS = non-significan

Regarding +*d*F/*d*t potentiation, WT muscles exhibited greater magnitudes than their skMLCK$^{-/-}$ counterparts both at Post 10 ($p = .024$) and Post 30 ($p < .001$). Additionally, in both genotypes at all lengths potentiation was greater at Post 10 than Post 30 (all $p < .001$). These findings are summarized in Table 14.

WT

Relative Muscle Length (L/Lo)	0.90	0.95	1	1.05	1.10
+*d*F/*d*t Potentiation Post 10	45.7 ± 4*†	20.5 ± 2.2*†	17.5 ± 1.7*†	22.1 ± 1.6*†	25.3 ± 1.6*†
+*d*F/*d*t Potentiation Post 30	40 ± 3.6**	17.5 ± 2**	15.6 ± 1.5**	20.2 ± 1.5**	23.2 ± 1.6**

skMLCK$^{-/-}$

Relative Muscle Length (L/Lo)	0.90	0.95	1	1.05	1.10
+*d*F/*d*t Potentiation Post 10	39.9 ± 8.7†	15.3 ± 1.9†	10.6 ± 1.6†	15.7 ± 1.3†	17.1 ± 1.7†
+*d*F/*d*t Potentiation Post 30	30 ± 5.7	10.4 ± 1.4	7 ± 1.4	11.5 ± 1	12.7 ± 1.4

Table 14. Mean +*d*F/*d*t potentiation (+ % Pre) values at Post 10 and Post 30, for WT (top, n=12) and skMLCK $^{-/-}$ (bottom, n=12) mouse EDL muscles, at all experimental lengths. Values are mean ± SEM. * significantly different than skMLCK $^{-/-}$ at the same time point and length ($p < .05$), ** significantly different than skMLCK $^{-/-}$ at the same time point and length ($p < .001$), † significantly different than Post 30 within genotype ($p < .001$)

+*d*F/*d*t potentiation was related to muscle length both at Post 10 ($p < .001$) and Post 30 ($p < .001$), but this effect was not dependent on genotype, as indicated by the absence of significant time x muscle length x genotype ($p < .05$), and muscle length x genotype ($p < .05$) interactions (Figure 14).

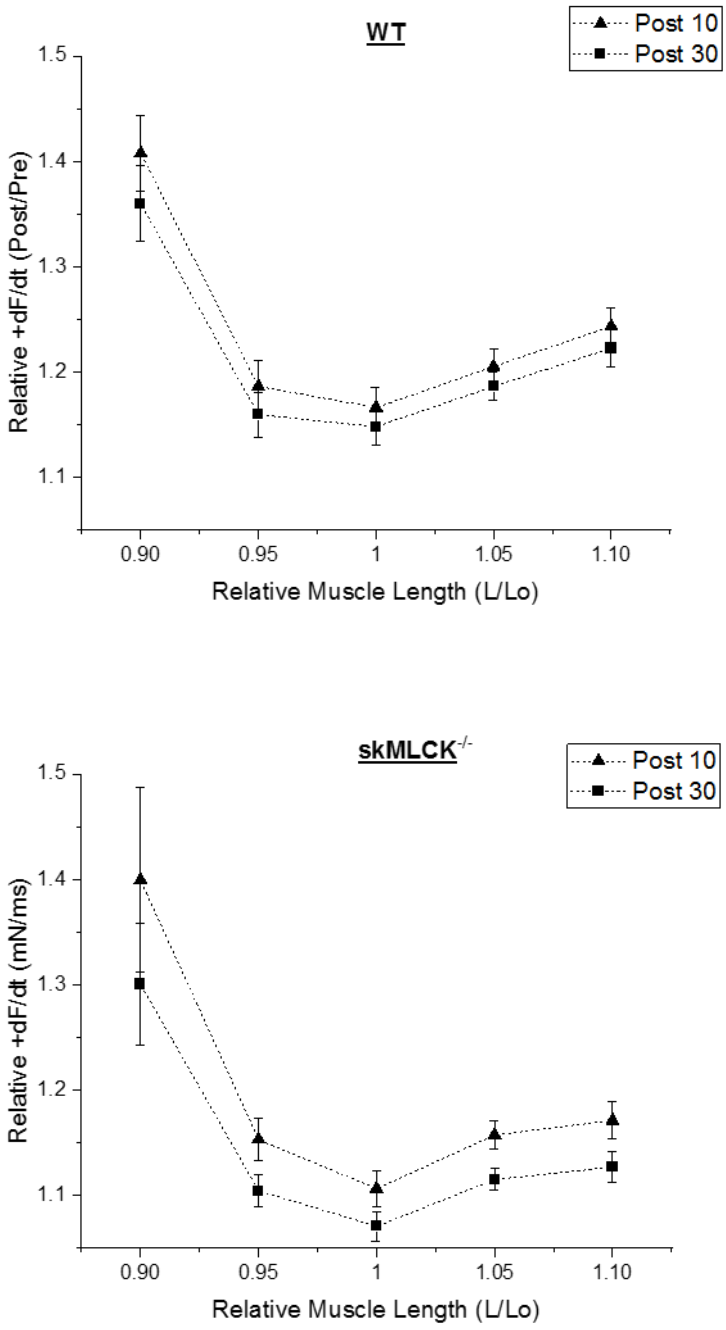

Fig. 14. Relative +*d*F/*d*t – muscle length relationship for WT (top, n=12) and skMLCK$^{-/-}$ (bottom, n=12) EDL. Note that at both Post 10 and Post 30, WT > skMLCK$^{-/-}$ at all lengths. Additionally, in all cases, Post 10 > Post 30. Error bars represent SEM.

Subsequent trend analysis indicated that at both time points, the pattern of length-dependence was similar, with significant linear, quadratic and cubic trends (all $p < .001$) which could explain 33.78% and 29.83%, 55.22% and 57.80% and 10.92% and 12.37% of the total observed trends, respectively (Table 15).

Relative +*d*F/*d*t (Post/Pre)		
Time x Muscle Length - F: 7.547**	Post 10 - F: 29.447*	Post 30 - F: 34.339*
% Variance Accounted	Post 10	Post 30
Linear: Quadratic: Cubic: 4th Order:	33.78%* 55.22%* 10.92%* NS	29.83%* 57.80%* 12.37%* NS

Table 15. Trend components of the polynomial contrast analysis for the simple main effects of muscle length at each time point. The ANOVA F-values for the Time x Muscle Length interaction, as well as the simple main effects of length at each time point are presented. At the bottom of the table, the percent variance explained by each significant trend component for each simple main effect can be found. * $p < .001$, ** $p < .05$, NS = non-significant

Collectively, these findings indicate that: i) the pattern of length-dependence of +*d*F/*d*t potentiation was independent of genotype ii) it was also similar between Post 10 and Post 30, and iii) +*d*F/*d*t potentiation magnitude was greater in WT than skMLCK$^{-/-}$ muscles, regardless of time and length. As expected by previous literature (e.g., Vandenboom et al., 1995), +*d*F/*d*t potentiation characteristics closely corresponded to force potentiation in a qualitative manner.

V. -dF/dt and -dF/dt Potentiation

-*d*F/*d*t values were similar between WT and skMLCK$^{-/-}$ muscles both prior to and following the CS, at all lengths. Regardless of muscle length, -*d*F/*d*t decreased significantly after the CS and Post 10 values were significantly greater than Post 30 values (all $p < .001$), which in turn remained higher than Pre values (all $p < .001$) (i.e., Post 10 > Post 30 > Pre). These data are summarized in Table 16.

WT

Relative Muscle Length (L/Lo)	0.90	0.95	1	1.05	1.10
-*d*F/*d*t Pre	-2.8 ± 0.3	-3.3 ± 0.3	-2.8 ± 0.2	-2.1 ± 0.1	-1.4 ± 0.1
-*d*F/*d*t Post 10	-4.2 ± 0.2*†	-4 ± 0.3*†	-3.6 ± 0.2*†	-2.7 ± 0.1*†	-2.1 ± 0.1*†
-*d*F/*d*t Post 30	-4 ± 0.2*	-3.9 ± 0.2*	-3.5 ± 0.2*	-2.7 ± 0.1*	-2 ± 0.1*

skMLCK $^{-/-}$

Relative Muscle Length (L/Lo)	0.90	0.95	1	1.05	1.10
-*d*F/*d*t Pre	-2.7 ± 0.3	-3.3 ± 0.3	-2.6 ± 0.3	-1.9 ± 0.2	-1.2 ± 0.1
-*d*F/*d*t Post 10	-4 ± 0.3*†	-4.1 ± 0.3*†	-3.6 ± 0.3*†	-2.6 ± 0.2*†	-1.8 ± 0.1*†
-*d*F/*d*t Post 30	-3.6 ± 0.2*	-3.8 ± 0.3*	-3.3 ± 0.3*	-2.4 ± 0.2*	-1.7 ± 0.1*

Table 16. Mean -dF/dt at Pre, Post 10 and Post 30 for WT (top, n=12) and skMLCK$^{-/-}$ (bottom, n=12) mouse EDL muscles. Note that WT and skMLCK$^{-/-}$ values are not significantly different in any case. Values are mean ± SEM. *significantly different than Pre within genotype ($p < .001$), † significantly different than Post 30 within genotype ($p < .001$)

-*d*F/*d*t was dependent on muscle length, and the pattern of this relationship was not different between genotypes as shown by the non-significant time x muscle length x genotype ($p > .05$) and muscle length x genotype ($p > .05$) interactions (Figure 15). Trend analysis revealed that the length-dependence of -*d*F/*d*t differed pre- compared to post-CS. Specifically, at Pre, there were significant linear, quadratic and cubic trends (all $p < .001$), which could explain 74.85%, 19.04% and 5.78% of the total trend respectively. On the other hand, at Post 10 and Post 30, there were again significant linear, quadratic, and cubic trends (all $p < .001$), but the linear trends were markedly more pronounced, explaining 92.28% and 90.22% of the observed variance respectively (Table 17). This can be attributed to the relatively greater increase of -*d*F/*d*t at 0.9 L_o after the CS when compared to other lengths, as can be observed graphically. While Pre -*d*F/*d*t appeared to be lower at 0.9 L_o than 0.95 L_o, and then again progressively decrease as length increased, at Post 10 and Post 30 the relationship appeared mostly linear, with a steady decrease of -*d*F/*d*t as length increased.

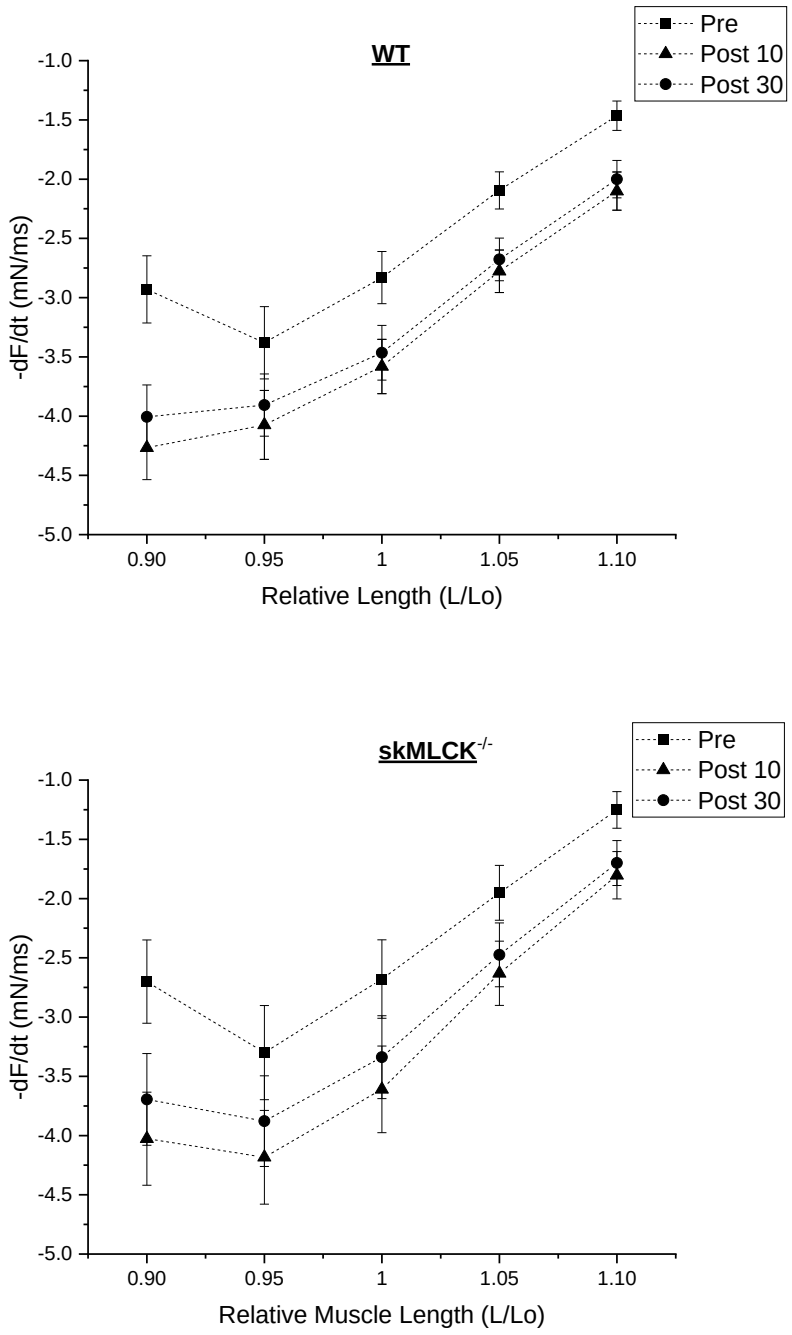

Fig. 15. -*d*F/*d*t – muscle length relationship for WT (top, n=12) and skMLCK$^{-/-}$ (bottom, n=12) EDL. Note that for both genotypes, at all lengths, Pre < Post 30 < Post 10. WT values not significantly different than skMLCK$^{-/-}$ values at all lengths and timepoints.

-dF/dt			
Time x Muscle Length - F: 24.869*	Pre – F: 71.892*	Post 10 - F: 143.961*	Post 30 - F: 126.776*
% Variance Accounted	Pre	Post 10	Post 30
Linear:	74.85%*	92.28%*	90.22%*
Quadratic:	19.04%*	6.5%*	8.42%*
Cubic:	5.78%*	1.16%*	1.28%
4th Order:	NS	NS	NS

Table 17. Trend components of the polynomial contrast analysis for the simple main effects of muscle length at each time point. The ANOVA F-values for the Time x Muscle Length interaction, as well as the simple main effects of length at each time point are presented. At the bottom of the table, the percent variance explained by each significant trend component for each simple main effect can be found. * $p < .001$, NS = non-significant

The above findings were somewhat expected, since prior literature suggests that the effects of a CS to accelerate twitch relaxation do not appear to be dependent on RLC phosphorylation, as discussed earlier (Vandenboom, 2017).

Potentiation of -*d*F/*d*t was similar between genotypes at all lengths and timepoints. In all cases, potentiation magnitude was greater at Post 10 than Post 30 (all $p < .001$). These observations are summarized in table 18.

WT

Relative Muscle Length (L/Lo)	0.90	0.95	1	1.05	1.10
-*d*F/*d*t Potentiation Post 10	52.1 ± 7.1*	23.7 ± 4.9*	28.9 ± 4.3*	33.8 ± 4.6*	44.3 ± 4.3*
-*d*F/*d*t Potentiation Post 30	43.7 ± 6.9	18.6 ± 4.3	24.6 ± 4.9	29.4 ± 3.7	37.3 ± 3.6

skMLCK $^{-/-}$

Relative Muscle Length (L/Lo)	0.90	0.95	1	1.05	1.10
-*d*F/*d*t Potentiation Post 10	62.6 ± 10.7*	33.1 ± 6*	40.7 ± 5.7*	39.3 ± 4.8*	47.1 ± 3.2*
-*d*F/*d*t Potentiation Post 30	46.2 ± 7.7	22.6 ± 5.2	29 ± 4.7	29.7 ± 3.6	38.6 ± 3.3

Table 18. Mean -*d*F/*d*t potentiation (+ % Pre) values at Post 10 and Post 30 for WT (top, n=12) and skMLCK $^{-/-}$ (bottom, n=12) mouse EDL muscles. No significant differences between genotypes. *significantly different than Post 30 within genotype ($p < .001$)

Furthermore, -dF/dt potentiation was related to muscle length at both Post 10 and Post 30 (Figure 16), with both time points exhibiting similar patterns of length-dependence as indicated by trend analysis. In detail, both time points exhibited significant quadratic (both $p < .001$), cubic (both $p < .001$) and 4^{th} order (both $p < .05$) trends, which could explain 73.46% and 74.97%, 15.81% and 16.87%, and 7.27% and 7.36% of the observed total trends respectively (Table 19). In both cases, the relationship reflected the -*d*F/*d*t observations, with potentiation being substantially greater at 0.9 L_o than 0.95 L_o and then increasing linearly as length increased (i.e., -*d*F/*d*t magnitude and potentiation were inversely related), thus explaining the dominant quadratic trend.

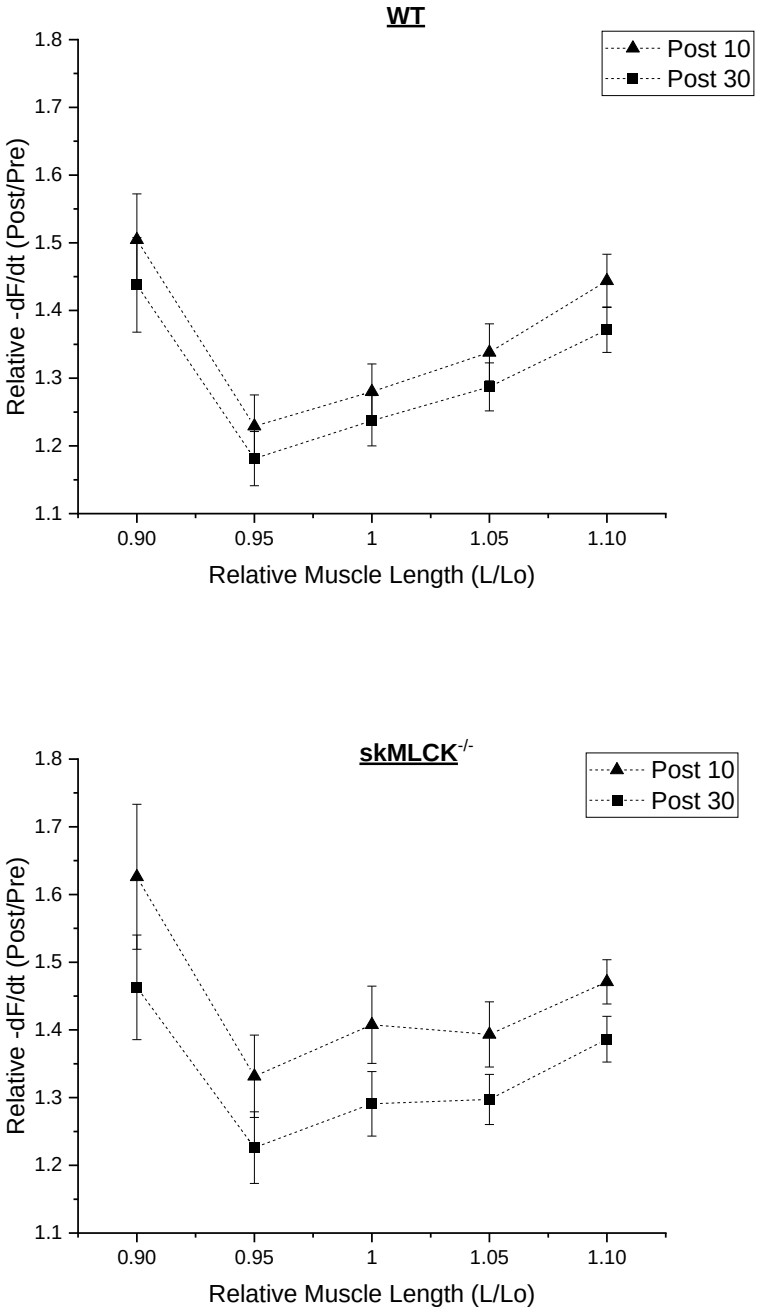

Fig. 16. Relative -*d*F/*d*t – muscle length relationship for WT (top, n=12) and skMLCK$^{-/-}$ (bottom, n=12) EDL mouse muscles. Note that for both genotypes, at all lengths, Post 30 < Post 10. Additionally, WT values did not differ significantly from skMLCK$^{-/-}$ values at all lengths and timepoints.

Relative -*d*F/*d*t (Post/Pre)		
Time x Muscle Length - F: 4.265**	Post 10 - F: 18.076*	Post 30 - F: 16.719*
% Variance Accounted	Post 10	Post 30
Linear: Quadratic: Cubic: 4th Order:	NS 73.46%* 15.81%* 7.27%**	NS 74.97%* 16.87%* 7.36%**

Table 19. Trend components of the polynomial contrast analysis for the simple main effects of muscle length at each time point. The ANOVA F-values for the Time x Muscle Length interaction, as well as the simple main effects of length at each time point are presented. At the bottom of the table, the percent variance explained by each significant trend component for each simple main effect can be found. * $p < .001$, ** $p < .05$, NS = non-significant

VI. ½ Relaxation Time and Time to Peak Tension

Unpotentiated ½ RT was similar between WT and skMLCK$^{-/-}$ muscles ($p > .05$). Following the CS, ½ RT time was significantly decreased at all lengths in both WT and skMLCK $^{-/-}$ muscles at both Post 10 and Post 30 (all $p <. 001$). Values were not significantly different between genotypes, both at Post 10 and Post 30 (both $p < .05$). In addition, Post 10 values were in all cases similar to Post 30 values ($p > .05$), indicating that the effects of the CS were retained until the 30-second timepoint (i.e., Post 10 = Post 30 < Pre). These data are summarized in Table 20.

WT

Relative Muscle Length (L/Lo)	0.90	0.95	1	1.05	1.10
½ RT Pre	10.3 ± 0.3	10.9 ± 0.4	13.7 ± 0.5	16.9 ± 0.5	22.3 ± 0.8
½ RT Post 10	7.7 ± 0.2*	9.1 ± 0.3*	11 ± 0.3*	13.6 ± 0.3*	16.5 ± 0.2*
½ RT Post 30	7.7 ± 0.2*	9.3 ± 0.3*	11.2 ± 0.3*	13.8 ± 0.5*	17.1 ± 0.6*

skMLCK $^{-/-}$

Relative Muscle Length (L/Lo)	0.90	0.95	1	1.05	1.10
½ RT Pre	10.1 ± 0.3	10.9 ± 0.3	14 ± 0.4	17.6 ± 0.7	23 ± 1.1
½ RT Post 10	6.7 ± 0.2*	7.7 ± 0.2*	9.7 ± 0.4*	12.5 ± 0.4*	15.5 ± 0.4*
½ RT Post 30	7 ± 0.2*	8.1 ± 0.2*	10 ± 0.4*	12.6 ± 0.4*	16 ± 0.6*

Table 20. Mean ½ RT (ms) at Pre, Post 10 and Post 30, for WT (top, n=12) and skMLCK $^{-/-}$ (bottom, n=12) mouse EDL muscles. Values are not significantly different between genotypes in any case. Note that for both genotypes, Post 10 values are not significantly different than Post 30 values at any length. *significantly different than Pre within genotype ($p < .001$)

½ RT was dependent on muscle length and this effect was similar between genotypes, as indicated by the absence of significant time x muscle length x genotype ($p > .05$) and muscle length x genotype ($p > .05$) interactions (Figure 17). The pattern of length-dependence of ½ RT appeared largerly unchanged across time; at Pre, there were significant linear ($p < .001$), quadratic ($p < .001$) and 4^{th} order ($p = .011$) trends, which could explain 93.29%, 6.53% and 0.15% of the observed variance respectively, while at Post 10 and Post 30 there were significant linear and quadratic trends (all $p < .001$), which could explain 97.35% and 97%, and 2.39% and 2.97% of the total trend respectively (Table 21). At all time points, ½ RT was greater with increasing muscle length.

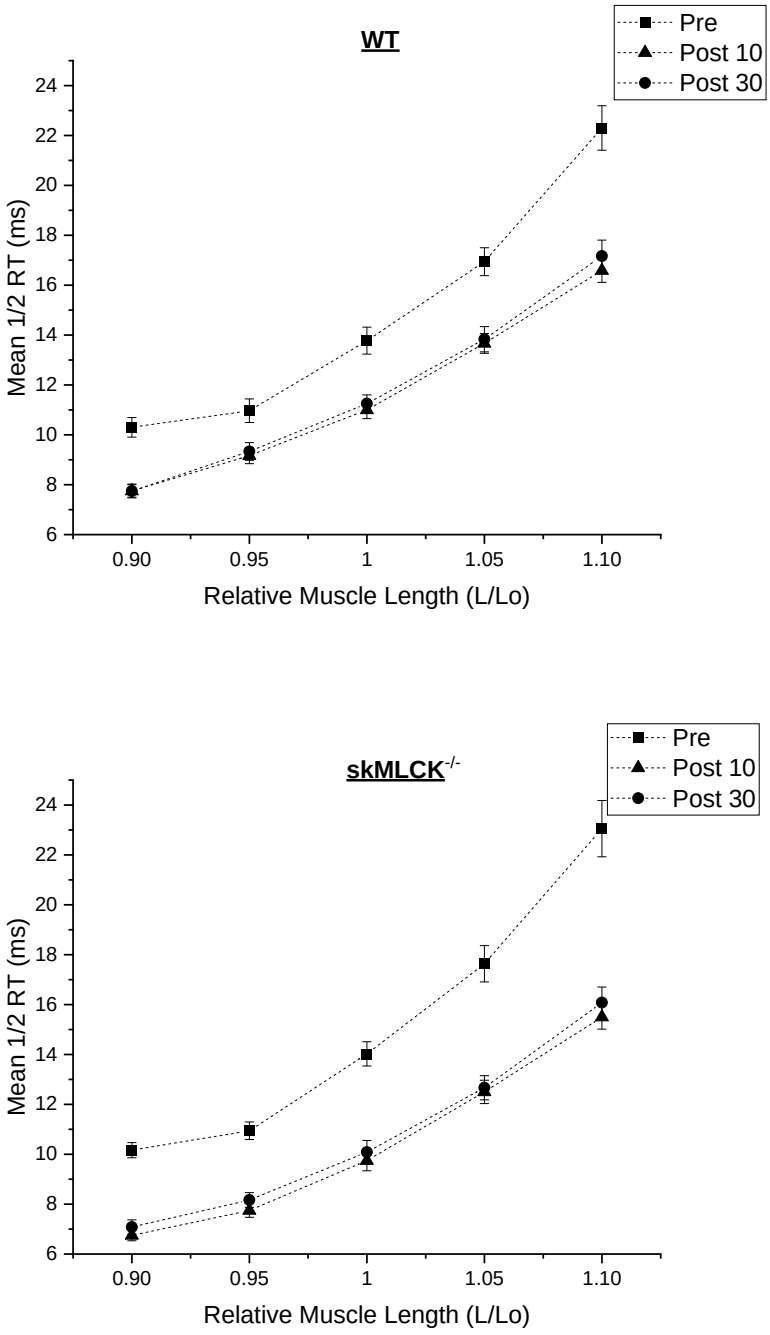

Fig. 17. ½ RT - muscle length relationship for WT (top, n=12) and skMLCK$^{-/-}$ (bottom, n=12) mouse EDL muscles. For both genotypes at all lengths, Pre > Post 10 = Post 30. WT values were not significantly different than skMLCK$^{-/-}$ values at any time point, at all lengths.

½ RT			
Time x Muscle Length - F: 32.821*	Pre – F: 267.395*	Post 10 - F: 576.818*	Post 30 - F: 317.889*
% Variance Accounted	Pre	Post 10	Post 30
Linear:	74.85%*	97.35%*	97%*
Quadratic:	19.04%*	2.39%	2.97%
Cubic:	NS	NS	NS
4th Order:	0.15%**	NS	NS

Table 21. Trend components of the polynomial contrast analysis for the simple main effects of muscle length at each time point. The ANOVA F-values for the Time x Muscle Length interaction, as well as the simple main effects of length at each time point are presented. At the bottom of the table, the percent variance explained by each significant trend component, for each simple main effect can be found. * $p < .001$, ** $p < .05$, NS = non-significant

In total, these findings indicate that: i) ½ RT was similar between WT and skMLCK$^{-/-}$ muscles both prior to and following the CS ii) ½ RT was positively associated with muscle length, and the pattern of this relationship was largely similar pre- and post-CS and iii) following the CS, ½ RT was significantly reduced, and this effect remained of the same magnitude until 30 s post-CS. These observations were not surprising, given that both WT and skMLCK$^{-/-}$ mouse EDL muscles have been shown to display reduced twitch duration and accelerated relaxation following a CS (Gittings et al., 2016).

TPT did not exhibit any significant interactions, but there were significant main effects of time ($p < .001$), length ($p < .001$) and genotype ($p < .05$). TPT was significantly greater in WT compared to skMLCK $^{-/-}$ muscles both prior to, and following the CS, at all lengths. In both genotypes, TPT was significantly reduced after the CS, with Post 10 values being similar to Post 30 values (all $p > .05$) at all lengths (all $p < .001$). These data are summarized in Table 22.

WT

Relative Muscle Length (L/Lo)	0.90	0.95	1	1.05	1.10
½ TPT Pre	15.3 ± 0.3	16 ± 0.2	17.1 ± 0.3	18.3 ± 0.2	19.2 ± 0.3
½ TPT Post 10	14.3 ± 0.2*	14.9 ± 0.2*	16.1 ± 0.2*	17 ± 0.2*	18 ± 0.2*
½ TPT Post 30	14.3 ± 0.2*	14.9 ± 0.3*	15.9 ± 0.2*	17 ± 0.2*	18 ± 0.2*

skMLCK $^{-/-}$

Relative Muscle Length (L/Lo)	0.90	0.95	1	1.05	1.10
½ TPT Pre	14.5 ± 3.3	15.3 ± 0.3	16.6 ± 0.3	17.8 ± 0.2	18.6 ± 0.3
½ TPT Post 10	13.1 ± 0.3*	13.9 ± 0.3*	15 ± 0.3*	15.9 ± 0.2*	16.8 ± 0.2*
½ TPT Post 30	12.9 ± 0.3*	13.5 ± 0.2*	14.9 ± 0.3*	16 ± 0.2*	17 ± 0.2*

Table 22. Mean TPT (ms) at Pre, Post 10 and Post 30 for WT (top, n=12) and skMLCK $^{-/-}$ (bottom, n=12) EDL mouse muscles. Note that at all time points and lengths, WT values are significantly greater than skMLCK $^{-/-}$ values. In both genotypes, Post 10 values are not significantly different than Post 30 values, at any length. *significantly different than Pre within genotype ($p < .001$)

Finally, TPT appeared to increase linearly with length (Figure 18), as also indicated by trend analysis; there was a significant linear trend ($p < .001$), which could explain 99.46% of the total trend, as well as a statistically significant but weak cubic trend ($p < .05$, accounting for 0.37% of total variance) (Table 23)

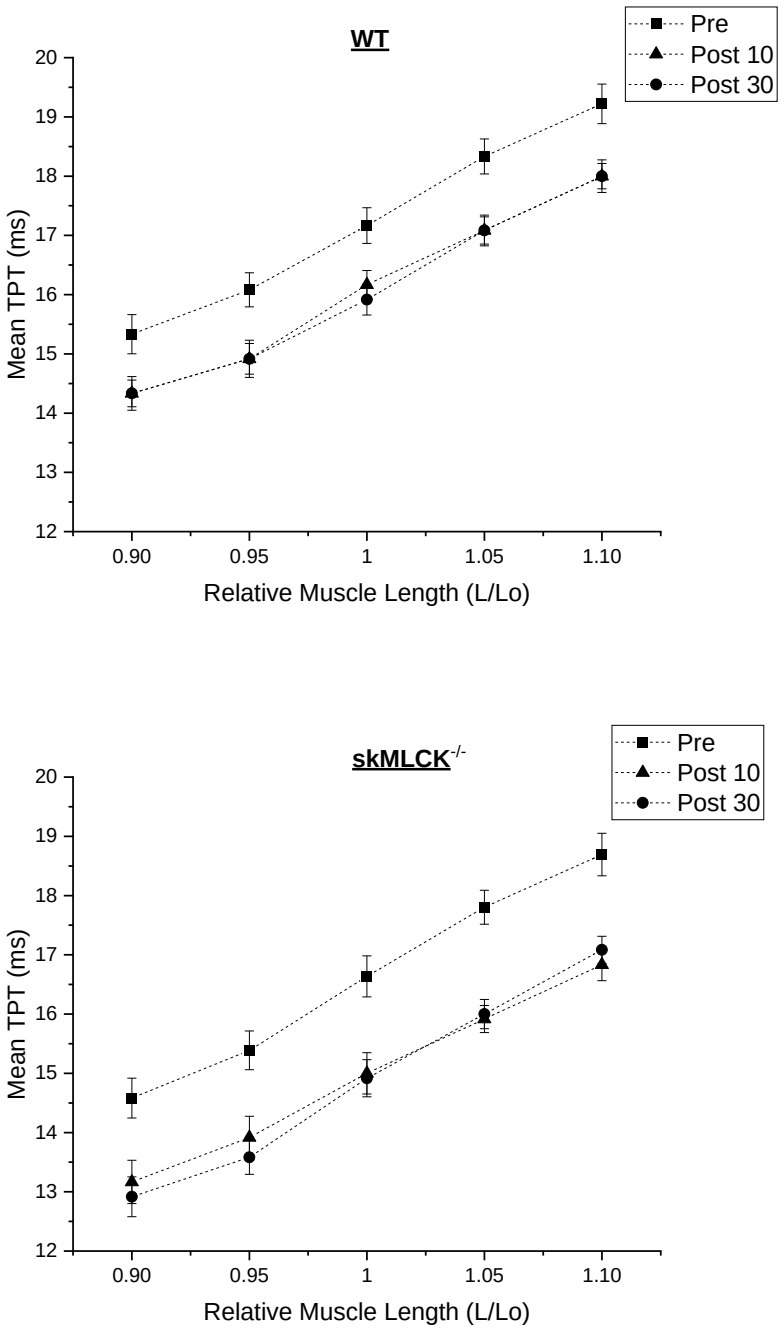

Fig. 18. TPT – muscle length relationship for WT (top, n=12) and skMLCK$^{-/-}$ (bottom, n=12) mouse EDL muscles. Note that for both genotypes at all lengths, Pre > Post 10 = Post 30. WT values were significantly greater than skMLCK$^{-/-}$ values at all lengths and timepoints.

TPT	
Main Effect: Muscle Length	F: 242.568*
% Variance Accounted	
Linear: 99,46%* Quadratic: NS Cubic: 0.37%** 4th Order: NS	

Table 23. Trend components of the polynomial contrast analysis for the main effect of muscle length. The ANOVA F-value for the main effect of length collapsed across genotypes and time is presented, along with the percent variance explained by each significant trend component. * $p < .001$, ** $p < .05$, NS = non-significant

Chapter Six: Discussion

The primary hypothesis of this thesis was that the length-dependence of activity-dependent force potentiation observed in rat gastrocnemius in situ (Rassier et al., 1997; 1998; Rassier & MacIntosh, 2000), and WT mouse EDL fiber bundles in vitro (Rassier & Herzog, 2002; Rassier & MacIntosh, 2002) would be attenuated in the skMLCK$^{-/-}$ mouse EDL. These findings have consistently shown that in wildtype experimental models, force potentiation appears to be inversely related to muscle or sarcomere length, with potentiation magnitude attenuated at long, and enhanced at short lengths. Even prior to the direct demonstration of the central role of RLC phosphorylation in potentiation by Zhi and coworkers through the skMLCK$^{-/-}$ model (Zhi et al., 2005), the length-dependence of potentiation had been attributed, at least partially, to the structural effects of RLC phosphorylation (e.g., Rassier et al., 1998). According to this model, the disorder/radial movement of myosin heads observed in

isolated thick filaments upon RLC phosphorylation (Levine et al., 1996), thought to structurally facilitate potentiation by increasing the potential for myosin-actin interactions (MacIntosh, 2010), would be redundant at long sarcomere lengths; since interfilament lattice spacing is reduced as sarcomere length is increased, actin-myosin interaction probability would already be high, and the radial displacement of myosin heads would not have a substantial additional effect (MacIntosh et al., 2010). Thus, since skMLCK$^{-/-}$ EDL muscles display attenuated post-tetanic and staircase potentiation in the absence of RLC phosphorylation (Zhi et al., 2005; Gittings et al., 2011; 2012; 2017), through as of yet unknown mechanisms, it was hypothesized that in this model, potentiation would not be dependent on muscle/sarcomere length to the same extent. Importantly, potentiation was still expected to differ between lengths, owing to length-dependent activation (Rassier et al., 1999). Specifically, the interaction of increased Ca^{2+} sensitivity and submaximal force at longer lengths with potentiation, as well as the fact that force differs with length in general (i.e., force is attenuated at short sarcomere lengths), would be expected to result in different potentiation magnitudes across sarcomere lengths, despite the absence of RLC phosphorylation.

Contrary to the initial hypothesis, the observed pattern of length-dependence of potentiation was similar between WT and skMLCK$^{-/-}$ EDL muscles. As expected, skMLCK ablation resulted in reduced potentiation across lengths, but the relationship of length with potentiation magnitude was surprisingly similar between genotypes. In accordance with previous findings (Rassier et al, 1997; 1998; Rassier & MacIntosh, 2000; 2002; Rassier & Herzog, 2002) potentiation appeared markedly enhanced at 0.9 L_o in comparison to other lengths. In contrast, although no direct comparisons were made, potentiation did not seem to differ markedly for lengths between 0.95 L_o and 1.10 L_o. This was supported by trend analysis, as both at Post 10 and Post 30, the linear

component explained approximately 50% of the total trend, and there were also substantial, statistically significant quadratic (~30%) and cubic (~10%) trends. Thus, both in WT and skMLCK$^{-/-}$ EDL, the robust linear relationship between muscle length and potentiation observed previously (Rassier et al., 1998; Rassier & Herzog, 2002; Rassier & MacIntosh, 2002), was not recapitulated. This does not necessarily mean that the findings presented here contradict prior observations. A potential explanation for this discrepancy is the fact that whole mouse EDL muscles were used here, in contrast to mouse EDL fiber bundles (Rassier & Herzog, 2002; Rassier & MacIntosh, 2002), and rat gastrocnemius (Rassier et al., 1997; 1998; Rassier & MacIntosh, 2000) in previous works. Although the viscoelastic properties and passive force-length relationships of mouse EDL and rat gastrocnemius have not been compared directly, mouse EDL fiber bundles could possibly be less compliant than a whole mouse EDL musculotendinous unit, due to the potential presence of a greater amount of tendon in the latter. Previous works have specifically attempted to minimize the amount of tendon in the fiber bundle preparations (Rassier & Herzog, 2002; Rassier & MacIntosh, 2002). Since sarcomere length was not controlled here, active force at the longer lengths used may have been underestimated, due to using the passive force value measured prior to contraction initiation for its calculation (for a review on this issue, see MacIntosh, 2017). In-series compliance due to the tendon would enable internal sarcomere shortening during the contraction, and thus the passive force present at the peak of force production would be lower than the value measured before the contraction. This effect would be apparent both in high and low frequency contractions, but it would be more pronounced in the tetani, as internal shortening magnitude would be greater (MacIntosh, 2017). In turn, this could mean that the longer relative lengths used here may not have corresponded to sarcomere lengths long enough to detect a substantial

reduction in potentiation magnitude. Essentially, despite forces appearing to decline at the longer lengths, it is possible that they nevertheless correspond to the plateau of the force-length relationship; this could have been verified if passive force at the final sarcomere length was used to calculate active force, as has been suggested (MacIntosh, 2017). Unfortunately, fascicle or sarcomere length measurements which would enable this were not available. If that is indeed the case, measurements at relative lengths longer than 1.10 L_o may have resulted in a more linear length-potentiation relationship, as well as revealed substantial differences between genotypes.

More generally, it is interesting to consider that factors affected by compliance may interact with potentiation in a length-dependent fashion. For example, in rat medial gastrocnemius, it has been shown that as muscle-tendon unit length increases, internal shortening magnitude, as well as shortening velocity, decrease (MacDougall et al., 2020). While this effect was apparent in both low and high-compliance conditions, it is worth exploring how it could interact with potentiation, considering that potentiation magnitude appears to be greater as contraction velocity is increased (Gittings et al., 2012; 2017). Thus, in preparations where substantial internal shortening is allowed, part of the difference in potentiation between shorter and longer lengths may be related to velocity-dependent differences in potentiation present at the level of the sarcomere, while the preparation remains isometric.

A final and more likely possibility is that the absence of a robust linear relationship in the current data may be an experimental artifact related to the CS being undertaken at different muscle lengths. It was shown here that fatigue (assessed through the change in force between the first and final tetanus of the CS) was significantly lower at long compared to optimal and short muscle lengths. Potentiation is known to be present in conjunction with fatigue (Rassier & MacIntosh, 2000b), and the reduced

fatigue at long lengths may have allowed for greater potentiation magnitudes to be manifested. On the other hand, the reduced fatigue observed at long lengths may have also been a fallacy; if active tetanic force was underestimated at long lengths owing to internal shortening, and passive force dropped throughout the CS due to force relaxation or slippage of the preparation, the difference in force between the first and last tetanus would potentially appear smaller than it actually was. Moreover, differences between unpotentiated and potentiated twitch active force would also appear exaggerated, since following the CS passive force would be lower. Notably, this effect could be present at all muscle lengths, but it would be substantially greater at longer lengths (MacIntosh, 2017), as mentioned previously.

Considering the above, there are still multiple potential explanations as to why skMLCK ablation may not influence the length-potentiation relationship. One possibility is that skMLCK$^{-/-}$ mice may differ at undiscovered loci from WT mice. Functionally, both genotypes appeared similar, with no statistically significant differences at baseline values of tetanic and twitch force as well as force kinetics, except for TPT, with WT muscles exhibiting greater values than their skMLCK$^{-/-}$ counterparts at all lengths. In spite of this, skMLCK ablation may in some unknown manner affect sarcomeric function and by extension, the observed length-potentiation relationship. However, it is unknown whether such differences exist and what their mechanistic influence would be.

Another consideration is that the proposed mechanism for the length-dependence of potentiation, i.e., the radial displacement/disorder of the myosin heads, may not be sufficient to explain this relationship. Given the recent realization that structural findings from isolated filaments and permeabilized fibers may not correspond to whole muscle function, both in skeletal (Caremani et al., 2019b; 2021) and cardiac

muscle (Caremani et al., 2019; Irving & Craig, 2019; Park-Holohan et al., 2021), it is conceivable that this initial model of RLC phosphorylation-mediated potentiation - which was based on findings in isolated thick filaments (Levine et al., 1996; Yang et al., 1998) and permeabilized fibers in the absence of osmotic compression (Yamaguchi et al., 2016) - might not directly correspond to the situation present in the whole muscle environment. As a relevant example of the observed discrepancies between levels of organization, in permeabilized mammalian cardiac trabeculae, RLC phosphorylation initially appeared to radially displace the myosin heads at rest, under non-physiological temperature and lattice spacing conditions (Kampourakis et al., 2016). However, when similar experiments on the same model were carried out at higher temperature and increased osmotic compression by dextran, thus more closely mimicking the physiological environment, similar amounts of RLC phosphate content did not significantly affect thick filament structure at rest (Park-Holohan et al., 2021). The structural effects of RLC phosphorylation in mammalian skeletal muscle have not been studied in a whole muscle model. While in intact tarantula skeletal muscle it has been directly demonstrated that a tetanus (and subsequent RLC phosphorylation) results in persistent radial displacement of the myosin heads in the physiological filament lattice environment (Padron et al., 2020), major differences in thick filament structure and function between tarantulas and vertebrates prevent extrapolation to mammalian skeletal muscle. These include: i) the absence of MyBP-C in tarantula skeletal muscle ii) the presence of a paramyosin core, which likely contributes to the minimal thick filament elongation observed upon activation (assessed by x-ray diffraction through the spacing of the M6 reflection), in stark contrast to vertebrate skeletal muscle iii) the lesser (if any) importance of the mechanosensing thick-filament regulation mechanism, reflected in the absence of thick filament elongation, and the preponderance of the

cooperative-phosphorylation activation mechanism instead and iv) differences in the RLC itself (long N-terminal extensions vs short in vertebrates, two phosphorylatable residues vs one in vertebrates) (Padron et al., 2020). A relevant observation from x-ray diffraction studies is that while following a tetanus both tarantula skeletal muscle and mouse EDL muscle exhibit persistent decreased intensity of the first (and fourth for tarantulas) myosin-layer line (ML1), which is indicative of disorder of the myosin heads and disruption of the helical array (Padron et al., 2020; Hill et al., 2021), the radial position of the heads appears to differ between the two models. Specifically, while in tarantula muscle, heads appear to remain in the vicinity of actin on the timescale of seconds (assessed through the 1,0 + 2,0 and 1,1 equatorial reflections, as well as their ratio) (Padron et al., 2020), in mouse EDL heads were observed to fold back on the filament backbone within 130 ms of the last stimulus of a tetanus (assessed through the axial profile of the third meridional myosin reflection, M3 and the aforementioned equatorial reflections) (Hill et al., 2021). Notably, the spacing of the M6 reflection (associated with thick filament elongation and activation in vertebrates) also remained increased within that timeframe in mouse EDL (Hill et al., 2021). It is possible that this observation is related to the different stimulation protocols; 2 s tetani were used in tarantula femur muscles (Padron et al., 2020), but only 100 ms in mouse EDLs (Hill et al., 2021). Thus, it may be that the stimulus used in the latter was not enough to elicit considerable RLC phosphorylation, and unfortunately, RLC phosphate content was not assessed (Hill et al., 2021). Nevertheless, considering the findings in cardiac muscle mentioned above (Park-Holohan et al., 2021), it is conceivable that post-tetanic potentiation may differ slightly between the two species: in tarantulas, persistent positioning of the myosin heads near actin may facilitate increased force production and rate of force development following a tetanic stimulus (Padron et al., 2020), while

in mice, it is possible that potentiation is mediated simply through the disruption of the helical array and persistent thick filament elongation, with subsequent enhanced responses of the mechanosensing mechanism (Caremani et al., 2019; Irving & Craig, 2019) and/or interfilament communication mechanisms to activate myosin heads. Additionally, it might be the case that RLC phosphorylation in the mouse EDL happens on a slower timescale than in tarantula skeletal muscle, and myosin heads may be radially displaced on a timescale of seconds following a tetanus, despite initially recovering their folded conformation. Regardless, the observation that in cardiac muscle RLC phosphorylation had markedly different structural effects than in tarantula skeletal muscle (although in the former RLC phosphorylation was not induced through tetanic stimulation) (Park-Holohan et al., 2021) suggests that additional research in this area is required in whole muscle mammalian models, utilizing x-ray diffraction or fluorescence polarization methods and parallel assessment of RLC phosphate content. In addition to the above, the notion that length-dependent force characteristics are related to decreased interfilament lattice spacing has itself been shown to be insufficient to explain the experimental observations both in cardiac (e.g., de Tombe et al., 2010; Ait-Mou et al., 2016) and skeletal muscle (Mateja et al., 2013; Williams et al., 2013; Li et al., 2016). Instead, it has become apparent that titin-mediated signaling mechanisms (de Tombe et al., 2010; Mateja et al., 2013; Reconditi et al., 2014; Ait-Mou et al., 2016; Zhang et al., 2017; Caremani et al., 2019; Park-Holohan et al., 2021), potentially involving thin and thick filament components as well as MyBP-C, may act concomitantly with the effects of lattice spacing (Williams et al., 2013). Thus, the proposed mechanistic model of the length-dependence of potentiation would have to also account for all these observations, and include thick filament-based regulation (Irving, 2017), molecular effects of lattice spacing on contraction (Williams et al.,

2010), and the emerging roles of MyBP-C (e.g., Song et al., 2021) and titin (e.g., Mateja et al., 2013) in the contractile process.

Other mechanisms of potentiation may also explain the experimental observations. Here, there are two possibilities to be considered; i) either the additional potentiation mechanisms present in skMLCK$^{-/-}$ muscles exhibit a dependence on muscle/sarcomere length very similar to the one of RLC phosphorylation-dominant potentiation, which in turn could indeed be related mainly to radial displacement of the myosin heads, or ii) alternatively, potentiation in and of its own, regardless of underlying mechanisms (RLC phosphorylation, Ca^{2+} handling, redox-related mechanisms) is dependent on sarcomere length through a common underlying mechanism. Unfortunately, both these scenarios are currently impossible to verify based on existing literature. Two recent discoveries are relevant in this regard; first, it has become apparent that in vertebrate skeletal muscle, the thick filament can be partially activated by passive tension at longer sarcomere lengths (Reconditi et al., 2014; Fusi et al., 2016). This was apparent both in frog tibialis anterior fiber bundles (Reconditi et al., 2014) and permeabilized rabbit psoas fibers under close-to-physiological conditions (Fusi et al., 2016). X-ray diffraction demonstrated that these changes include disruption of the helical array of myosin heads on the filament backbone (assessed through ML1 intensity) and elongation of the backbone (assessed through S6), but not radial displacement of heads (assessed through the axial profile of M3) (Reconditi et al., 2014). At increased sarcomere lengths, it is possible that this incomplete thick filament activation may result in a suboptimal effect of potentiation, to the extent the latter is dependent on recruitment of myosin heads or enhanced probability of interaction with actin, through decreased required time for thick-filament activation. Regarding RLC phosphorylation specifically, this partial activation may

render its structural effects redundant, thus adding another layer of complexity to the mechanistic explanation of the length-dependence of potentiation. On the other hand, it has recently been demonstrated that calcium release during a tetanic stimulus is inhibited at short sarcomere lengths, in mouse flexor digitorum brevis fibers (Rassier & Minozzo, 2016). Earlier, it was believed that calcium release in mouse muscle is symmetric across sarcomere lengths (Balnave & Allen, 1996). While it is unclear whether this effect would be meaningful during twitch contractions, it nevertheless points towards the possibility that the enhanced potentiation observed at short sarcomere lengths may additionally be related to sarcoplasmic [Ca^{2+}].

When considered together, all the above observations indicate that the mechanistic underpinnings of the length-dependence of potentiation may involve a number of factors and be more complex than initially thought. The fact that calcium sensitivity itself differs with sarcomere length (i.e., length-dependent activation) further complicates the situation. Additionally, while recent findings have demonstrated that RLC phosphorylation-independent potentiation may be related to increased resting [Ca^{2+}] and alterations in calcium kinetics (Smith et al., 2013; 2014), the molecular mechanisms of this and other potential alternative potentiation mechanisms have not been elucidated. Nevertheless, it has become clear that potentiation cannot be thought of solely as an effect of RLC phosphorylation (Vandenboom, 2017). The demonstration here that the length-dependence of potentiation is not related to RLC phosphorylation per se, but is also displayed in a similar manner by the alternative potentiation mechanism(s), points towards the need for more research regarding both the structural effects of RLC phosphorylation in mammalian skeletal muscle, as well as the alternative mechanism(s) of potentiation and its molecular mechanisms. Until more data are available, models of why potentiation is dependent on muscle length can only

be hypothetical. When considered at the whole-muscle level, interactions of internal sarcomere shortening-related effects (MacIntosh, 2017; MacDougall et al., 2020) with potentiation, as well as biomechanical effects related to fiber and fascicle spatial organization (i.e., pennation angle, gearing etc.) further complicate interpretation.

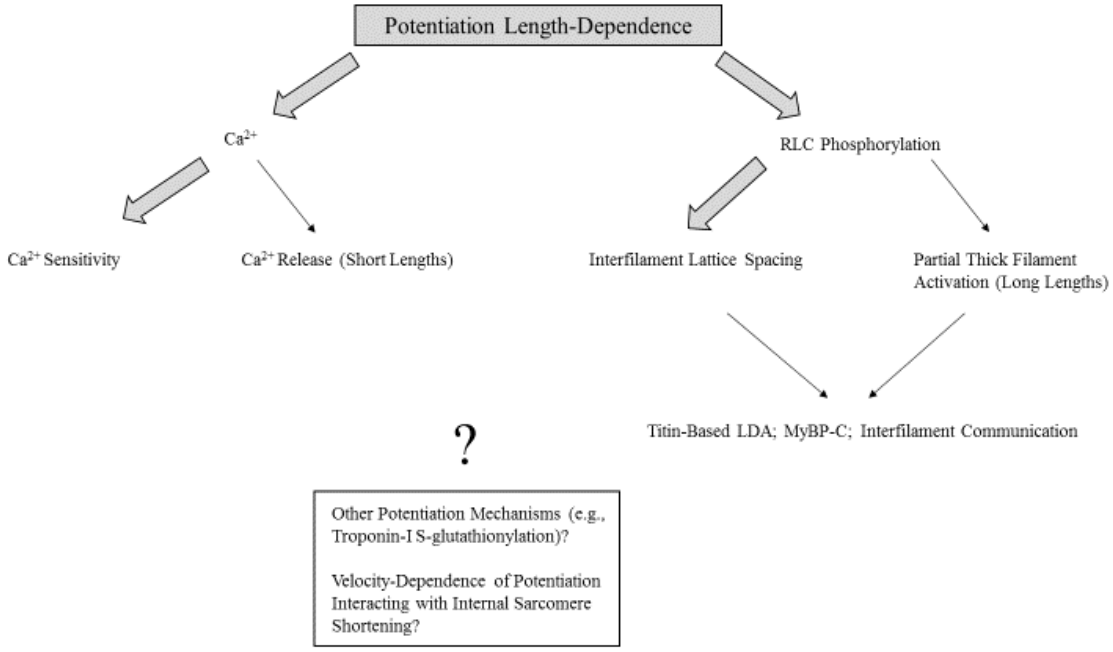

Fig. 19. Possible mechanisms involved in potentiation length-dependence. Arrow size indicates strength of evidence. Box with question mark includes less explored factors.

Findings regarding force kinetics were generally in agreement with prior literature. In both genotypes, rate of force development, reflected in $+dF/dt$, had a curvilinear relationship with length, appearing maximal at L_o, and decreasing as length either decreased or increased, as has been shown before in rat gastrocnemius muscle in

situ (Rassier et al., 1997; Rassier & MacIntosh, 2002b). Basal +*d*F/*d*t values were not different between genotypes, but potentiation of +*d*F/*d*t was greater in WT, in accordance with past findings (Gittings et al., 2016; Morris, Gittings & Vandenboom, 2018). Potentiation of +*d*F/*d*t reflected the pattern of +*d*F/*d*t, being greater at short and long lengths, with no difference in pattern between genotypes. Despite this asymmetrical potentiation, the length dependence of +*d*F/*d*t was mostly similar pre- and post-CS. While no clear mechanistic explanation exists for the length-dependent differences in rate of force development (Rassier & MacIntosh, 2002b), these may include inhibition of Ca^{2+} release at shorter sarcomere lengths (Rassier & Minozzo, 2016), and the observed slowing of crossbridge cycling kinetics at longer lengths, thought to be due to slowed ADP release (Fenwick et al., 2016; 2021). However, the latter observations were made in slow-twitch soleus muscle preparations, and it is unclear whether they can be extrapolated to the mouse EDL. Other possible mediators of this effect include lattice spacing-related effects on force production (Williams et al., 2010) and disruption of MyBP-C interactions with the thin filament as overlap of actin with the C-zone is abolished with increased sarcomere length (Reconditi et al., 2014). Factors related to tendon compliance must also be considered (MacDougall et al., 2020). All of these possible mechanisms remain unexplored.

In both genotypes, -*d*F/*d*t exhibited linear and quadratic trends. It appeared maximal at 0.95 L_o and decreased markedly as length increased, and to a lesser extent towards shorter lengths. These observations are in agreement with past findings, again in rat gastrocnemius in situ (Rassier et al., 1997; Rassier & MacIntosh, 2002b). Basal rates of -*d*F/*d*t were not different between genotypes. Following the CS, rate of force relaxation was enhanced at all lengths and this effect was independent of genotype. In addition, the linear trends became dominant both at 10- and 30- seconds post-CS,

reflecting the greater relative increase of -*d*F/*d*t at 0.9 L_o. Potentiation of -*d*F/*d*t mirrored this pattern, appearing greater at 0.9 L_o than 0.95 L_o and then displaying a linear increase with increasing length. It has been previously demonstrated that enhanced post-tetanic rates of twitch force relaxation are not necessarily related to RLC phosphorylation, as this effect has been observed in lumbrical muscles (Smith et al., 2013), which exhibit potentiation in the absence of RLC phosphorylation (Smith et al., 2013; 2014). Unfortunately, it is again unclear what the mechanisms of this effect (Vandenboom, 2017) as well as its length-dependence could be.

Both TPT and ½ RT were positively related to length, with both genotypes exhibiting longer twitch contraction times as muscle length increased. These findings are in accordance with previous literature in rat EDL and gastrocnemius in situ (Wallinga-de Jonge et al., 1980; Rassier et al., 1997; Rassier & MacIntosh, 2002b). Following the CS, both TPT and ½ RT were reduced at all lengths, and their relationship with length remained linear, as shown by trend analysis (linear trend accounting for > 90% of total variance). For both variables, values were not different between the 10 and 30 second timepoint after the CS. ½ RT was similar at all time points between WT and skMLCK$^{-/-}$ muscles at all lengths, in agreement with previous findings (Gittings et al., 2011). Interestingly, however, there was a main effect of genotype for TPT, with WT muscles exhibiting longer times than their skMLCK$^{-/-}$ counterparts. The reason for this difference is unknown. Reduced TPT following the CS is likely associated with the enhanced rate of force development traditionally observed with potentiation, both in WT (e.g., Vandenboom et al., 1995; Gittings et al., 2011) and skMLCK$^{-/-}$ (Gittings et al., 2011) EDL. The shorter ½ RT values following the CS in both genotypes are at least partially related to the mechanisms of enhanced -*d*F/*d*t, which are currently unclear as discussed above.

Chapter 7: Conclusions and Significance

The main finding of the current experiments was that the length-dependence of post-tetanic potentiation was similar between WT and skMLCK$^{-/-}$ EDL mouse muscles. The potentiation exhibited by the skMLCK$^{-/-}$ EDL is related to the additional mechanisms of potentiation, which unfortunately remain unclear. Nevertheless, the findings here indicate that at least in the model and experimental conditions utilized, these mechanisms facilitate potentiation which is dependent on length in a manner similar to RLC phosphorylation-dominant potentiation.

While these findings are not sufficient for a mechanistic interpretation of the length-dependence of potentiation, they indicate that either the existing model, based on the structural effects of RLC phosphorylation, cannot sufficiently explain this relationship, or alternatively, that the additional potentiation mechanisms exhibit the same dependence on sarcomere length as RLC phosphorylation. The existence of length-dependent activation further complicates interpretation, as Ca^{2+} sensitivity and submaximal force production are increased at longer sarcomere lengths. It is conceivable, although likely simplistic, that while RLC phosphorylation results in greater magnitudes of potentiation than the alternative mechanisms, the underlying downstream effects converge and length-dependence of potentiation reflects mostly the existence of length-dependent activation (i.e., potentiation magnitude is inversely related to Ca^{2+} sensitivity regardless of mechanism).

In total, these findings indicate that more research is necessary, in two main directions; i) elucidating the structural mechanisms of RLC phosphorylation in a whole muscle mammalian model in order to better understand how it facilitates potentiation and ii) further exploring the additional mechanisms of potentiation in order to

understand how functional relationships like the one observed here can be explained in their context. Moreover, it is becoming apparent that findings regarding activity-dependent potentiation have to be interpreted in the context of both thick-filament regulation and in the future, as more data become available, MyBP-C, which can potentially be of central importance to length-dependent aspects of contraction. The current findings support this notion, by demonstrating that the length-dependence of potentiation, a relationship with important implications for the underlying mechanisms of potentiation, cannot necessarily be attributed to RLC phosphorylation and its structural effects in a whole muscle model.

In addition to the above, past findings regarding length-dependent aspects of contraction have been recapitulated here, both in WT mouse EDL, and importantly, also in skMLCK$^{-/-}$ mouse EDL muscles. Both rates of force development and relaxation appear to be related to length in a curvilinear manner, with their values increasing as muscle length becomes shorter or longer than optimal, while TPT and ½ RT exhibited a positive linear dependence on muscle length. Furthermore, the conditioning stimulus influenced force kinetics in a manner consistent with existing literature, with $+dF/dt$ enhancement closely corresponding to force potentiation in a quantitative manner in both genotypes, while $-dF/dt$ was increased independent of RLC phosphorylation. Thus, with the exception of generally higher TPT in WT muscles, the origin of which is unknown, these findings further demonstrate the functional similarity of the skMLCK$^{-/-}$ EDL model with WT EDL, and reinforce the notion of its use as a negative control for the effects of RLC phosphorylation.

7.2 Model Sufficiency

Mouse EDL muscles have been extensively utilized to study activity-dependent potentiation, owing to their fast-twitch phenotype (Gittings et al., 2011) and robust potentiation responses (Vandenboom et al., 2013). In addition, at the experimental temperature used here (25 ^{o} C), they are able to undergo moderate contractile protocols without exhibiting diffusion-related decrements in central oxygenation (and related functional impairments), due to their relatively small size (Barclay, 2005). SkMLCK$^{-/-}$ EDL muscles are a strong experimental model for examining mechanistic aspects of potentiation, as they provide a direct negative control to the effects of RLC phosphorylation (Zhi et al, 2005), while retaining the fast-fiber composition of WT EDL (Gittings et al., 2011). Potential undiscovered effects of knocking out skMLCK cannot be excluded (i.e., alterations in signaling pathways or other sarcomeric proteins), however no outstanding functional differences aside from potentiation characteristics have been observed. Thus, isolation of the effects of additional mechanisms of potentiation in a whole muscle model becomes possible. On the other hand, WT EDL muscles allowed for replication of previous findings under the experimental conditions used here, and direct comparison with skMLCK $^{-/-}$ EDLs.

7.3 Limitations

A major limitation of this study was the inability to track sarcomere length, which can be problematic when length-dependent force characteristics are assessed in fixed end contractions (de Tombe & ter Keurs, 2016; MacIntosh, 2017). Consequently, interpretation of the current data in the context of potentiation mechanisms becomes more difficult, as a number of confounding factors are present, including internal sarcomere shortening (MacIntosh, 2017) and sarcomere inhomogeneities (Rassier,

2017). The absence of sarcomere length control can additionally result in misrepresentation of active force at longer lengths (MacIntosh, 2017), and extend the plateau of the force-length relationship (Rassier, 2017).

Another important limitation was that RLC phosphorylation was not assessed at the different lengths tested. While previous research has shown that RLC phosphate content does not differ following a staircase conditioning stimulus at different lengths (Rassier et al., 1997), this finding cannot be extrapolated to tetanic stimuli, considering that high-frequency Ca^{2+} release may be inhibited at shorter sarcomere lengths (Rassier & Minozzo, 2016). The increased post-tetanic potentiation observed at shorter sarcomere lengths both here and previously (Rassier & MacIntosh, 2002) indicates that the potentiating effects are more pronounced there, perhaps partially due to the potentially attenuated Ca^{2+} release. How this effect is related to RLC phosphorylation and other potentiation mechanisms is currently uncertain.

Finally, possible length-dependent fatigue effects (MacNaughton & MacIntosh, 2007), due to the conditioning stimuli being administered at different lengths must be taken into account. Potentiation is known to be manifested concomitantly with fatigue (Rassier & MacIntosh, 2000b) and any length-dependent differences of the latter would confound the observed effect. Under the present experimental conditions, fatigue appeared greater at short (0.9 L_o, 0.95 L_o, L_o) compared to long (1.05 L_o, 1.10 L_o) relative muscle lengths. However, these observations must be considered in the context of the aforementioned potential errors in active force calculation, and likely represent an experimental artifact more so than true differences in fatigue (MacIntosh, 2017).

References:

Ackermann, M. A., & Kontrogianni-Konstantopoulos, A. (2011). Myosin binding protein-C slow is a novel substrate for protein kinase A (PKA) and C (PKC) in skeletal muscle. *Journal of Proteome Research*, *10*(10), 4547–4555. https://doi.org/10.1021/pr200355w

Ait-Mou, Y., Hsu, K., Farman, G. P., Kumar, M., Greaser, M. L., Irving, T. C., & De Tombe, P. P. (2016). Titin strain contributes to the Frank-Starling law of the heart by structural rearrangements of both thin- and thick-filament proteins. *Proceedings of the National Academy of Sciences of the United States of America*, *113*(8), 2306–2311. https://doi.org/10.1073/pnas.1516732113

Alamo, L., Qi, D., Wriggers, W., Pinto, A., Zhu, J., Bilbao, A., Gillilan, R. E., Hu, S., & Padrón, R. (2016). Conserved Intramolecular Interactions Maintain Myosin Interacting-Heads Motifs Explaining Tarantula Muscle Super-Relaxed State Structural Basis. *Journal of Molecular Biology*, *428*(6), 1142–1164. https://doi.org/10.1016/j.jmb.2016.01.027

Alamo, L., Koubassova, N., Pinto, A., Gillilan, R., Tsaturyan, A., & Padrón, R. (2017). Lessons from a tarantula: new insights into muscle thick filament and myosin interacting-heads motif structure and function. *Biophysical Reviews*, *9*(5), 461–480. https://doi.org/10.1007/s12551-017-0295-1

Alamo, L., Pinto, A., Sulbarán, G., Mavárez, J., & Padrón, R. (2018). Lessons from a tarantula: new insights into myosin interacting-heads motif evolution and its implications on disease. *Biophysical Reviews*, *10*(5), 1465–1477. https://doi.org/10.1007/s12551-017-0292-4

Allen, D. G., Lamb, G. D., & Westerblad, H. (2008). Skeletal muscle fatigue: Cellular mechanisms. *Physiological Reviews*, *88*(1), 287–332. https://doi.org/10.1152/physrev.00015.2007

Al-Khayat, H. A., Kensler, R. W., Squire, J. M., Marston, S. B., & Morris, E. P. (2013). Atomic model of the human cardiac muscle myosin filament. *Proceedings of the National Academy of Sciences of the United States of America*, *110*(1), 318–323. https://doi.org/10.1073/pnas.1212708110

Anderson, D. M., Anderson, K. M., Chang, C. L., Makarewich, C. A., Nelson, B. R., McAnally, J. R., Kasaragod, P., Shelton, J. M., Liou, J., Bassel-Duby, R., & Olson, E. N. (2015). A micropeptide encoded by a putative long noncoding RNA regulates muscle performance. *Cell*, *160*(4), 595–606. https://doi.org/10.1016/j.cell.2015.01.009

Aracena, P., Sánchez, G., Donoso, P., Hamilton, S. L., & Hidalgo, C. (2003). S-Glutathionylation Decreases Mg^{2+} Inhibition and S-Nitrosylation Enhances Ca^{2+} Activation of RyR1 Channels. *Journal of Biological Chemistry*, *278*(44), 42927–42935. https://doi.org/10.1074/jbc.M306969200

Aracena, P., Tang, W., Hamilton, S. L. & Hidalgo, C. (2005) Effects of S-Glutathionylation and S-Nitrosylation on Calmodulin Binding to Triads and FKBP12 Binding to Type 1 Calcium Release Channels. *Antioxidants & Redox Signaling*, *7*(7-8), 870-881. https://doi.org/10.1089/ars.2005.7.870

Aracena-Parks, P., Goonasekera, S. A., Gilman, C. P., Dirksen, R. T., Hidalgo, C., & Hamilton, S. L. (2006). Identification of cysteines involved in S-nitrosylation, S-glutathionylation, and oxidation to disulfides in ryanodine receptor type 1. *Journal of Biological Chemistry*, *281*(52), 40354–40368. https://doi.org/10.1074/jbc.M600876200

Balnave, C. D., & Allen, D. G. (1996). The effect of muscle length on intracellular calcium and force in single fibres from mouse skeletal muscle. *Journal of Physiology, 492*(3), 705–713. https://doi.org/10.1113/jphysiol.1996.sp021339

Balnave, C. D., & Allen, D. G. (1998). Evidence for Na^+/Ca^{2+} exchange in intact single skeletal muscle fibers from the mouse. *American Journal of Physiology - Cell Physiology*, *274*(4 43-4), 940–946. https://doi.org/10.1152/ajpcell.1998.274.4.c940

Barclay, C.J. (2005). Modelling diffusive O_2 supply to isolated preparations of mammalian skeletal and cardiac muscle. *Journal of Muscle Research & Cell Motility 26***,** 225–235. https://doi.org/10.1007/s10974-005-9013-x

Barclay, C. J. (2012). Quantifying Ca^{2+} release and inactivation of Ca^{2+} release in fast- and slow-twitch muscles. *The Journal of Physiology*, *590*(23), 6199–6212. https://doi.org/10.1113/jphysiol.2012.242073

Baudry, S., & Duchateau, J. (2004). Postactivation potentiation in human muscle is not related to the type of maximal conditioning contraction. *Muscle and Nerve*, *30*(3), 328–336. https://doi.org/10.1002/mus.20101

Baylor, S. M., & Hollingworth, S. (2003). Sarcoplasmic reticulum calcium release compared in slow-twitch and fast-twitch fibres of mouse muscle. *The Journal of Physiology*, *551*(1), 125–138. https://doi.org/10.1113/jphysiol.2003.041608

Baylor, Stephen M., & Hollingworth, S. (2011). Calcium indicators and calcium signalling in skeletal muscle fibres during excitation-contraction coupling. *Progress in Biophysics and Molecular Biology*, *105*(3), 162–179. https://doi.org/10.1016/j.pbiomolbio.2010.06.001

Baylor, Stephen M., & Hollingworth, S. (2012). Intracellular calcium movements during excitation-contraction coupling in mammalian slow-twitch and fast-twitch muscle fibers. *Journal of General Physiology*, *139*(4), 261–272. https://doi.org/10.1085/jgp.201210773

Beard, N.A., Wei, L., & Dulhunty A.F. (2008). Control of muscle ryanodine receptor calcium release channels by proteins in the sarcoplasmic reticulum lumen. *Proceedings of the Australian Physiological Society, 39*: 123-129

Block, B. A., Imagawa, T., Campbell, K. P., & Franzini-Armstrong, C. (1988). Structural evidence for direct interaction between the molecular components of the transverse tubule/sarcoplasmic reticulum junction in skeletal muscle. *Journal of Cell Biology, 107*: 2587–2600

Boncompagni, S., Rossi, A. E., Micaroni, M., Beznoussenko, G. V, Polishchuk, R. S., Dirksen, R. T., & Protasi, F. (2009). Mitochondria Are Linked to Calcium Stores in Striated Muscle by Developmentally Regulated Tethering Structures. *Molecular Biology of the Cell, 20*(3), 1058–1067. https://doi.org/10.1091/mbc.E08

Boncompagni, S., Thomas, M., Lopez, J. R., Allen, P. D., Yuan, Q., Kranias, E. G., Franzini-Armstrong, C., & Perez, C. F. (2012). Triadin/junctin double null mouse reveals a differential role for triadin and junctin in anchoring CASQ to the jSR and regulating Ca^{2+} homeostasis. *PLoS ONE, 7*(7). https://doi.org/10.1371/journal.pone.0039962

Bowslaugh, J., Gittings, W., & Vandenboom, R. (2016). Myosin light chain phosphorylation is required for peak power output of mouse fast skeletal muscle in vitro. *Pflugers Archiv-European Journal of Physiology*, *468*(11–12), 2007–2016. https://doi.org/10.1007/s00424-016-1897-3

Brenner, B. (1988). Effect of Ca^{2+} on cross-bridge turnover kinetics in skinned single rabbit psoas fibers: Implications for regulation of muscle contraction. *Proceedings of the National Academy of Sciences of the United States of America*, *85*(9), 3265–3269. https://doi.org/10.1073/pnas.85.9.3265

Brillantes, A. M. B., Ondrias, K., Scott, A., Kobrinsky, E., Ondriašová, E., Moschella, M. C., Jayaraman, T., Landers, M., Ehrlich, B. E., & Marks, A. R. (1994). Stabilization of calcium release channel (ryanodine receptor) function by FK506-binding protein. *Cell*, *77*(4), 513–523. https://doi.org/10.1016/0092-8674(94)90214-3

Brito, R., Alamo, L., Lundberg, U., Guerrero, J. R., Pinto, A., Sulbarán, G., Gawinowicz, M. A., Craig, R., & Padrón, R. (2011). A molecular model of phosphorylation-based activation and potentiation of tarantula muscle thick filaments. *Journal of Molecular Biology*, *414*(1), 44–61. https://doi.org/10.1016/j.jmb.2011.09.017

Calderón, J. C., Bolaños, P., Torres, S. H., Rodríguez-Arroyo, G., & Caputo, C. (2009). Different fibre populations distinguished by their calcium transient characteristics in enzymatically dissociated murine flexor digitorum brevis and soleus muscles. *Journal of Muscle Research and Cell Motility*, *30*(3–4), 125–137. https://doi.org/10.1007/s10974-009-9181-1

Calderón, J. C., Bolaños, P., & Caputo, C. (2010). Myosin heavy chain isoform composition and Ca^{2+} transients in fibres from enzymatically dissociated murine soleus and extensor digitorum longus muscles. *The Journal of Physiology, 588*(1), 267–279. https://doi.org/10.1113/jphysiol.2009.180893

Calderón, J. C., Bolaños, P., & Caputo, C. (2014). Tetanic Ca^{2+} transient differences between slow- and fast-twitch mouse skeletal muscle fibres: a comprehensive experimental approach. *Journal of Muscle Research and Cell Motility*, *35*(5–6), 279–293. https://doi.org/10.1007/s10974-014-9388-7

Campbell, K. S. (2011). Impact of myocyte strain on cardiac myofilament activation. *Pflugers Archiv European Journal of Physiology*, *462*(1), 3–14. https://doi.org/10.1007/s00424-011-0952-3

Caremani, M., Pinzauti, F., Powers, J. D., Governali, S., Narayanan, T., Stienen, G. J. M., Reconditi, M., Linari, M., Lombardi, V., & Piazzesi, G. (2019). Inotropic interventions do not change the resting state of myosin motors during cardiac diastole. *Journal of General Physiology*, *151*(1), 53–65. https://doi.org/10.1085/jgp.201812196

Caremani, M., Brunello, E., Linari, M., Fusi, L., Irving, T. C., Gore, D., Piazzesi, G., Irving, M., Lombardi, V., & Reconditi, M. (2019b). Low temperature traps myosin motors of mammalian muscle in a refractory state that prevents activation. *Journal of General Physiology*, *151*(11), 1272–1286. https://doi.org/10.1085/jgp.201912424

Caremani, M., Fusi, L., Linari, M., Reconditi, M., Piazzesi, G., Irving, T. C., Narayanan, T., Irving, M., Lombardi, V., & Brunello, E. (2021). Dependence of thick filament structure in relaxed mammalian skeletal muscle on temperature and interfilament spacing. *Journal of General Physiology*, *153*(3). https://doi.org/10.1085/JGP.202012713

Caterini, D., Gittings, W., Huang, J., & Vandenboom, R. (2011). The effect of work cycle frequency on the potentiation of dynamic force in mouse fast twitch skeletal muscle. *The Journal of Experimental Biology*, *214*(23), 3915 LP – 3923. https://doi.org/10.1242/jeb.061150

Chen, S. R. W., Leong, P., Imredy, J. P., Bartlett, C., Zhang, L., & MacLennan, D. H. (1997). SinglECChannel properties of the recombinant skeletal muscle Ca^{2+} release channel (ryanodine receptor). *Biophysical Journal*, *73*(4), 1904–1912. https://doi.org/10.1016/S0006-3495(97)78221-3

Colson, B. A., Locher, M. R., Bekyarova, T., Patel, J. R., Fitzsimons, D. P., Irving, T. C., & Moss, R. L. (2010). Differential roles of regulatory light chain and myosin binding protein-C phosphorylations in the modulation of cardiac force development. *The Journal of Physiology*, *588*(6), 981–993. https://doi.org/10.1113/jphysiol.2009.183897

Colson, B. A., Petersen, K. J., Collins, B. C., Lowe, D. A., & Thomas, D. D. (2015). The myosin super-relaxed state is disrupted by estradiol deficiency. *Biochemical and Biophysical Research Communications*, *456*(1), 151–155. https://doi.org/10.1016/j.bbrc.2014.11.050

Cooke, R. (2011). The role of the myosin ATPase activity in adaptive thermogenesis by skeletal muscle. *Biophysical Reviews*, *3*(1), 33–45. https://doi.org/10.1007/s12551-011-0044-9

Craig, R., & Woodhead, J. L. (2006). Structure and function of myosin filaments. *Current Opinion in Structural Biology*, *16*(2), 204–212. https://doi.org/10.1016/j.sbi.2006.03.006

Darbellay, B., Arnaudeau, S., Bader, C. R., Konig, S., & Bernheim, L. (2011). STIM1L is a new actin-binding splice variant involved in fast repetitive Ca 2+ release. *Journal of Cell Biology*, *194*(2), 335–346. https://doi.org/10.1083/jcb.201012157

Davis, J. S., Satorius, C. L., & Epstein, N. D. (2002). Kinetic Effects of Myosin Regulatory Light Chain Phosphorylation on Skeletal Muscle Contraction. *Biophysical Journal*, *83*(1), 359–370. https://doi.org/10.1016/S0006-3495(02)75175-8

Debold, E. P., Fitts, R. H., Sundberg, C. W., & Nosek, T. M. (2016) Muscle fatigue from the perspective of a single crossbridge. *Medicine & Science in Sports & Exercise*, *48*(11), 2270-2280 doi: 10.1249/mss.0000000000001047

Denniss, A., Dulhunty, A. F., & Beard, N. A. (2018). Ryanodine receptor Ca 2+ release channel post-translational modification: Central player in cardiac and skeletal muscle disease. *International Journal of Biochemistry and Cell Biology*, *101*, 49–53. https://doi.org/10.1016/j.biocel.2018.05.004

Desmond, P. F., Muriel, J., Markwardt, M. L., Rizzo, M. A., & Bloch, R. J. (2015). Identification of small ankyrin 1 as a novel sarco(endo)plasmic reticulum Ca^{2+}-ATPase 1 (SERCA1) regulatory protein in skeletal muscle. *Journal of Biological Chemistry*, 290(46), 27854–27867. https://doi.org/10.1074/jbc.M115.676585

Desmond, P. F., Labuza, A., Muriel, J., Markwardt, M. L., Mancini, A. E., Rizzo, M. A., & Bloch, R. J. (2017). Interactions between small ankyrin 1 and sarcolipin coordinately regulate activity of the sarco(endo)plasmic reticulum Ca^{2+}-ATPase (SERCA1). *Journal of Biological Chemistry*, *292*(26), 10961–10972. https://doi.org/10.1074/jbc.M117.783613

de Tombe, P. P., Mateja, R. D., Tachampa, K., Mou, Y. A., Farman, G. P., & Irving, T. C. (2010). Myofilament length dependent activation. *Journal of Molecular and Cellular Cardiology*, *48*(5), 851–858. https://doi.org/10.1016/j.yjmcc.2009.12.017

de Tombe, P. P., & ter Keurs, H. E. D. J. (2016). Cardiac muscle mechanics: Sarcomere length matters. *Journal of Molecular and Cellular Cardiology*, *91*, 148–150. https://doi.org/10.1016/j.yjmcc.2015.12.006

Dirksen, R. T. (2009). Checking your SOCCs and feet: The molecular mechanisms of Ca^{2+} entry in skeletal muscle. *The Journal of Physiology*, 587(13), 3139–3147. https://doi.org/10.1113/jphysiol.2009.172148

Dutka, T., L., Mollica, J. P., Lamboley, C. R., Weerakkody, V. C., Greening, D. W., Posterino, G. S., Murphy, R. M. & Lamb G. D. (2017) S-nitrosylation and S-glutathionylation of Cys134 on troponin I have opposing competitive actions on Ca^{2+} sensitivity in rat fast-twitch muscle fibers. *American Journal of Physiology-Cell Physiology*, *312*(3), C316-C327

Fajardo V.A., Bombardier E., Vigna C., Devji T., Bloemberg D., Gamu, D., Gramolini, A. O., Quadrilatero, J. & Tupling, A. R. (2013). Co-Expression of SERCA Isoforms, Phospholamban and Sarcolipin in Human Skeletal Muscle Fibers. *PLOS ONE*, *8*(12): e84304. https://doi.org/10.1371/journal.pone.0084304

Fenwick, A. J., Leighton, S. R., & Tanner, B. C. W. (2016). Myosin MgADP Release Rate Decreases as Sarcomere Length Increases in Skinned Rat Soleus Muscle Fibers. *Biophysical Journal*, *111*(9), 2011–2023. https://doi.org/10.1016/j.bpj.2016.09.024

Fenwick, A. J., Lin, D. C., & Tanner, B. C. W. (2021). Myosin cross-bridge kinetics slow at longer muscle lengths during isometric contractions in intact soleus from mice. *Proceedings of the Royal Society B: Biological Sciences*, *288*(1950). https://doi.org/10.1098/rspb.2020.2895

Franks-Skiba, K., Lardelli, R., Goh, G., & Cooke, R. (2007). Myosin light chain phosphorylation inhibits muscle fiber shortening velocity in the presence of vanadate. *American Journal of Physiology - Regulatory Integrative and Comparative Physiology*, *292*(4), 1603–1612. https://doi.org/10.1152/ajpregu.00499.2006

Fuchs., F., & Wang, Y.P. (1991). Force, length, and $Ca(^{2+})$-troponin C affinity in skeletal muscle. *American Journal of Physiology-Cell Physiology 261*(5), 787-792. https://doi.org/10.1152/ajpcell.1991.261.5.C787

Fusi, L., Huang, Z., & Irving, M. (2015). The Conformation of Myosin Heads in Relaxed Skeletal Muscle: Implications for Myosin-Based Regulation. *Biophysical Journal*, *109*(4), 783–792. https://doi.org/10.1016/j.bpj.2015.06.038

Fusi, L., Brunello, E., Yan, Z., & Irving, M. (2016). Thick filament mechano-sensing is a calcium-independent regulatory mechanism in skeletal muscle. *Nature Communications*, *7*, 1–9. https://doi.org/10.1038/ncomms13281

Fusi, L., Percario, V., Brunello, E., Caremani, M., Bianco, P., Powers, J. D., Reconditi, M., Lombardi, V., & Piazzesi, G. (2017). Minimum number of myosin motors accounting for shortening velocity under zero load in skeletal muscle. *The Journal of Physiology*, *595*(4), 1127–1142. https://doi.org/10.1113/JP273299

Gaburjakova, M., Gaburjakova, J., Reiken, S., Huang, F., Marx, S. O., Rosemblit, N., & Marks, A. R. (2001). FKBP12 Binding Modulates Ryanodine Receptor Channel Gating. *Journal of Biological Chemistry*, *276*(20), 16931–16935. https://doi.org/10.1074/jbc.M100856200

Gamu, D., Juracic, E. S., Fajardo, V. A., Rietze, B. A., Tran, K., Bombardier, E., & Tupling, A. R. (2019). Phospholamban deficiency does not alter skeletal muscle SERCA pumping efficiency or predispose mice to diet-induced obesity. *American Journal of Physiology - Endocrinology and Metabolism*, *316*(3), E432–E442. https://doi.org/10.1152/ajpendo.00288.2018

Geeves, M. A., & Holmes, K. C. (2005). The molecular mechanism of muscle contraction. *Advances in Protein Chemistry*, *71*, 161–193. https://doi.org/10.1016/S0065-3233(04)71005-0

Geeves, M. A. (2012). Thin filament regulation. *Comprehensive Biophysics*, *4*, 251–267. https://doi.org/10.1016/B978-0-12-374920-8.00416-1

Geeves, Michael A., Lehrer, S. S., & Lehman, W. (2019). The mechanism of thin filament regulation: Models in conflict? *The Journal of General Physiology*, *151*(11), 1265–1271. https://doi.org/10.1085/jgp.201912446

Geist, J., Ward, C. W., & Kontrogianni-Konstantopoulos, A. (2018). Structure before function: Myosin binding protein-C slow is a structural protein with regulatory properties. *FASEB Journal*, *32*(12), 6385–6394. https://doi.org/10.1096/fj.201800624R

Gittings, W., Huang, J., Smith, I. C., Quadrilatero, J., & Vandenboom, R. (2011). The effect of skeletal myosin light chain kinase gene ablation on the fatigability of mouse fast muscle. *Journal of Muscle Research and Cell Motility*, *31*(5–6), 337–348. https://doi.org/10.1007/s10974-011-9239-8

Gittings, W., Huang, J., & Vandenboom, R. (2012). Tetanic force potentiation of mouse fast muscle is shortening speed dependent. *Journal of Muscle Research and Cell Motility*, *33*(5), 359–368. https://doi.org/10.1007/s10974-012-9325-6

Gittings, W., Aggarwal, H., Stull, J. T., & Vandenboom, R. (2015). The force dependence of isometric and concentric potentiation in mouse muscle with and without skeletal myosin light chain kinase. *Canadian Journal of Physiology and Pharmacology*. *93*(1): 23-32. https://doi.org/10.1139/cjpp-2014-0118

Gittings, W., Bunda, J., Stull, J.T., & Vandenboom, R. (2016), Interaction of posttetanic potentiation and the catchlike property in mouse skeletal muscle. *Muscle Nerve*, *54*, 308-316. https://doi.org/10.1002/mus.25053

Gittings, W., Bunda, J., & Vandenboom, R. (2017). Shortening speed dependent force potentiation is attenuated but not eliminated in skeletal muscles without myosin phosphorylation. *Journal of Muscle Research and Cell Motility*, *38*(2), 157–162. https://doi.org/10.1007/s10974-017-9465-9

Goonasekera, S. A., Beard, N. A., Groom, L., Kimura, T., Lyfenko, A. D., Rosenfeld, A., Marty, I., Dulhunty, A. F., & Dirksen, R. T. (2007). Triadin binding to the C-terminal luminal loop of the ryanodine receptor is important for skeletal muscle excitation-contraction coupling. *Journal of General Physiology*, *130*(4), 365–378. https://doi.org/10.1085/jgp.200709790

Gordon, A. M., Huxley, A. F., & Julian, F. J. (1966). The variation in isometric tension with sarcomere length in vertebrate muscle fibres. *The Journal of Physiology*, *184*(1), 170–192. https://doi.org/10.1113/jphysiol.1966.sp007909

Gordon, A. M., Homsher, E., & Regnier, M. (2000). Regulation of contraction in striated muscle. *Physiological Reviews*, *80*(2), 853–924. https://doi.org/10.1152/physrev.2000.80.2.853

Grange, R. W., Cory, C. R., Vandenboom, R., & Houston, M. E. (1995). Myosin phosphorylation augments force-displacement and force-velocity relationships of mouse fast muscle. *American Journal of Physiology-Cell Physiology*, *269*(3), C713-C724. https://doi.org/10.1152/ajpcell.1995.269.3.C713

Greenberg, M. J., Mealy, T. R., Watt, J. D., Jones, M., Szczesna-Cordary, D. & Moore J. R. (2009). The molecular effects of skeletal muscle myosin regulatory light chain phosphorylation. *American Journal of Physiology-Regulatory, Integrative and Comparative Physiology*, *297*(2), R265-R274. https://doi.org/10.1152/ajpregu.00171.2009

Greenberg, M. J., Mealy, T. R., Jones, M., Szczesna-Cordary, D. & Moore J. R. (2010). The direct molecular effects of fatigue and myosin regulatory light chain phosphorylation on the actomyosin contractile apparatus. *American Journal of Physiology-Regulatory, Integrative and Comparative Physiology*, *298*(4), R989-R996. https://doi.org/10.1152/ajpregu.00566.2009

Hanft, L. M., Fitzsimons, D. P., Hacker, T. A., Moss, R. L., & McDonald, K. S. (2020). Cardiac MyBP-C phosphorylation regulates the Frank-Starling relationship in murine hearts. *Journal of General Physiology*, *7*(7), 1–10. https://doi.org/10.1085/JGP.202012770

Harris, S. P. (2020). Making waves: A proposed new role for myosin-binding protein C in regulating oscillatory contractions in vertebrate striated muscle. *Journal of General Physiology*, *153*(3), 1–16. https://doi.org/10.1085/JGP.202012729

Heling, L. W. H. J., Geeves, M. A., & Kad, N. M. (2020). MyBP-C: one protein to govern them all. *Journal of Muscle Research and Cell Motility*, 41(1), 91–101. https://doi.org/10.1007/s10974-019-09567-1

Henderson, C. A., Gomez, C. G., Novak, S. M., Mi-Mi, L., & Gregorio, C. C. (2017). Overview of the muscle cytoskeleton. *Comprehensive Physiology*, *7*(3), 891–944. https://doi.org/10.1002/cphy.c160033

Hill, C., Brunello, E., Fusi, L., Ovejero, J. G., & Irving, M. (2021). Myosin-based regulation of twitch and tetanic contractions in mammalian skeletal muscle. *ELife*, *10*. https://doi.org/10.7554/elife.68211

Hollingworth, S., Kim, M.M. and Baylor, S.M. (2012), Measurement and simulation of myoplasmic calcium transients in mouse slow-twitch muscle fibres. *The Journal of Physiology, 590*, 575-594. doi:10.1113/jphysiol.2011.220780

Hollingworth, S., & Baylor, S.M. (2013). Return of myoplasmic calcium (Ca) to resting levels following stimulation of fast- and slow-twitch mouse muscle fibers. *Biophysical Journal*, *104*, 291a–292a. http://dx.doi.org/10.1016/j.bpj.2012.11.1629

Holmes, K. C., & Lehman, W. (2008). Gestalt-binding of tropomyosin to actin filaments. *Journal of Muscle Research and Cell Motility*, *29*(6–8), 213–219. https://doi.org/10.1007/s10974-008-9157-6

Holt, N. C., & Williams, C. D. (2018). Can strain dependent inhibition of cross-bridge binding explain shifts in optimum muscle length? *Integrative and Comparative Biology*, *58*(2), 174–185. https://doi.org/10.1093/icb/icy050

Hooijman, P., Stewart, M. A., & Cooke, R. (2011). A new state of cardiac myosin with very slow ATP turnover: A potential cardioprotective mechanism in the heart. *Biophysical Journal*, *100*(8), 1969–1976. https://doi.org/10.1016/j.bpj.2011.02.061

Houdusse, A., & Sweeney, H. L. (2016). How Myosin Generates Force on Actin Filaments. *Trends in Biochemical Sciences*, *41*(12), 989–997. https://doi.org/10.1016/j.tibs.2016.09.006

Inchingolo, A. V., Previs, S. B., Previs, M. J., Warshaw, D. M., & Kad, N. M. (2019). Revealing the mechanism of how cardiac myosin-binding protein C N-terminal fragments sensitize thin filaments for myosin binding. *Proceedings of the National Academy of Sciences of the United States of America*, *116*(14), 6828–6835. https://doi.org/10.1073/pnas.1816480116

Irving, M. (2017). Regulation of Contraction by the Thick Filaments in Skeletal Muscle. *Biophysical Journal*, *113*(12), 2579–2594. https://doi.org/10.1016/j.bpj.2017.09.037

Irving, T. C., & Craig, R. (2019). Getting into the thick (and thin) of it. *Journal of General Physiology*, *151*(5), 610–613. https://doi.org/10.1085/jgp.201812307

Joumaa, V., & Herzog, W. (2010). Force depression in single myofibrils. *Journal of Applied Physiology*, *108*(2), 356–362. https://doi.org/10.1152/japplphysiol.01108.2009

Joumaa, V., MacIntosh, B. R., & Herzog, W. (2012). New insights into force depression in skeletal muscle. *Journal of Experimental Biology*, *215*(12), 2135–2140. https://doi.org/10.1242/jeb.060863

Joumaa, V., Smith, I. C., Fakutani, A., Leonard, T., Ma, W., Irving, T., & Herzog, W. (2018). Evidence for Actin Filament Structural Changes after Active Shortening in Skinned Muscle Bundles. *Biophysical Journal*, *114*(3), 135a. https://doi.org/10.1016/j.bpj.2017.11.765

Jung, H. S., Komatsu, S., Ikebe, M., & Craig, R. (2008). Head–Head and Head–Tail Interaction: A General Mechanism for Switching Off Myosin II Activity in Cells. *Molecular Biology of the Cell*, *19*(8), 3234–3242. https://doi.org/10.1091/mbc.e08-02-0206

Kampourakis, T., & Irving, M. (2015). Phosphorylation of myosin regulatory light chain controls myosin head conformation in cardiac muscle. *Journal of Molecular and Cellular Cardiology*, *85*, 199–206. https://doi.org/10.1016/j.yjmcc.2015.06.002

Kampourakis, T., Sun, Y. B., & Irving, M. (2016). Myosin light chain phosphorylation enhances contraction of heart muscle via structural changes in both thick and thin filaments. *Proceedings of the National Academy of Sciences of the United States of America*, *113*(21), E3039–E3047. https://doi.org/10.1073/pnas.1602776113

Karatzaferi, C., Franks-Skiba, K., & Cooke, R. (2008). Inhibition of shortening velocity of skinned skeletal muscle fibers in conditions that mimic fatigue. *American Journal of Physiology - Regulatory Integrative and Comparative Physiology*, *294*(3), 948–955. https://doi.org/10.1152/ajpregu.00541.2007

Kawai, M., Wray, J. S., & Zhao, Y. (1993). The effect of lattice spacing change on cross-bridge kinetics in chemically skinned rabbit psoas muscle fibers. I. Proportionality between the lattice spacing and the fiber width. *Biophysical Journal*, *64*(1), 187–196. https://doi.org/10.1016/S0006-3495(93)81356-0

Kensler, R. W., Craig, R., & Moss, R. L. (2017). Phosphorylation of cardiac myosin binding protein C releases myosin heads from the surface of cardiac thick filaments. *Proceedings of the National Academy of Sciences of the United States of America*, *114*(8), E1355–E1364. https://doi.org/10.1073/pnas.1614020114

Koenig, X., Choi, R. H., & Launikonis, B. S. (2018). Store-operated Ca^{2+} entry is activated by every action potential in skeletal muscle. *Communications Biology*, *1*(1). https://doi.org/10.1038/s42003-018-0033-7

Koenig, X., Choi, R. H., Schicker, K., Singh, D. P., Hilber, K., & Launikonis, B. S. (2019). Mechanistic insights into store-operated Ca 2+ entry during excitation-contraction coupling in skeletal muscle. *Biochimica et Biophysica Acta - Molecular Cell Research*, *1866*(7), 1239–1248. https://doi.org/10.1016/j.bbamcr.2019.02.014

Konhilas, J. P., Irving, T. C., & De Tombe, P. P. (2002). Length-dependent activation in three striated muscle types of the rat. *The Journal of Physiology*, *544*(1), 225–236. https://doi.org/10.1113/jphysiol.2002.024505

Konhilas, J. P., Irving, T. C., & De Tombe, P. P. (2002b). Myofilament calcium sensitivity in skinned rat cardiac trabeculae: Role of interfilament spacing. *Circulation Research*, *90*(1), 59–65. https://doi.org/10.1161/hh0102.102269

Kumar, M., Govindan, S., Zhang, M., Khairallah, R. J., Martin, J. L., Sadayappan, S., & De Tombe, P. P. (2015). Cardiac myosin-binding protein C and troponin-I phosphorylation independently modulate myofilament length-dependent activation. *Journal of Biological Chemistry*, *290*(49), 29241–29249. https://doi.org/10.1074/jbc.M115.686790

Lamb, G. D., & Posterino, G. S. (2003). Effects of oxidation and reduction on contractile function in skeletal muscle fibres of the rat. *The Journal of Physiology 546*, 149–163. https://doi.org/10.1113/jphysiol.2002.027896

Launikonis, B. S., Zhou, J., Royer, L., Shannon, T. R., Brum, G., & Ríos, E. (2006). Depletion “skraps” and dynamic buffering inside the cellular calcium store. *Proceedings of the National Academy of Sciences of the United States of America*, *103*(8), 2982–2987. https://doi.org/10.1073/pnas.0511252103

Lee, K. H., Sulbarán, G., Yang, S., Mun, J. Y., Alamo, L., Pinto, A., Sato, O., Ikebe, M., Liu, X., Korn, E. D., Sarsoza, F., Bernstein, S. I., Padrón, R., & Craig, R. (2018). Interacting-heads motif has been conserved as a mechanism of myosin II inhibition since before the origin of animals. *Proceedings of the National Academy of Sciences of the United States of America*, *115*(9), E1991–E2000. https://doi.org/10.1073/pnas.1715247115

Lehman, W. (2016). Thin filament structure and the steric blocking model. *Comprehensive Physiology*, *6*(2), 1043–1069. https://doi.org/10.1002/cphy.c150030

Lehman, W. (2017). Switching Muscles On and Off in Steps: The McKillop-Geeves Three-State Model of Muscle Regulation. *Biophysical Journal*, *112*(12), 2459–2466. https://doi.org/10.1016/j.bpj.2017.04.053

Lehman, W., Rynkiewicz, M. J., & Moore, J. R. (2020). A new twist on tropomyosin binding to actin filaments: perspectives on thin filament function, assembly and biomechanics. *Journal of Muscle Research and Cell Motility*, 41, 23-38. https://doi.org/10.1007/s10974-019-09501-5

Levine, R. J. C., Kensler, R. W., Yang, Z., Stull, J. T., & Sweeney, H. L. (1996). Myosin Light Chain Phosphorylation Affects the Structure of Rabbit Skeletal Muscle Thick Filaments. *Biophysical Journal*, *71*(2), 898–907. https://doi.org/10.1016/S0006-3495(96)79293-7

Levine, R. J. C., Epstein, N. D., Fananapazir, L., Stull, J. T., & Sweeney, H. L. (1998). Structural and Functional Responses of Mammalian Thick Filaments to Alterations in Myosin Regulatory Light Chains. *Journal of Structural Biology*, *122*(1-2), 149–161. https://doi.org/10.1006/jsbi.1998.3980

Li, Y., Lang, P., & Linke, W. A. (2016). Titin stiffness modifies the force-generating region of muscle sarcomeres. *Scientific Reports*, *6*, 1–9. https://doi.org/10.1038/srep24492

Li, K. L., Methawasin, M., Tanner, B. C. W., Granzier, H. L., Solaro, R. J., & Dong, W. J. (2019). Sarcomere length-dependent effects on Ca 2+ - troponin regulation in myocardium expressing compliant titin. *Journal of General Physiology*, *151*(1), 30–41. https://doi.org/10.1085/jgp.201812218

Linari, M., Brunello, E., Reconditi, M., Fusi, L., Caremani, M., Narayanan, T., Piazzesi, G., Lombardi, V., & Irving, M. (2015). Force generation by skeletal muscle is controlled by mechanosensing in myosin filaments. *Nature*, *528*(7581), 276–279. https://doi.org/10.1038/nature15727

Linke, W. A. (2018). Titin Gene and Protein Functions in Passive and Active Muscle. *Annual Review of Physiology*, *80*(1), 389–411. https://doi.org/10.1146/annurev-physiol-021317-121234

Llinas, P., Isabet, T., Song, L., Ropars, V., Zong, B., Benisty, H., Sirigu, S., Morris, C., Kikuti, C., Safer, D., Sweeney, H. L., & Houdusse, A. (2015). How Actin Initiates the Motor Activity of Myosin. *Developmental Cell*, *33*(4), 401–412. https://doi.org/10.1016/j.devcel.2015.03.025

Luther, P. K., Winkler, H., Taylor, K., Zoghbi, M. E., Craig, R., Padrón, R., Squire, J. M., & Liu, J. (2011). Direct visualization of myosin-binding protein C bridging myosin and actin filaments in intact muscle. *Proceedings of the National Academy of Sciences of the United States of America*, *108*(28), 11423–11428. https://doi.org/10.1073/pnas.1103216108

Lymn, R. W., & Taylor, E. W. (1971). Mechanism of Adenosine Triphosphate Hydrolysis by Actomyosin. *Biochemistry*, *10*(25), 4617–4624. https://doi.org/10.1021/bi00801a004

McDonald, K. S., Wolff, M. R., & Moss, R. L. (1997). Sarcomere length dependence of the rate of tension redevelopment and submaximal tension in rat and rabbit skinned skeletal muscle fibres. *Journal of Physiology*, *501*(3), 607–621. https://doi.org/10.1111/j.1469-7793.1997.607bm.x

MacDougall, K. B., Kristensen, A. M., & MacIntosh, B. R. (2020). Additional in-series compliance does not affect the length dependence of activation in rat medial gastrocnemius. *Experimental Physiology*,*105*: 1907– 1917. https://doi.org/10.1113/EP088940

MacIntosh, B. R., & Willis, J. C. (2000). Force-frequency relationship and potentiation in mammalian skeletal muscle. *Journal of Applied Physiology*, *88*(6), 2088–2096. https://doi.org/10.1152/jappl.2000.88.6.2088

MacIntosh, B. R., & MacNaughton, M. B. (2005). The length dependence of muscle active force: Considerations for parallel elastic properties. *Journal of Applied Physiology*, *98*(5), 1666–1673. https://doi.org/10.1152/japplphysiol.01045.2004

MacIntosh, B.R. (2010). Cellular and whole muscle studies of activity dependent potentiation. In: Rassier D. (eds) *Muscle Biophysics*. Advances in Experimental Medicine and Biology, vol 682 (pp. 315-342). Springer, New York, NY. https://doi.org/10.1007/978-1-4419-6366-6_18

MacIntosh, B. R. (2017). Recent developments in understanding the length dependence of contractile response of skeletal muscle. *European Journal of Applied Physiology*, *117*(6), 1059–1071. https://doi.org/10.1007/s00421-017-3591-3

MacLennan, D. H., & Kranias, E. G. (2003). Phospholamban: A crucial regulator of cardiac contractility. *Nature Reviews Molecular Cell Biology*, *4*(7), 566–577. https://doi.org/10.1038/nrm1151

MacNaughton, M. B., & MacIntosh, B. R. (2007). Impact of length during repetitive contractions on fatigue in rat skeletal muscle. *Pflugers Archiv European Journal of Physiology*, *455*(2), 359–366. https://doi.org/10.1007/s00424-007-0273-8

Mair, P., & Wilcox, R. (2019). Robust statistical methods in R using the WRS2 package. *Behavior Research Methods*, *52*(2), 464–488. https://doi.org/10.3758/s13428-019-01246-w

Mamidi, R., Gresham, K. S., & Stelzer, J. E. (2014). Length-dependent changes in contractile dynamics are blunted due to cardiac myosin binding protein-C ablation. *Frontiers in Physiology*, *5*(Nov), 1–11. https://doi.org/10.3389/fphys.2014.00461

Mammucari, C., Raffaello, A., Vecellio Reane, D., Gherardi, G., De Mario, A., & Rosario, R. (2018) Mitochondrial calcium uptake in organ physiology: from molecular mechanism to animal models. *Pflugers Archiv - European Journal Physiology*,*470*, 1165–1179. https://doi.org/10.1007/s00424-018-2123-2

Manning, D. R., & Stull, J. T. (1979). Myosin light chain phosphorylation and phosphorylase a activity in rat extensor digitorum longus muscle. *Biochemical and Biophysical Research Communications*, *90*(1), 164–170. https://doi.org/10.1016/0006-291X(79)91604-8

Manning, D. R., & Stull, J. T. (1982). Myosin light chain phosphorylation-dephosphorylation in mammalian skeletal muscle. *American Journal of Physiology- Cell Physiology*,*242*(3), C234-C241. https://doi.org/10.1152/ajpcell.1982.242.3.C234

Manno, C., Figueroa, L. C., Gillespie, D., Fitts, R., Kang, C., Franzini-Armstrong, C., & Rios, E. (2017). Calsequestrin depolymerizes when calcium is depleted in the sarcoplasmic reticulum of working muscle. *Proceedings of the National Academy of Sciences of the United States of America*, *114*(4), E638–E647. https://doi.org/10.1073/pnas.1620265114

Martyn, D. A., & Gordon, A. M. (2001). Influence of length on force and activation-dependent changes in troponin C structure in skinned cardiac and fast skeletal muscle. *Biophysical Journal*, *80*(6), 2798–2808. https://doi.org/10.1016/S0006-3495(01)76247-9

Marx, S. O., Ondrias, K., & Marks, A. R. (1998). Coupled gating between individual skeletal muscle Ca^{2+} release channels (ryanodine receptors). *Science*, *281*(5378), 818–821. https://doi.org/10.1126/science.281.5378.818

Mateja, R. D., Greaser, M. L., & de Tombe, P. P. (2013). Impact of titin isoform on length dependent activation and cross-bridge cycling kinetics in rat skeletal muscle. *Biochimica et Biophysica Acta - Molecular Cell Research*, *1833*(4), 804–811. https://doi.org/10.1016/j.bbamcr.2012.08.011

McKillop, D. F., & Geeves, M. A. (1993). Regulation of the interaction between actin and myosin subfragment 1: evidence for three states of the thin filament. *Biophysical Journal*, *65*(2), 693–701. https://doi.org/10.1016/S0006-3495(93)81110-X

McNamara, J. W., Li, A., dos Remedios, C. G., & Cooke, R. (2014). The role of super-relaxed myosin in skeletal and cardiac muscle. *Biophysical Reviews*, *7*(1), 5–14. https://doi.org/10.1007/s12551-014-0151-5

McNamara, J. W., Li, A., Smith, N. J., Lal, S., Graham, R. M., Kooiker, K. B., van Dijk, S. J., Remedios, C. G. do., Harris, S. P., & Cooke, R. (2016). Ablation of cardiac myosin binding protein-C disrupts the super-relaxed state of myosin in murine cardiomyocytes. *Journal of Molecular and Cellular Cardiology*, *94*, 65–71. https://doi.org/10.1016/j.yjmcc.2016.03.009

McNamara, J. W., & Sadayappan, S. (2018). Skeletal myosin binding protein-C: An increasingly important regulator of striated muscle physiology. *Archives of Biochemistry and Biophysics*, *660*, 121–128. https://doi.org/10.1016/j.abb.2018.10.007

Metzger, J. M., Greaser, M. L., & Moss, R. L. (1989). Variations in cross-bridge attachment rate and tension with phosphorylation of myosin in mammalian skinned skeletal muscle fibers: Implications for twitch potentiation in intact muscle. *Journal of General Physiology*, *93*(5), 855–883. https://doi.org/10.1085/jgp.93.5.855

Michelucci, A., Boncompagni, S., Pietrangelo, L., Takano, T., Protasi, F., & Dirksen, R. T. (2020). Pre-assembled Ca 2 + entry units and constitutively active Ca 2 + entry in skeletal muscle of calsequestrin-1 knockout mice. *Journal of General Physiology*, *152*(10): e202012617. doi: https://doi.org/10.1085/jgp.202012617

Møller, J. V., Olesen, C., Winther, A. M. L., & Nissen, P. (2010). The sarcoplasmic Ca^{2+}-ATPase: design of a perfect chemi-osmotic pump. *Quarterly Reviews of Biophysics, 43*(4), 501-66. DOI:10.1017/S003358351000017X

Mollica, J. P., Dutka, T. L., Merry, T. L., Lamboley, C. R., Mcconell, G. K., Mckenna, M. J., Murphy, R. M., & Lamb, G. D. (2012). S -Glutathionylation of troponin I (fast) increases contractile apparatus Ca^{2+} sensitivity in fast-twitch muscle fibres of rats and humans. *The Journal of Physiology, 590*, 1443–1463. https://doi.org/10.1113/jphysiol.2011.224535

Moore, C. P., Zhang, J. Z., & Hamilton, S. L. (1999). A role for cysteine 3635 of RYR1 in redox modulation and calmodulin binding. *Journal of Biological Chemistry, 274*(52), 36831–36834. https://doi.org/10.1074/jbc.274.52.36831

Moore, R. L., & Stull, J. T. (1984). Myosin light chain phosphorylation in fast and slow skeletal muscles in situ. *American Journal of Physiology - Cell Physiology, 16*(3), 462–471. https://doi.org/10.1152/ajpcell.1984.247.5.c462

Moore, R. L., Palmer, B. M., Williams, S. L., Tanabe, H., Grange, R. W., & Houston, M. E. (1990). Effect of temperature on myosin phosphorylation in mouse skeletal muscle. *American Journal of Physiology - Cell Physiology, 259*(3 28-3). https://doi.org/10.1152/ajpcell.1990.259.3.c432

Moore, R. L., & Persechini, A. (1990). Length-dependence of isometric twitch tension potentiation and myosin phosphorylation in mouse skeletal muscle. *Journal of Cellular Physiology, 143*, 257-262. doi:10.1002/jcp.1041430209

Morris, S. R., Gittings, W., & Vandenboom, R. (2018). Epinephrine augments posttetanic potentiation in mouse skeletal muscle with and without myosin phosphorylation. *Physiological Reports, 6* (9), e13690, https://doi.org/10.14814/phy2.13690

Moss, R. L., & Fitzsimons, D. P. (2010). Regulation of contraction in mammalian striated muscles the plot thick-ens. *Journal of General Physiology, 136*(1), 21–27. https://doi.org/10.1085/jgp.201010471

Moss, R. L., Fitzsimons, D. P., & Ralphe, J. C. (2015). Cardiac MyBP-C regulates the rate and force of contraction in mammalian myocardium. *Circulation Research, 116*(1), 183–192. https://doi.org/10.1161/CIRCRESAHA.116.300561

Mukund, K., & Subramaniam, S. (2020). Skeletal muscle: A review of molecular structure and function, in health and disease. *Wiley Interdisciplinary Reviews: Systems Biology and Medicine, 12*(1), 1–46. https://doi.org/10.1002/wsbm.1462

Naber, N., Cooke, R., & Pate, E. (2011). Slow myosin ATP turnover in the super-relaxed state in tarantula muscle. *Journal of Molecular Biology, 411*(5), 943–950. https://doi.org/10.1016/j.jmb.2011.06.051

Nag, S., & Trivedi, D. V. (2021). To lie or not to lie: Super-relaxing with myosins. *ELife, 10*, 1–21. https://doi.org/10.7554/eLife.63703

Nelson, B. R., Makarewich, C. A., Anderson, D. M., Winders, B. R., Troupes, C. D., Wu, F., Reese, A. L., McAnally, J. R., Chen, X., Kavalali, E. T., Cannon, S. C., Houser, S. R., Bassel-Duby, R., & Olson, E. N. (2016). A peptide encoded by a transcript annotated as long noncoding RNA enhances SERCA activity in muscle. *Science*, *351*(6270), 271 LP – 275. https://doi.org/10.1126/science.aad4076

Nyitrai, M., & Geeves, M. A. (2004). Adenosine diphosphate and strain sensitivity in myosin motors. *Philosophical Transactions of the Royal Society B: Biological Sciences*, *359*(1452), 1867–1877. https://doi.org/10.1098/rstb.2004.1560

Oddoux, S., Brocard, J., Schweitzer, A., Szentesi, P., Giannesini, B., Brocard, J., Fauré, J., Pernet-Gallay, K., Bendahan, D., Lunardi, J., Csernoch, L., & Marty, I. (2009). Triadin deletion induces impaired skeletal muscle function. *Journal of Biological Chemistry*, *284*(50), 34918–34920. https://doi.org/10.1074/jbc.M109.022442

Padron, R., Ma, W., Duno Miranda, S., Koubassova, N., Lee, K., Tiwari, P., Pinto, A., Bolaños, P., Tsaturyan, A., Irving, T. C., & Craig, R. (2020). Thick Filament Activation and Post-Tetanic Potentiation Mechanisms Evolved Differently in Invertebrate and Vertebrate Striated Muscle. *Biophysical Journal*, *118*(3, Supplement 1), 496a. https://doi.org/https://doi.org/10.1016/j.bpj.2019.11.274

Park-Holohan, S. J., Brunello, E., Kampourakis, T., Rees, M., Irving, M., & Fusi, L. (2021). Stress-dependent activation of myosin in the heart requires thin filament activation and thick filament mechanosensing. *Proceedings of the National Academy of Sciences of the United States of America*, *118*(16). https://doi.org/10.1073/pnas.2023706118

Patel, B. G., Wilder, T., & John Solaro, R. (2013). Novel control of cardiac myofilament response to calcium by S-glutathionylation at specific sites of myosin binding protein C. *Frontiers in Physiology*, (November), 2–11. https://doi.org/10.3389/fphys.2013.00336

Patel, J. R., McDonald, K. S., Wolff, M. R., & Moss, R. L. (1997). Ca^{2+} binding to troponin C in skinned skeletal muscle fibers assessed with caged Ca^{2+} and a Ca^{2+} fluorophore. Invariance of Ca^{2+} binding as a function of sarcomere length. *Journal of Biological Chemistry*, *272*(9), 6018–6027. https://doi.org/10.1074/jbc.272.9.6018

Patel, J. R., Diffee, G. M., Xu, P. H., & Moss, R. L. (1998). Phosphorylation of myosin regulatory light chain eliminates force- dependent changes in relaxation rates in skeletal muscle. *Biophysical Journal*, *74*(1), 360–368. https://doi.org/10.1016/S0006-3495(98)77793-8

Pavlov, D. A., & Landesberg, A. (2016). The cross-bridge dynamics is determined by two length-independent kinetics: Implications on muscle economy and Frank-Starling Law. *Journal of Molecular and Cellular Cardiology*, *90*, 94–101. https://doi.org/10.1016/j.yjmcc.2015.11.007

Pavlov, I., Novinger, R., & Rassier, D. E. (2009). The mechanical behavior of individual sarcomeres of myofibrils isolated from rabbit psoas muscle. *American Journal of Physiology - Cell Physiology*, *297*(5), 1211–1219. https://doi.org/10.1152/ajpcell.00233.2009

Periasamy, M., & Kalyanasundaram, A. (2007). SERCA pump isoforms: Their role in calcium transport and disease. *Muscle Nerve*, *35*: 430-442. doi:10.1002/mus.20745

Pinto, A., Sánchez, F., Alamo, L., & Raúl Padrón (2012). The myosin interacting-heads motif is present in the relaxed thick filament of the striated muscle of scorpion. *Journal of Structural Biology*, *180*(3), 469-478. https://doi.org/10.1016/j.jsb.2012.08.010.

Ponnam, S., Sevrieva, I., Sun, Y. B., Irving, M., & Kampourakis, T. (2019). Site-specific phosphorylation of myosin binding protein-C coordinates thin and thick filament activation in cardiac muscle. *Proceedings of the National Academy of Sciences of the United States of America*, *116*(31), 15485–15494. https://doi.org/10.1073/pnas.1903033116

Posterino, G. S., Cellini, M. A., & Lamb, G. D. (2003). Effects of oxidation and cytosolic redox conditions on excitation – contraction coupling in rat skeletal muscle. *The Journal of Physiology*, *547*: 807–823. https://doi.org/10.1113/jphysiol.2002.035204

Previs, M. J., Mun, J. Y., Michalek, A. J., Beck Previs, S., Gulick, J., Robbins, J., Warshaw, D. M., & Craig, R. (2016). Phosphorylation and calcium antagonistically tune myosin-binding protein C's structure and function. *Proceedings of the National Academy of Sciences of the United States of America*, *113*(12), 3239–3244. https://doi.org/10.1073/pnas.1522236113

Protasi, F., Pietrangelo, L., & Boncompagni, S. (2020). Calcium entry units (CEUs): perspectives in skeletal muscle function and disease. *Journal of Muscle Research and Cell Motility*. https://doi.org/10.1007/s10974-020-09586-3

Prosser, B. L., Hernández-Ochoa, E. O., & Schneider, M. F. (2011). S100A1 and calmodulin regulation of ryanodine receptor in striated muscle. *Cell Calcium*, *50*(4), 323–331. https://doi.org/10.1016/j.ceca.2011.06.001

R Core Team (2021). R: A language and environment for statistical computing. R Foundation for Statistical Computing, Vienna, Austria. URL https://www.R-project.org/.

RStudio Team (2016). RStudio: Integrated Development for R. RStudio, Inc., Boston, MA URL http://www.rstudio.com/.

Rassier, D. E., Tubman, L. A., & MacIntosh, B. R. (1997). Length-dependent potentiation and myosin light chain phosphorylation in rat gastrocnemius muscle. *American Journal of Physiology - Cell Physiology*, *273*(1 42-1). https://doi.org/10.1152/ajpcell.1997.273.1.c198

Rassier, D. E., Tubman, L. A., & MacIntosh, B. R. (1998). Caffeine and length dependence of staircase potentiation in skeletal muscle. *Canadian Journal of Physiology and Pharmacology*, *76*(10–11), 975–982. https://doi.org/10.1139/y98-117

Rassier, D. E., MacIntosh, B. R., & Herzog, W. (1999). Length dependence of active force production in skeletal muscle. *Journal of Applied Physiology*, *86*(5), 1445-1457, https://doi.org/10.1152/jappl.1999.86.5.1445

Rassier, D. E., Tubman, L. A., & MacIntosh, B. R. (1999b). Staircase in mammalian muscle without light chain phosphorylation. *Brazilian Journal of Medical and Biological Research*, *32*(1), 121–129. https://doi.org/10.1590/s0100-879x1999000100018

Rassier, D. E., & MacIntosh, B. R. (2000). Length dependence of staircase potentiation: Interactions with caffeine and dantrolene sodium. *Canadian Journal of Physiology and Pharmacology*, *78*(4), 350–357. https://doi.org/10.1139/y99-143

Rassier, D. E., & MacIntosh, B. R. (2000). Coexistence of potentiation and fatigue in skeletal muscle. *Brazilian Journal of Medical and Biological Research*, *33*(5), 499–508. https://doi.org/10.1590/S0100-879X2000000500003

Rassier, D. R., & Herzog, W. (2002). Effects of pH on the length-dependent twitch potentiation in skeletal muscle. *Journal of Applied Physiology*, *92*: 1293-1299. https://doi.org/10.1152/japplphysiol.00912.2001.

Rassier, D. E., & Macintosh, B. R. (2002). Sarcomere Length-Dependence of Activity-Dependent Twitch Potentiation in Mouse Skeletal Muscle. *BMC Physiology*, *8*, 1–8.

Rassier, D. E., & MacIntosh, B. R. (2002b). Length-dependent twitch contractile characteristics of skeletal muscle. *Canadian Journal of Physiology and Pharmacology*, *80*(10), 993–1000. https://doi.org/10.1139/y02-127

Rassier, D. E., & Herzog, W. (2004). Considerations on the history dependence of muscle contraction. *Journal of Applied Physiology*, *96*(2), 419–427. https://doi.org/10.1152/japplphysiol.00653.2003

Rassier, D. E., & Minozzo, F. C. (2016). Length-dependent Ca^{2+} activation in skeletal muscle fibers from mammalians. *American Journal of Physiology - Cell Physiology*, *311*(2), C201–C211. https://doi.org/10.1152/ajpcell.00046.2016

Rassier, D. E. (2017). Sarcomere mechanics in striated muscles: From molecules to sarcomeres to cells. *American Journal of Physiology - Cell Physiology*, *313*(2), C134–C145. https://doi.org/10.1152/ajpcell.00050.2017

Raymackers, J. M., Gailly, P., Colson-Van Schoor, M., Pette, D., Schwaller, B., Hunziker, W., Celio, M. R., & Gillis, J. M. (2000). Tetanus relaxation of fast skeletal muscles of the mouse made parvalbumin deficient by gene inactivation. *The Journal of Physiology*, *527*(2), 355–364. https://doi.org/10.1111/j.1469-7793.2000.00355.x

Rebbeck, R. T., Karunasekara, Y., Board, P. G., Beard, N. A., Casarotto, M. G., & Dulhunty, A. F. (2014). Skeletal muscle excitation-contraction coupling: Who are the dancing partners? *International Journal of Biochemistry and Cell Biology*, *48*(1), 28–38. https://doi.org/10.1016/j.biocel.2013.12.001

Reconditi, M., Brunello, E., Fusi, L., Linari, M., Martinez, M. F., Lombardi, V., Irving, M., & Piazzesi, G. (2014). Sarcomere-length dependence of myosin filament structure in skeletal muscle fibres of the frog. *The Journal of Physiology*, *592*(5), 1119–1137. https://doi.org/10.1113/jphysiol.2013.267849

Reconditi, M., Brunello, E., Linari, M., Bianco, P., Narayanan, T., Panine, P., Piazzesi, G., Lombardi, V., & Irving, M. (2011). Motion of myosin head domains during activation and force development in skeletal muscle. *Proceedings of the National Academy of Sciences of the United States of America*, *108*(17), 7236–7240. https://doi.org/10.1073/pnas.1018330108

Reconditi, M., Caremani, M., Pinzauti, F., Powers, J. D., Narayanan, T., Stienen, G. J. M., Linari, M., Lombardi, V., & Piazzesi, G. (2017). Myosin filament activation in the heart is tuned to the mechanical task. *Proceedings of the National Academy of Sciences of the United States of America*, *114*(12), 3240–3245. https://doi.org/10.1073/pnas.1619484114

Robert-Paganin, J., Pylypenko, O., Kikuti, C., Sweeney, H. L., & Houdusse, A. (2020). Force Generation by Myosin Motors: A Structural Perspective. *Chemical Reviews*, *120*(1), 5–35. https://doi.org/10.1021/acs.chemrev.9b00264

Robinett, J. C., Hanft, L. M., Geist, J., Kontrogianni-Konstantopoulos, A., & McDonald, K. S. (2019). Regulation of myofilament force and loaded shortening by skeletal myosin binding protein C. *Journal of General Physiology*, *151*(5), 645–659. https://doi.org/10.1085/jgp.201812200

Rossi, D., Gamberucci, A., Pierantozzi, E., Amato, C., Migliore, L., & Sorrentino, V. (2020). Calsequestrin, a key protein in striated muscle health and disease. *Journal of Muscle Research and Cell Motility*, 0123456789. https://doi.org/10.1007/s10974-020-09583-6

Schiaffino, S., & Reggiani, C. (2011). Fiber types in mammalian skeletal muscles. *Physiological Reviews*, *91*(4), 1447–1531. https://doi.org/10.1152/physrev.00031.2010

Schwaller, B., Dick, J., Dhoot, G., Carroll, S., Vrbova, G., Nicotera, P., Pette, D., Wyss, A., Bluethmann, H., Hunziker, W., & Celio, M. R. (1999). Prolonged contraction-relaxation cycle of fast-twitch muscles in parvalbumin knockout mice. *American Journal of Physiology - Cell Physiology*, *276*(2 45-2), 395–403. https://doi.org/10.1152/ajpcell.1999.276.2.c395

Scorzeto M., Giacomello M., Toniolo L., Canato M., Blaauw B., Paolini, C., Protasi, F., Reggiani, C. & Stienen, G. J. M. (2013) Mitochondrial Ca^{2+}-Handling in Fast Skeletal Muscle Fibers from Wild Type and Calsequestrin-Null Mice. *PLOS ONE*, *8*(10): e74919. https://doi.org/10.1371/journal.pone.0074919

Sequeira, V., & van der Velden, J. (2017). The Frank–Starling Law: a jigsaw of titin proportions. *Biophysical Reviews*, *9*(3), 259–267. https://doi.org/10.1007/s12551-017-0272-8

Shaikh, S. A., Sahoo, S. K., & Periasamy, M. (2016). Phospholamban and sarcolipin: Are they functionally redundant or distinct regulators of the Sarco(Endo)Plasmic Reticulum Calcium ATPase? *Journal of Molecular and Cellular Cardiology*, *91*, 81–91. https://doi.org/10.1016/j.yjmcc.2015.12.030

Shishmarev, D. (2020). Excitation-contraction coupling in skeletal muscle: recent progress and unanswered questions. *Biophysical Reviews*, *12*(1), 143–153. https://doi.org/10.1007/s12551-020-00610-x

Smith, I. C., Gittings, W., Huang, J., McMillan, E. M., Quadrilatero, J., Tupling, R. R., & Vandenboom, R. (2013). Potentiation in mouse lumbrical muscle without myosin light chain phosphorylation: Is resting calcium responsible? *Journal of General Physiology*, *141*(3), 297–308. https://doi.org/10.1085/jgp.201210918

Smith, I. C., Vandenboom, R., & Tupling, A. R. (2014). Juxtaposition of the changes in intracellular calcium and force during staircase potentiation at 30 and 37°C. *Journal of General Physiology*, *144*(6), 561–570. https://doi.org/10.1085/jgp.201411257

Smith, I. C., Vandenboom, R., & Tupling, A. R. (2017). Contraction-induced enhancement of relaxation during high force contractions of mouse lumbrical muscle at 37°C. *Journal of Experimental Biology*, *220*(16), 2870–2873. https://doi.org/10.1242/jeb.158998

Smith, I. C., Vandenboom, R., & Tupling, A. R. (2019). Caffeine attenuates contraction-induced diminutions of the intracellular calcium transient in mouse lumbrical muscle ex vivo. *Canadian Journal of Physiology and Pharmacology*. *97*(5): 429-435. https://doi.org/10.1139/cjpp-2018-0658

Solís, C., & Solaro, R. J. (2021). Novel insights into sarcomere regulatory systems control of cardiac thin filament activation. *The Journal of General Physiology*, *153*(7), 1–25. https://doi.org/10.1085/jgp.202012777

Song, T., McNamara, J. W., Ma, W., Landim-Vieira, M., Lee, K. H., Martin, L. A., Heiny, J. A., Lorenz, J. N., Craig, R., Pinto, J. R., Irving, T., & Sadayappan, S. (2021). Fast skeletal myosin-binding protein-C regulates fast skeletal muscle contraction. *Proceedings of the National Academy of Sciences of the United States of America*, *118*(17), 2–9. https://doi.org/10.1073/pnas.2003596118

Sun, J., Xin, C., Eu, J. P., Stamler, J. S., & Meissner, G. (2001). Cysteine-3635 is responsible for skeletal muscle ryanodine receptor modulation by NO. *Proceedings of the National Academy of Sciences of the United States of America*, *98*(20), 11158–11162. https://doi.org/10.1073/pnas.201289098

Sun, J., Xu, L., Eu, J. P., Stamler, J. S., & Meissner, G. (2003). Nitric oxide, NOC-12, and S-nitrosoglutathione modulate the skeletal muscle calcium release channel/ryanodine receptor by different mechanisms: An allosteric function for O_2 in S-nitrosylation of the channel. *Journal of Biological Chemistry*, *278*(10), 8184–8189. https://doi.org/10.1074/jbc.M211940200

Sun, Q. A., Hess, D. T., Nogueira, L., Yong, S., Bowles, D. E., Eu, J., Laurita, K. R., Meissner, G., & Stamler, J. S. (2011). Oxygen-coupled redox regulation of the skeletal muscle ryanodine receptor-Ca^{2+} release channel by NADPH oxidase 4. *Proceedings of the National Academy of Sciences of the United States of America*, *108*(38), 16098–16103. https://doi.org/10.1073/pnas.1109546108

Sun, Q. A., Wang, B., Miyagi, M., Hess, D. T., & Stamler, J. S. (2013). Oxygen-coupled redox regulation of the skeletal muscle ryanodine receptor/Ca^{2+} release channel (RyR1): Sites and nature of oxidative modification. *Journal of Biological Chemistry*, *288*(32), 22961–22971. https://doi.org/10.1074/jbc.M113.480228

Stehle, R., & Tesi, C. (2017). Kinetic coupling of phosphate release, force generation and rate-limiting steps in the cross-bridge cycle. *Journal of Muscle Research and Cell Motility*, *38*(3–4), 275–289. https://doi.org/10.1007/s10974-017-9482-8

Stephenson, G. M. M., & Stephenson, D. G. (1993). Endogenous MLC2 phosphorylation and Ca^{2+}-activated force in mechanically skinned skeletal muscle fibres of the rat. *Pflügers Archiv-European Journal of Physiology*, *424*(1), 30–38. https://doi.org/10.1007/BF00375099

Stewart, M., Franks-Skiba, K., & Cooke, R. (2009). Myosin regulatory light chain phosphorylation inhibits shortening velocities of skeletal muscle fibers in the presence of the myosin inhibitor blebbistatin. *Journal of Muscle Research and Cell Motility*, *30*(1–2), 17–27. https://doi.org/10.1007/s10974-008-9162-9

Stull, J. T., Kamm, K. E., & Vandenboom, R. (2011). Myosin light chain kinase and the role of myosin light chain phosphorylation in skeletal muscle. *Archives of Biochemistry and Biophysics*, *510*(2), 120–128. https://doi.org/10.1016/j.abb.2011.01.017

Sweeney, H. L., & Kushmesrick, M. J. (1985). Myosin phosphorylation in permeabilized rabbit psoas fibers. *American Journal of Physiology - Cell Physiology*, *18*(2), 18–21. https://doi.org/10.1152/ajpcell.1985.249.3.c362

Sweeney, H. L., & Stull, J. T. (1986). Phosphorylation of myosin in permeabilized mammalian cardiac and skeletal muscle cells. *American Journal of Physiology - Cell Physiology*, *250*(4). https://doi.org/10.1152/ajpcell.1986.250.4.c657

Sweeney, H. Lee, & Stull, J. T. (1990). Alteration of cross-bridge kinetics by myosin light chain phosphorylation in rabbit skeletal muscle: Implications for regulation of actin-myosin interaction. *Proceedings of the National Academy of Sciences of the United States of America*, *87*(1), 414–418. https://doi.org/10.1073/pnas.87.1.414

Sweeney, H. L., Bowman, B. F., & Stull, J. T. (1993). Myosin light chain phosphorylation in vertebrate striated muscle: Regulation and function. *American Journal of Physiology - Cell Physiology*, *264*(5 33-5), 85–95. https://doi.org/10.1152/ajpcell.1993.264.5.c1085

Sweeney, H. L., Yang, Z., Zhi, G., Stull, J. T., & Trybus, K. M. (1994). Charge replacement near the phosphorylatable serine of the myosin regulatory light chain mimics aspects of phosphorylation. *Proceedings of the National Academy of Sciences of the United States of America*, *91*(4), 1490–1494. https://doi.org/10.1073/pnas.91.4.1490

Sweeney, H. L., & Houdusse, A. (2010). Structural and Functional Insights into the Myosin Motor Mechanism. *Annual Review of Biophysics*, *39*(1), 539–557. https://doi.org/10.1146/annurev.biophys.050708.133751

Szczesna, D., Zhao, J., Jones, M., Zhi, G., Stull, J., & Potter, J. D. (2002). Phosphorylation of the regulatory light chains of myosin affects Ca^{2+} sensitivity of skeletal muscle contraction. *Journal of Applied Physiology*, *92*(4), 1661–1670. https://doi.org/10.1152/japplphysiol.00858.2001

Tachampa, K., Wang, H., Farman, G. P., & De Tombe, P. P. (2007). Cardiac troponin I threonine 144: Role in myofilament length-dependent activation. *Circulation Research*, *101*(11), 1081–1083. https://doi.org/10.1161/CIRCRESAHA.107.165258

Toepfer, C., Caorsi, V., Kampourakis, T., Sikkel, M. B., West, T. G., Leung, M. C., Al-Saud, S. A., MacLeod, K. T., Lyon, A. R., Marston, S. B., Sellers, J. R., & Ferenczi, M. A. (2013). Myosin regulatory light chain (RLC) phosphorylation change as a modulator of cardiac muscle contraction in disease. *Journal of Biological Chemistry*, *288*(19), 13446–13454. https://doi.org/10.1074/jbc.M113.455444

Tupling, R. A. (2009). The decay phase of Ca^{2+} transients in skeletal muscle: Regulation and physiology. *Applied Physiology, Nutrition and Metabolism*, *34*(3), 373–376. https://doi.org/10.1139/H09-033

Tupling, A. R., Bombardier, E., Gupta, S. C., Hussain, D., Vigna, C., Bloemberg, D., Quadrilatero, J., Trivieri, M. G., Babu, G. J., Backx, P. H., Periasamy, M., Maclennan, D. H., & Gramolini, A. O. (2011). Enhanced Ca^{2+} transport and muscle relaxation in skeletal muscle from sarcolipin-null mice. *American Journal of Physiology - Cell Physiology*, *301*(4), 841–849. https://doi.org/10.1152/ajpcell.00409.2010

Unger, M., & Debold, E. P. (2019). Acidosis decreases the Ca^{2+} sensitivity of thin filaments by preventing the first actomyosin interaction. *American Journal of Physiology - Cell Physiology*, *317*(4), C714–C718. https://doi.org/10.1152/ajpcell.00196.2019

Vandenboom, R., Grange, R. W., & Houston, M. E. (1993). Threshold for force potentiation associated with skeletal myosin phosphorylation. *American Journal of Physiology - Cell Physiology*, *265*(6 34-6). https://doi.org/10.1152/ajpcell.1993.265.6.c1456

Vandenboom, R., Grange, R. W., & Houston, M. E. (1995). Myosin phosphorylation enhances rate of force development in fast-twitch skeletal muscle. *American Journal of Physiology - Cell Physiology*, *268*(3 37-3). https://doi.org/10.1152/ajpcell.1995.268.3.c596

Vandenboom, R., Claflin, D. R., & Julian, F. J. (1998). Effects of rapid shortening on rate of force regeneration and myoplasmic $[Ca^{2+}]$ in intact frog skeletal muscle fibres. *Journal of Physiology*, *511*(1), 171–180. https://doi.org/10.1111/j.1469-7793.1998.171bi.x

Vandenboom, R., Gittings, W., Smith, I.C., Grange, R. W., & Stull, J. T. (2013). Myosin phosphorylation and force potentiation in skeletal muscle: evidence from animal models. *Journal of Muscle Research and Cell Motility*, *34*, 317–332 (2013). https://doi.org/10.1007/s10974-013-9363-8

Vandenboom, R. (2017). Modulation of skeletal muscle contraction by myosin phosphorylation. *Comprehensive Physiology*, *7*(1), 171–212. https://doi.org/10.1002/cphy.c150044

Vinogradova, M. V., Stone, D. B., Malanina, G. G., Karatzaferi, C., Cooke, R., Mendelson, R. A., & Fletterick, R. J. (2005). Ca^{2+}-regulated structural changes in troponin. *Proceedings of the National Academy of Sciences of the United States of America*, *102*(14), 5038–5043. https://doi.org/10.1073/pnas.0408882102

Walklate, J., Ujfalusi, Z., & Geeves, M. A. (2016). Myosin isoforms and the mechanochemical cross-bridge cycle. *Journal of Experimental Biology*, *219*(2), 168–174. https://doi.org/10.1242/jeb.124594

Wallinga-De Jonge, W., Boom, H. B. K., & Boon, K. L. (1980). Force development of fast and slow skeletal muscle at different muscle lengths. *American Journal of Physiology - Cell Physiology*, *8*(2), 0–6. https://doi.org/10.1152/ajpcell.1980.239.3.c98

Wang, Y., Li, X., Duan, H., Fulton, T. R., Eu, J. P., & Meissner, G. (2009). Altered stored calcium release in skeletal myotubes deficient of triadin and junctin. *Cell Calcium*, *45*(1), 29–37. https://doi.org/10.1016/j.ceca.2008.05.006

Wei, L., Gallant, E. M., Dulhunty, A. F., & Beard, N. A. (2009). Junctin and triadin each activate skeletal ryanodine receptors but junctin alone mediates functional interactions with calsequestrin. *International Journal of Biochemistry and Cell Biology*, *41*(11), 2214–2224. https://doi.org/10.1016/j.biocel.2009.04.017

Williams, C., Regnier, M., & Daniel, T. L. (2010). Axial and radial forces of cross-bridges depend on lattice spacing. *PLoS Computational Biology*, *6*(12). https://doi.org/10.1371/journal.pcbi.1001018

Williams, C. D., Salcedo, M. K., Irving, T. C., Regnier, M., & Daniel, T. L. (2013). The length-tension curve in muscle depends on lattice spacing. *Proceedings of the Royal Society B: Biological Sciences*, *280*(1766). https://doi.org/10.1098/rspb.2013.0697

Williams, G. S. B., Boyman, L., Chikando, A. C., Khairallah, R. J., & Lederer, W. J. (2013) Mitochondrial calcium uptake. *Proceedings of the National Academy of Sciences* ,*110*(26) 10479-10486. DOI: 10.1073/pnas.1300410110

Willigems, K., & Efremov, R. G. (2017). Structural details of the ryanodine receptor calcium release channel and its gating mechanism. In: Krebs J. (eds) *Membrane Dynamics and Calcium Signalling*. Advances in Experimental Medicine and Biology, vol 981 (pp.179-204). Springer International Publishing AG, part of Springer Nature 2017. https://doi.org/10.1007/978-3-319-55858-5_8

Willingham, T.B., Kim, Y., Lindberg, E., Bleck, C. K. E., & Glancy, B. (2020). The unified myofibrillar matrix for force generation in muscle. *Nature Communications*, *11*, 3722. https://doi.org/10.1038/s41467-020-17579-6

Xeni, J., Gittings, W. B., Caterini, D., Huang, J., Houston, M. E., Grange, R. W., & Vandenboom, R. (2011). Myosin light-chain phosphorylation and potentiation of dynamic function in mouse fast muscle. *Pflugers Archiv European-Journal of Physiology*, *462*(2), 349–358. https://doi.org/10.1007/s00424-011-0965-y

Yamada, Y., Namba, K., & Fujii, T. (2020). Cardiac muscle thin filament structures reveal calcium regulatory mechanism. *Nature Communications*, *11*(1), 1–3. https://doi.org/10.1038/s41467-019-14008-1

Yamaguchi, M., Kimura, M., Li, Z. B., Ohno, T., Takemori, S., Hoh, J. F. Y., & Yagi, N. (2016). X-ray diffraction analysis of the effects of myosin regulatory light chain phosphorylation and butanedione monoxime on skinned skeletal muscle fibers. *American Journal of Physiology - Cell Physiology*, *310*(8), C692–C700. https://doi.org/10.1152/ajpcell.00318.2015

Yamaguchi, N., Prosser, B. L., Ghassemi, F., Xu, L., Pasek, D. A., Eu, J. P., Hernández-Ochoa, E. O., Cannon, B. R., Wilder, P. T., Lovering, R. M., Weber, D., Melzer, W., Schneider, M. F., & Meissner, G. (2011). Modulation of sarcoplasmic reticulum Ca^{2+} release in skeletal muscle expressing ryanodine receptor impaired in regulation by calmodulin and S100A1. *American Journal of Physiology - Cell Physiology*, *300*(5), 998–1012. https://doi.org/10.1152/ajpcell.00370.2010

Yang, Z., Stull, J. T., Levine, R. J. C., & Sweeney, H. L. (1998). Changes in interfilament spacing mimic the effects of myosin regulatory light chain phosphorylation in rabbit psoas fibers. *Journal of Structural Biology*, *122*(1–2), 139–148. https://doi.org/10.1006/jsbi.1998.3979

Zhang, X., Kampourakis, T., Yan, Z., Sevrieva, I., Irving, M., & Sun, Y. B. (2017). Distinct contributions of the thin and thick filaments to length-dependent activation in heart muscle. *ELife*, *6*, 1–16. https://doi.org/10.7554/eLife.24081

Zhi, G., Ryder, J. W., Huang, J., Ding, P., Chen, Y., Zhao, Y., Kamm, K. E., & Stull, J. T. (2005). Myosin light chain kinase and myosin phosphorylation effect frequency-dependent potentiation of skeletal muscle contraction. *Proceedings of the National Academy of Sciences of the United States of America*, *102*(48), 17519–17524. https://doi.org/10.1073/pnas.0506846102

Zoghbi, M. E., Woodhead, J. L., Moss, R. L., & Craig, R. (2008). Three-dimensional structure of vertebrate cardiac muscle myosin filaments. *Proceedings of the National Academy of Sciences of the United States of America*, *105*(7), 2386–2390. https://doi.org/10.1073/pnas.0708912105